TUM

Technische Universität München
Ingenieurfakultät Bau Geo Umwelt

Lehrstuhl für Wasserbau und Wasserwirtschaft

Numerical Modeling of Sediment Transport in Dasu-Tarbela Reservoir using Neural Networks and TELEMAC Model System

Sardar Ateeq-Ur-Rehman

Vollständiger Abdruck der von der Ingenieurfakultät Bau Geo Umwelt der Technischen Universität München zur Erlangung des akademischen Grades eines

Doktor-Ingenieurs

genehmigten Dissertation.

Vorsitzender: Prof. Dr.-Ing. Jörg E. Drewes
Prüfer der Dissertation:
1. Prof. Dr. sc. techn. Peter Rutschmann
2. Prof. Dr. George S. Constantinescu
3. Prof. Dr.-Ing. Jochen Aberle

Die Dissertation wurde am 05.10.2018 bei der Technischen Universität München eingereicht und durch die Ingenieurfakultät Bau Geo Umwelt am 19.12.2018 angenommen.

Dies ist eine kumulative Dissertation basierend auf Veröffentlichungen in internationalen

Fachzeitschriften.

Acknowledgement

First and foremost, I would like to thank my Mentor Dr. Ing. Minh Duc Bui and Supervisor Prof. Dr. Peter Rutschmann for years of guidance, mentoring, and encouragement. Without their valuable help, I could never have completed this dissertation. I am also grateful to my fellow students and staff members in the Chair of Hydraulic and Water Resources Engineering, for their help in my research.

Finally I am deeply grateful to the Higher Education Commission (HEC) of Pakistan and German Academic Exchange Service (DAAD) for supporting me financially in my doctoral studies. Without their financial support, none of my achievements would have been possible.

Sardar Ateeq Ur Rehman

Chair of Hydraulic and Water Resources Engineering

Technical University of Munich

Arcisstr. 21, 80333 Munich, Germany

Tel: +92 300 760 8181

Email: engr.ateeq@yahoo.com
       sardar.ateeq@tum.de

Abstract

High rates of soil loss and high sediment loads in rivers require efficient quantification methodologies for the design of effective reservoir sediment management strategies. A cascade modelling of sediment management in reservoirs is a useful approach to address these issues. Quantifying sediment load using conventional sediment rating curves, however, poorly accounts for the hysteresis phenomenon and hydrological variations. Wavelet transform coupled with artificial neural networks (WA-ANNs) makes it possible to study large basins and set more precise estimation of sediment load boundary conditions for reservoir sedimentation models. Following this approach, a cascade modelling algorithm was developed by the Chair of Hydraulic and Water Resources Engineering, Technical University of Munich, which was applied to the Indus River and the Tarbela dam in northern Pakistan. The methodological framework consists of five steps: (I) analysis of sediment management using 1D modelling and reservoir sedimentation techniques (II) analysis of sediment load estimation using artificial neural networks (ANNs) (III) development of wavelet-ANN (WA-ANN) model for estimation of suspended sediment load, (IV) based on WA-ANN estimates, investigation of sediment load trends, and (V) use more accurate sediment load boundary conditions for modelling of reservoir sedimentation at the Tarbela dam. The analysis carried out on the Indus River has enabled a better understanding of reservoir sedimentation in the basin.

The analysis of sediment load techniques in this study indicates that WA-ANN can precisely estimate the sediment load by accounting for the hysteresis phenomenon and hydrological variations using a temporal resolution of approximately one year. It also demonstrates that, contrary to the conventional model, the sediment load at the Tarbela dam gauge station is only 160 million tons per year and has been showing a decreasing trend caused by desynchronization between glacier melt and monsoon rainfall. Investigation of sediment load trends reveals statistically significant disproportional spatio-temporal trends between sediment loads and discharges caused primarily by intra-annual shifts in flows. This disproportional behaviour and the significant trends strongly disconfirm the hypothesis that future sediment loads are similar to the previous ones.

In modelling reservoir sedimentation, the uncertainty in predicting the river bed-level changes can be diminished by using a cascading modelling approach, which uses more precise sediment load boundary conditions estimated by WA-ANN. The morphodynamic model, which was hydrodynamically calibrated with a coefficient of determination (R^2)=0.97, Nash-Sutcliffe Efficiency (NSE)=0.96 also better predicted (form 1985 to 1990)

the river bed changes (especially delta) at the Tarbela dam with R^2=0.96 and NSE=0.95. Due to the desynchronization effect primarily caused by projected warmer climate and subsequent decrease of 17% in the sediment supply to the Tarbela dam, the modelling showed stabilization in the sediment delta in the future. The presented modelling algorithm can be used to improve and design sediment management strategies for the existing and planned hydraulic structures in the Upper Indus Basin and similar un-gauged or poorly gauged catchments around the world.

Abstract

Hohe Bodenverlustraten und hohe Sedimentfrachten in Flüssen erfordern effiziente Quantifizierungsmethoden, um effektive Sedimentmanagementstrategien zu entwickeln. Um an diese Probleme heranzugehen ist eine Kaskadenmodellierung des Sedimentmanagements in Reservoirs ein nützlicher Ansatz . Die Quantifizierung der Sedimentfracht unter Verwendung konventioneller Sediment-Bewertungskurven (SRCs) berücksichtigt jedoch schlecht das Hysteresephänomen und die hydrologischen Variationen. Die Wavelet-Transformation in Verbindung mit künstlichen neuronalen Netzen (WA-ANNs) ermöglicht die Untersuchung großer Becken und eine genauere Abschätzung der Sedimentfrachtbedingungen für Sedimentationsmodelle. Nach diesem Ansatz wurde am Lehrstuhl für Wasserbau und Wasserwirtschaft der Technischen Universität München ein Kaskadenmodellierungsalgorithmus entwickelt, der auf den Indus und den Tarbela-Staudamm im Norden Pakistans angewendet wurde. Der methodische Rahmen besteht aus fünf Schritten: (I) Gegenstandsanalyse des Sedimentmanagements mittels 1D-Modellierung und Reservoirsedimentationstechniken (II) Analyse der Sedimentfracht mit künstlichen neuronalen Netzen (ANN) (III) Entwicklung eines Wavelet-ANN (WA-ANN) Modells zur Abschätzung der Schwebstofffracht, (IV) basierend auf WA-ANN-Schätzungen, Untersuchung der Sedimentfrachttrends und (V) Modellierung der Reservoirsedimentation für den Tarbela-Staudamm. Die am Indus durchgeführte Analyse ermöglicht ein besseres Verständnis der Reservoirssedimentation im Becken.

Die Analyse der Sedimentfrachttechniken in dieser Studie zeigt, dass das WA-ANN die Sedimentfracht genau abschätzen kann, indem das Hysteresephänomen und die hydrologischen Variationen mit einer zeitlichen Auflösung von ungefähr einem Jahr berücksichtigt werden. Es zeigt auch, dass die Sedimentfracht an der Talstation der Tarbela-Talsperre im Gegensatz zum konventionellen Modell nur 160 Millionen Tonnen pro Jahr beträgt und aufgrund der Desynchronisation zwischen Gletscherschmelze und Monsunregen eine abnehmende Tendenz aufweist. Die Untersuchung der Sedimentfrachttrends zeigt statistisch signifikante disproportional verhaltende raumzeitliche Trends zwischen Sedimentfrachten und Abflüssen, die hauptsächlich durch innerjährliche Veränderung der Strömung verursacht werden. Dieses disproportionale Verhalten und die signifikanten Trends widerlegen stark die Hypothese, dass zukünftige Sedimentfrachten den vorherigen ähnlich sind.

Bei der Modellierung der Reservoirsedimentation kann die Unsicherheit bei der Vorhersage der Höhenveränderung des Flussbettes durch einen kaskadischen Modellierungsansatz, der präzisere vom WA-ANN abgeschätzte Sedimentfracht-Randbedingungen verwendet,

verringert werden. Das morphodynamische Modell, das hydrodynamisch mit einem Bestimmtheitsmaß von $R^2 = 0,97$ und der Nash-Sutcliffe-Efficiency (NSE) $= 0,96$ kalibriert wurde, konnte die Flussbettveränderungen(besonders im Delta) an der Tarbela-Staumauer mit $R^2 = 0,96$ und NSE $= 0,95$ (von 1985 bis 1990) gut vorhersagen. Aufgrund des Desynchronisationseffekts, der vor allem durch das projizierte wärmere Klima und die anschließende Abnahme der Sedimentzufuhr zum Tarbela-Damm von 17% verursacht wurde, zeigte die Modellierung eine Stabilisierung im Sedimentdelta in der Zukunft. Der vorgestellte Modellierungsalgorithmus kann verwendet werden, um Sediment-Management-Strategien für die bestehenden und geplanten hydraulischen Strukturen im Oberindus-Becken und ähnlichen nicht gemessenen oder schlecht ausgestatteten Einzugsgebieten auf der ganzen Welt zu verbessern.

Preface

This cumulative dissertation is based on the following conference and journal papers:

(I) Ateeq-Ur-Rehman, S.; Riaz, Z.; Bui, M.D.; Rutschmann, P., Application of a 1-D numerical model for sediment management in Dasu Hydropower Project. In *Proceedings of the 14th International Conference on Environmental Science and Technology*; Lekkas, D., Ed.; Global CEST: Rohdes, Greece, 2015; ISBN. 978-960-7475-52-7

(II) Ateeq-Ur-Rehman, S.; Bui, M.D.; Riaz, Z.; Rutschmann, P., Estimation of sediment yield for Dasu Hydropower Project using artificial neural networks. In *18. Wasserbau-Symposium*; Rutschmann, P., Ed.; Freunde des Lehrstuhls für Wasserbau und Wasserwirtschaft, TU Munich: Wallgau, Germany, 2016; Vol. Nr. 134/2016, pp. 326–337, ISBN. 978-3-943683

(III) Ateeq-Ur-Rehman, S.; Bui, M.D.; Rutschmann, P. Development of a wavelet-ANN model for estimating suspended sediment load in the upper Indus River. *Submitted to International Journal of River Basin Management* **2017**

(IV) Ateeq-Ur-Rehman, S.; Bui, M.D.; Rutschmann, P. Variability and trend detection in the sediment load of the Upper Indus River. *Water (Switzerland)* **2018**, *10*, 1–24, doi:10.3390/w10010016

(V) Ateeq-Ur-Rehman, S.; Bui, M.D.; Hasson, S.u.; Rutschmann, P. An innovative approach to minimizing uncertainty in sediment load boundary conditions for modelling sedimentation in reservoirs. *Water (Switzerland)* **2018**, *10*, 1–27, doi:10.3390/w10101411

In the introduction chapter I defines the state of the art and research gaps. Based on these research gaps, I selected and justified the used methods. At the end I concluded the overall contribution of the study. The introduction section also contains a summary of the above mentioned papers along with a declaration of consent of authors and their contributions.

Contents

List of Figures

List of Tables

Chapter 1

Introduction

1.1 Research background

Sediments are transported in the form of bed and suspended loads to reservoirs. There are a number of reasons for the velocity deceleration in a reservoir such as sudden inlet expansion, deep river bed, and reservoir operation rules, which decrease the sediment load carrying capacity of the river and result in sediment becoming trapped. Predictions/estimation of accurate amount of incoming sediments to the reservoir, sediment load trends, modelling of sediment deposition and their accumulation with the passage of time remains a significant challenge due to the following reasons in hydraulic engineering.

1.1.1 Sediment load estimation

The most common conventional method for sediment load estimation is the sediment rating curve approach, which is based on a relatively simple relationship between flow discharge and sediment concentration [8]. However, in real-world scenarios, multiple variables act on the given circumstances of the sampled data, which is why sediment rating curve mostly results in over or under estimations of the sediment load. This can have dire consequences. For example, a number of dams in Pakistan have silted up earlier than expected due to under-estimation or are inefficient due to over-estimation of sediment load - instances include the Warsak and Mangla dams [9, 10]. The cause of this problem is the significant variance in suspended sediment load (SSL) estimates on which the design and operation of these dams are based [3]. The variance in SSL estimates at Besham Qila gauge station used for the Tarbela dam range from 200 million tons per year (Mt yr^{-1}) to 675 Mt yr^{-1} (Tab. 1.1). Such variance might not only skew calculations of sediment load boundary conditions in reservoir sedimentation studies but also negatively influence

subsequent decisions and diminish associated benefits.

Table 1.1: Estimates published on the suspended sediment load (SSL) of the Upper Indus River [3, 4].

Suspended sediment yield (Mt yr^{-1})	Estimated by
480	[11]
400	[12]
475	[13]
200	[14] reported by [15]
675	[16]
300	[17]
200	[18]
197[1]	[19]
138[2]	[19]
200	[6]

SSL estimation has become vastly more challenging, in particular under the influence of climate change, where disproportional spatio-temporal trends between SSLs and flow discharges exist primarily due to intra-annual shifts in flows [20, 21, 4]. This highlights the need for sediment models which operate in real time and are able to provide a better estimates of sediment load for the planning of new hydraulic structures or better management of existing ones. This particularly applies to the Upper Indus River, where the presence of complex sediment transport processes related to the hysteresis phenomena and marked hydrological variations, such as: (a) the fluvial erosion and transport processes which interact with other sediment producing processes, (b) temporary sediment storage in the main river channel [22], (c) aggradation and degradation phases of landslides [23], (d) on average 5-10 high flow waves of an average 10-12 days duration during the monsoon period, (e) different transit times of discharge and sediment and their different lag times from several sources to the gauge stations, and (f) a recently noted Karakoram anomaly where desynchronization between glacier melt and monsoon rainfall is projected for the future [24], all pose a challenge for a accurate SSL estimation. In addition, hydro-morphological processes are highly nonlinear in nature, and in many cases, modelling of these variables with conceptual models may be limited by a poor understanding of the complex iterations involved. In such cases, artificial neural networks (ANNs) are often viewed as an appealing alternative, as they have the ability to extract the nonlinear relationship from the data without requiring an in depth knowledge of the physics occurring within the system [25]. Similarly, the application of wavelet transforms (WT) has also been found

---

[1]Besham Qila
[2]Partab Bridge

to be effective in dealing with hysteresis phenomenon issues. WT is a mathematical tool that can improve the performance of ANN models by simultaneously considering both the spectral and the temporal information contained in the input data. This information is revealed by decomposing the main time series data into its sub-components. These models have been performing well over the last decade of estimating and forecasting of SL [26, 27].

WA-ANNs can decompose the data time series up to several levels in time, space and frequency domains and reveal the information from a given data scenario [28]. This decomposition of data is required where the sediment transport process is subjected to temporary sediment storage, strong hysteresis phenomena and parallel aggradation and degradation of landslides. Data decomposition beyond level one can lead to a low efficiency [29], however, the concept of appropriate decomposition levels of data for rivers with temporary substantial sediment load storage is still not understood. ANNs sediment load estimation abilities with semi-monthly sediment loads using simple ANN structures have only been tested for rivers that have small catchments [30]. Moreover, WA-ANNs have not been tested for filling the gaps between intermittent suspended sediment concentration (SSC) samples; in the state-of-the-art techniques [26, 31], they have only been applied on continuous (daily) data time series. In granting the importance to hydraulic structures as non-renewable resources, therefore, it was necessary to quantitatively and qualitatively evaluate the performance (and uncertainties originating using) of these (sediment rating curve, ANN and WA-ANN) methods for rivers with complex sediment transport processes.

1.1.2 Sediment load trends

As with the problems related to more accurate estimation of the suspended sediment loads (SSL) for better planning of sediment management (yield reduction, routing, and removal) [32, 6, 33, 34, 35], the temporal variations and changes in SSLs are also important not only for setting correct sediment load boundary conditions for predictions of reservoir sedimentation but also to assess the effectiveness of existing watershed management practices or tectonic and land-sliding activities in the catchment area. Although there are many studies assessing the climate-induced adverse impacts on the Upper Indus River flow patterns [20, 36, 37, 38, 21, 39, 40], few have investigated the impact of flow pattern changes on the sediment yield and reservoirs [41, 42]. This might be due to the absence of more accurate sediment load estimation methods, while the studies conducted in this regard using conventional sediment rating curve differ widely in their suggested

estimates. For instance, the SSL for Tarbela Dam (the country's largest) or at the immediately upstream Besham Qila discharge gauge is reported to range from 200 Mt yr^{-1} to 675 Mt yr^{-1} over the past 50 years (Tab. 1.1). Such uncertainty leads to poor design quality of the operating rules for existing and under-construction dams. Especially, when the past SL data is used for predictions without modification. For example, variation in predictions using sediment rating curve were as high as approximately 40% of the mean difference of the measurements reported for the Tarbela dam over a mere 26 years [3]. Apparently, the assumption that future flows and SLs are similar to past ones is not appropriate for reservoir sedimentation studies for the existing and planned dams at the Indus River [43, 44, 45, 37, 21, 46]. This can result in plausible over or under estimates of the trapped sediment volume for long term sediment modelling.

In assessing the temporal dynamics of SSLs and discharges, non-parametric tests are assumed to be more robust as compared to their parametric counterparts due to the fact that the sediment load data are not normally distributed on account of the highly nonlinear nature of the sediment transport processes. However, several non-parametric tests may also result in distinct estimates, which requires employing a suite of successful non-parametric methods and then quantifying their associated uncertainty to build more confidence in the results.

By analysing discharges and SSCs at two different sites over the past 50 years, this study for the first time shows how changes in the flow patterns are affecting the sediment transport capacity of the UIB for the meltwater-dominated zone (up to the Partab Bridge site) and for the whole UIB (up to Besham Qila), which is additionally influenced by the summer monsoonal rainfall period. The gaps between intermittently sampled SSCs are filled using the wavelet transforms coupled with artificial neural networks (WA-ANNs). The temporal discharge and SSL dynamics are robustly assessed using a suite of three widely used non-parametric approaches, including, (1) the innovative trend analysis (ITA), which can analyse the trends in low, medium and high annual SSLs without requiring any assumptions, such as serial correlation, non-normality, sample numbers and others [47]; (2) the Mann-Kendall (MK) and the seasonal Kendall (SK) tests together with the Sen's slope method; the MK test detects a trend in a time series without requiring normally distributed input data [48, 49]; the Sen's slope method estimates its true slope, while SK analyses annual trends by removing the seasonal cycles in a time series; (3) a change point detection test, which reveals the changing tendency in the SSL series on monthly and annual scales [50, 51]; (4) mean monthly variations, which detect monthly changes based on differences from the (a) first and last decades, and (b) monthly

regression equations of the analysed records.

1.1.3 Reservoir sedimentation

A river basin conveys water, sediments, heat, chemical substances, biological inhabitants, etc. from the catchment to downstream flat lands, lakes, seas and oceans. The construction of an impounding structure across the river interrupts these fluxes, causing sediments to deposit upstream and lacking downstream, resulting in loss of water storage capacity [52]. The reservoir sedimentation process completes by filling water storing capacity with sediments. However, the reservoirs are non-renewable resources and their silting up not only has impacts on the river morphology but also diminishes the associated benefits.

On an average, the annual rate of decrease in the world's reservoirs' storage capacity is approximately 1%. This indicates that water supply is in crisis, largely due to increasing world population, non-sustainable development, use of water resources and the imminent threat associated with climate change [53, 54]. In Asia alone, 80% of the useful storage capacity for hydropower production will be lost by 2035, while 70% of the storage volume used for irrigation will be lost to sedimentation by 2025 [52]. Pakistan, where no new large storage dam has been constructed since the Tarbela dam in 1974, is facing a similar situation. Being a water stressed country amongst the top ten most climate-affected countries [55, 56], Pakistan has a total water storage capacity of only 30 days (equal to 10% of the annual available water), which has been depleting due to a heavy sedimentation transported through the Indus river system from the young Hindukush-Karakoram-Himalaya (HKH) ranges [45]. The decrease in water supply from reservoirs such as Tarbela will affect millions of people who depend on the water supply and may lead to internal migration and severe geopolitical crises [20, 46]. Therefore, it is not only necessary to operate the existing water storage capacities efficiently but also to construct reservoirs that trap less sediments - especially in a scenario where reservoirs are the key infrastructure in mitigating the effects of climate change by their capacity to store and regulate water supply since the expected increase for the hydrologic variability will demand more water regulation capacity [52]. In addition, optimizing reservoir sedimentation will require new sediment load (SL) estimation techniques, as conventional methods are no longer adequate or reliable.

The Tarbela dam is used as a standard for the designing of planned hydraulic structures in the Upper Indus Basin (UIB). In particular, the development of numerical models for reservoir sedimentation studies [57] and designing of sediment routing facilities (invert

level of low level outlets, bypass tunnels or location of power tunnels intakes). In the previous studies only 1D numerical models (HEC-RAS, HEC6-KC, RESSASS) have been used for Tarbela and other planned structures in UIB, due to their simplicity and lower computational time [58, 15, 6, 1, 59]. A 1D model can be used in simple topography to assess an average sediment deposition or erosion only at cross section and the life of the reservoirs. The sediment boundary conditions in these models were based on sediment rating curve estimates. However, the SL boundary conditions based on sediment rating curve estimates can lead to a false conclusion. On the other hand, designers (in detailed design stage) also need a more accurate estimate of sediment concentrations with regard to different outlets, tunnels, etc., (and at different locations), which enables them to optimize sedimentation related facilities [60]. A 2D model with more accurate boundary conditions can deliver this information in both simple and complex topographies anywhere in the domain, which makes them suitable for Tarbela and other similar existing and planned hydraulic structures.

For SL estimation, WA-ANNs have performed well due to their ability to adjust for the hysteresis phenomena by decomposing the data time series in the time-frequency domain and revealing the information from a given data scenario [26]. However, there is a research gap in the literature with respect to reducing the uncertainty factor (contributing to accumulation of sediments in reservoirs) using WA-ANN estimated sediment loads (SLs) as model of boundary conditions. Apart from that the computation time of 2D models for simulating large systems such as the Tarbela dam, with hundreds of thousands mesh elements, is also very high. To address these research gaps, a TELEMAC-SISYPHE 2D open source model [61, 62] was modified and employed for the study. The modification increased the stability and flexibility of the TELEMAC-SISYPHE system by solving the fractional distribution of sediment particles equal to 100% [63]. In order to include all fractions of particular sizes class in the morphodynamic calculation process, the SISYPHE code was also updated. The wet-dry problem of the mesh was solved by specifying a 1 cm water depth in the whole domain and no morphodynamic calculations for a water depth below 1 cm. The 2D model is suitable for shallow waters such as in the Tarbela dam, where, due to high ratio water depth (20 m to 150 m) to river width (500 m to 5.3 km), vertical variations of flow and sediment concentration are very small compared to that in the horizontal direction. Calibration is the process of setting the parameters of the model to ensure that the calculated values agree with the measured values. The validation process demonstrates whether the predictions of the calibrated model agree with the observed data set that is different from the data used in the calibration process. Therefore, the model was calibrated using hydrological and morphological data of the

Besham Qila and Tarbela dam from 1983 (first comprehensive survey after its construction in 1974) to 1985, while the data from 1990 was used for the validation process. The calibration period of two years covers both (dry and wet) hydrological variations of the river. For example, 1984, with a flow volume of 83.8 billion m^3 (BCM) and SL of 209.6 million tons (Mt) was among highest peak flow/SL year from 1969-2008, whereas 1985 has a lower flow/SL than corresponding averages. Similarly, the validation period of five years (1986-1990) also covers both dry and wet periods [4]. The computational time for hydrodynamic calibration was reduced using an automatic calibration method, which updates roughness for each mesh node using backward error propagation. The boundary condition of the morphodynamic model (in cascade modelling) was modified based on [3] studies where (due to the strong hysteresis phenomena) daily SL series was more accurately reconstructed from non-continuous suspended sediment (SSC) samples using WA-ANN.

1.1.4 Need for research

The modelling of reservoir sedimentation is widely influenced by a correct representation of sediment load (SL) boundary conditions, reservoir geometry, and coefficients in the empirical formulae [64, 5]. A correct representation of SL boundary conditions requires a clear understanding of a wide variety of erosional, depositional and transport processes over a varying spatio-temporal scale [19]. However, studies in this direction so far have only been conducted for relatively small catchments ranges from hundred hectares to a few hundred square kilometres [30]. Sediment load estimations for large river basins require adjustment of hysteresis phenomenon and hydrological variations in the modelling process [3]. As per available literature, no study has been done in this direction, which contrast to many studies on flow trends [43, 44, 45, 37, 21, 46] hinder sediment load trends (due to lake of accurate load estimation) as well. Consequently, designers and engineers only have the choice to set SL boundary conditions using conventional sediment rating curves along-with re-use of the sediment rating curve estimate in predictions [58, 15, 6, 1, 59].

Another aspect in modelling of reservoir sedimentation is related to selection of numerical models, where designers need more accurate estimate of sediment concentration with regards to different outlets, tunnels, etc., which enables them to optimise sedimentation related facilities. There was a need to develop a model with more accurate sediment load boundary conditions, which can deliver this information (in both simple and complex topographies) anywhere in the domain and can be used for reservoir sedimentation studies for the Indus River.

1.2   Study area

The Indus River is one of the largest rivers in south Asia, with a total length of 2,880 km and a drainage area of 912,000 km^2 extending across portions of the Pakistan, India, China and Afghanistan. The drainage area of the Indus River is divided into upper and lower parts, typically at the Besham Qila discharge gauge station or around 65 km downstream at, so far, it's only reservoir, Tarbela, which is one of the largest earth-filled dams in the world (Fig. 1.1). The Upper Indus Basin upstream of the Tarbela dam is 1,125 km long with a drainage area of 219,830 km^2. To help in regulating the seasonal flow both for irrigation and power generation the dam was constructed in 1974 at the Indus River. The dam supplies 50% of the total irrigation releases and 40% of the total energy production in Pakistan.
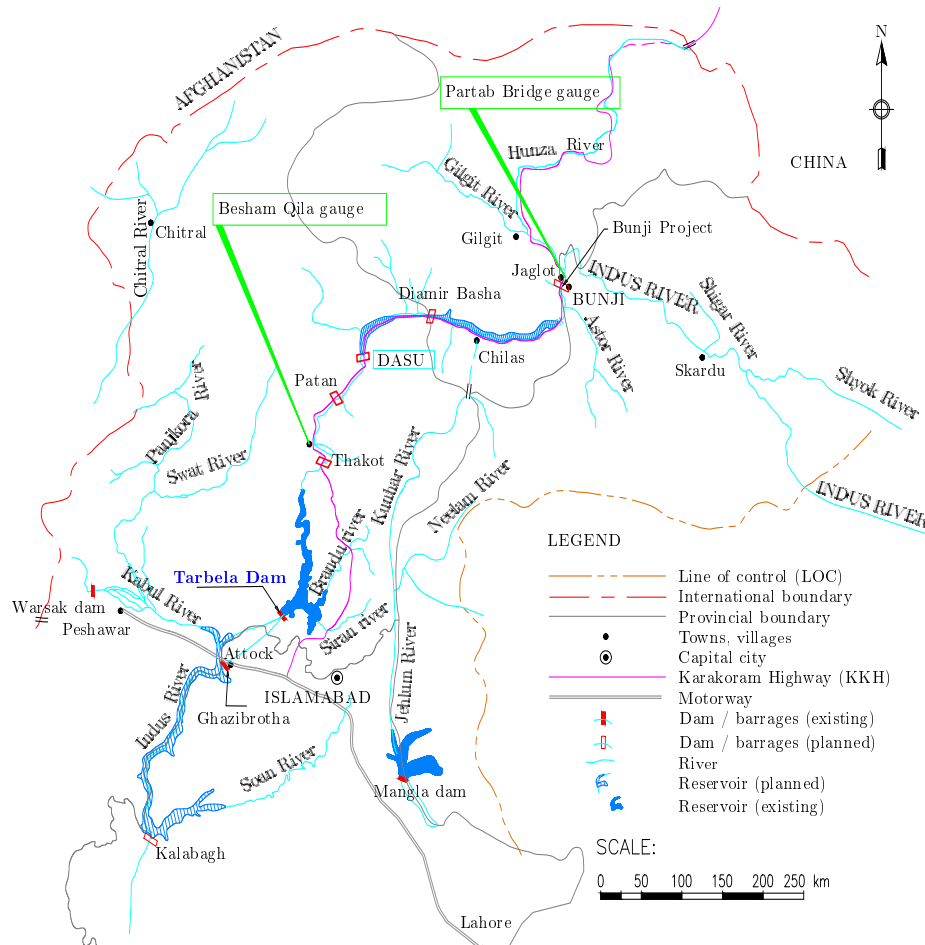
Figure 1.1: Location map of the study area. Modified from [6].

The Tarbela reservoir is embanked by three dams, the main embankment has a length of 2,750 m and height of 143 m. The reservoir had an initial water storage capacity of 11.6

billion m^3 (BCM) with a reservoir length extending to approximately 80 km. The outlet works consist of four tunnels cut through the right abutment of the main dam plus a fifth tunnel between the main dam and the spillways on the left bank. The total installed capacity of the dam is currently at 4,500 MW, 83% more than it was originally envisaged in the initial design, with several turbines installed on tunnels 1-4 (Fig. 1.2). Recently a new scheme had been installed on tunnel 4 which increased the power generation capacity by 1,410 MW.

Sedimentation at Tarbela dam has been a concern for a number of years due to very high supply of sediments from the Upper Indus River, i.e. approximately 160-200 Mt/yr. This is largely due to the erosion effect of the glaciers that supply much of the flow. The Indus basin upstream of the Tarbela dam has an area of 169,650 km^2 (Fig. 1.1). Over 90% lies between the great Karakoram and the Himalaya ranges. The snowmelt waters from this region contributes to the major part of the annual flow reaching into the reservoir. The remainder of the basin lying immediately upstream of the dam (Fig. 1.1) is subject to monsoon rainfall primarily during the months of July-September. Peak flows due to snowmelt can be as high as 5,660 m^3/s to 11,300 m^3/s with an additional rainfall contribution typically reaching a maximum of 5,660 m^3/s. The average annual inflow to Tarbela reservoir is 81 BCM [65].

[3] showed that 1969-2008 annual sediment inflows in the dam vary between 92-270 MT, which reduced the water storage capacity by 35% (Fig. 1.2). The decrease in storage is a concern as it may result in reduction of irrigation releases and power supply. In addition, the impact of delta created by the sediment deposits approaching towards the main dam may also block the power intakes. As the storage capacity of the reservoir reduces, more sediment will pass through the intakes. A major concern is the amount and representative sizes of the sediment that may pass through the turbines. The problems may be aggravated by the instability of the downstream sloping face of the delta [14] and the occurrence of an earthquake [65].

1.3 Research objectives

The overall objective of this study was to develop a set of models for a more accurate reservoir sedimentation and apply it to the Tarbela dam in the Upper Indus Basin (UIB). The UIB represents a unique topography with high mountains of the Himalayas, Karako-ram, Hindukush, with a huge catchment area that still exists in its natural conditions
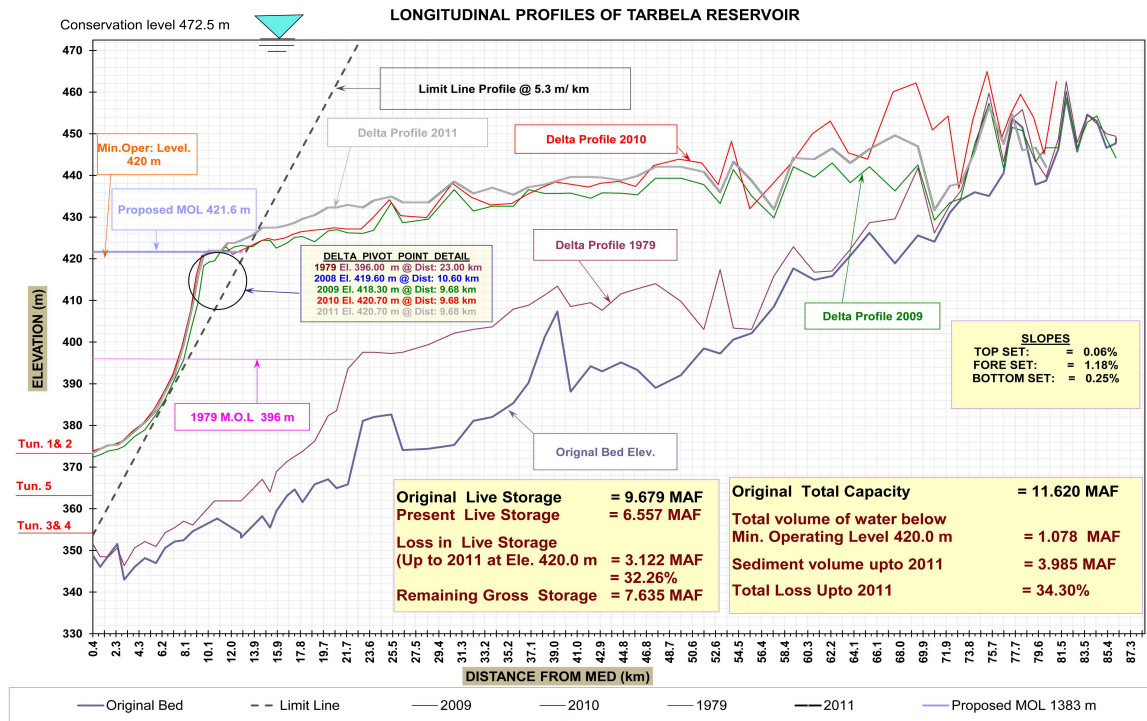
Figure 1.2: Sediment delta development in the Tarbela dam [5]

without any major human activities and has not received much attention in the past. In the view of serious energy and water crises in Pakistan where 14,000 MW hydropower projects and many water storage reservoirs are planned, more accurate reservoir sedimentation model seems to be timely and desirable. In order to address the relevant research needs and gaps in reservoir sedimentation for large scale drainage basin raised in sections 1.1.4 and learned in my preliminary studies [1, 2], the following were the sequential aims of this study:

- Estimation of more accurate sediment load in the Upper Indus River by filling the gaps between intermittent suspended sediment load samples.

- Asses spatio-temporal trends between sediment load and discharges using more accurate estimate.

- To develop cascade modelling approach for sediment management in reservoir by setting more accurate sediment load boundary conditions along-with hydrodynamic calibration using back error propagation.

1.4 Research methodology

Modelling reservoir sedimentation requires a clear understanding of the dynamics of sediment transport processes at the Upper Indus River. To gain this knowledge, the study has utilized multiple data types and sources includes the hydrological and sediment records, annual reservoir inspection surveys, literature about the Indus River, and recent published work on the reservoir sedimentation [1, 2, 3, 4, 5]. It is argued that occasionally collected suspended sediment load data series can be used in WA-ANN models for reconstruction of missing data for large rivers such as the Indus. The future sediment loads in absence of any upstream hydraulic structures can be estimated using projections of corresponding future discharges. Projections of both sediment loads and discharges can be used for the prediction of erosion and deposition processes in the reservoirs.

The methodological framework of numerical modelling of sediment transport in the Upper Indus River presented in this study consists of five distinct steps.

(I) Identification of the research gaps in estimation of reservoir sedimentation using conventional methods

(II) Preliminary investigation of the suitability of artificial neural networks (ANNs) for estimation of sediment yield

(III) Development of wavelet-ANN models for the estimation of sediment loads in the Upper Indus Basin, particularly at Besham Qila gauge station of the Tarbela dam

(IV) Detection of trends in sediment loads at the upper Indus River

(V) Carrying out 2D reservoir sedimentation calculations based on wavelet-ANN estimated sediment loads, and trends in the predictions of sediment delta development in the Tarbela dam

1.5   Thesis structure and authors contribution

The thesis is based on the series of five documents published in context with numerical modelling of reservoir sedimentation studies for Pakistani reservoirs conducted in the Chair of Hydraulic and Water Resources Engineering, Technical University of Munich. A brief summary of each publication along-with the division of work between the authors is given below.

1.5.1   1-D numerical modelling of Dasu Hydropower Project

The main findings of the publication "Application of a 1-D numerical model for sediment management in Dasu Hydropower Project" are discussed briefly. The study was published in the proceedings of the *14th International Conference on Environmental Science and Technology* in 2015 [1].

Main results: The first study of the PhD project was conducted to evaluate the suitability of flushing types (pressurized or free flow) for 4,320 MW planned Dasu Hydropower Project on the Indus River using 1D HEC-RAS model. In the modelling process two sediment rating curves were used to estimate sediment load (SL) for boundary conditions. To predict the reservoir life for 2027-2066, the past data (estimated SL and flow discharges) from 1969-2008 was repeated in future, without any modification. The estimated reservoir life was validated using [66] curves.

The modelling results reveal that free flow flushing is suitable for the project and can increase the reservoir life from 15 years to a minimum of 40 years. As sediment rating curve method has high variations in SL estimation due to transport processes related to hysteresis phenomenon and hydrological variations, the modelling boundary conditions and subsequent predictions also contain high uncertainties. In addition, the assumption that the future flow and SLs are similar to the past ones and can be used as boundary conditions in modelling of reservoir sedimentation [67, 57, 58, 15, 6, 33, 59], particularly under climate change [20, 36, 37, 38, 21], needs to be investigated. Although 1D modelling is sufficient for pre-feasibility studies, to have a reliable design of low level outlets and flushing tunnels in detailed/construction design, a 2D modelling is recommended for having the information of sediment concentrations or accumulation of sediments with regards to different outlets.

Authors' contribution: The model was developed by Sardar Ateeq Ur Rehman under guidance of Minh Duc Bui and Peter Rutschmann. Idea and concept of the paper were formulated by Sardar Ateeq Ur Rehman and discussed with Zeeshan Riaz. Sardar Ateeq Ur Rehman prepared the manuscript with the support of Minh Duc Bui.

1.5.2   Estimation of sediment yield using artificial neural networks (ANN)

The main findings of the publication "Estimation of Sediment Yield for Dasu Hydropower Project Using Artificial Neural Networks" are discussed briefly. The study was published in the proceedings of the 18th *Wasserbau-Symposium* in 2016 [2]. The main findings are summarized below.

Main results: In order to find more accurate sediment load (SL) estimation technique for reconstruction of missing data for the gauge stations at the Indus River, initially (in this publication) the output of the 1D sediment model of Dasu Hydropower Project [1] using artificial neural networks (ANNs) was tested. The inputs of ANNs (2027-2066) were same as of the 1D HEC-RAS model, i.e. daily inflows to the planned dam (m^3/day), daily outflows from the dam (m^3/day). The target of the ANNs was the output of the HEC-RAS, i.e. volume of sediment retained (m^3/day).

Due to the ANNs learning abilities and extraction of the nonlinear relationship from the data without requiring an in depth knowledge of the physics occurring within the system [25], the modelling results showed that the ANNs can accurately model the patterns of sediment deposits in the reservoir and flushing volume out of the reservoir on a daily time scale. In addition, ANNs also well captured the dry and wet hydrological cycles in the modelling process.

The ANN models outputs close to the HEC-RAS estimation motivated us to use these models (instead of sediment rating curves) to reconstruct occasionally measured suspended sediment concentration (SSC) samples (collected at gauge stations on the Indus River) on a daily time scale for trend detection (under sediment load variability scenarios) and implementation of more accurate sediment load boundary conditions (in predictions) for numerical modelling of the Tarbela reservoir.

Authors' contribution: The ANN architectures were created by Sardar Ateeq Ur Rehman under guidance of Minh Duc Bui, and Peter Rutschmann. Idea and concept of the paper were formulated by Sardar Ateeq Ur Rehman and discussed with Minh Duc Bui. Zeeshan Riaz helped for the data collection and raw data interpretation. Sardar Ateeq Ur Rehman prepared the manuscript with the support of Minh Duc Bui.

1.5.3 Development of wavelet-ANN for suspended sediment load

The publication "Development of a wavelet-ANN model for estimating suspended sediment load in the upper Indus River" [3] was submitted in *International Journal of River Basin Management* in 2017. The main findings of the publication are discussed below.

Main results: The accurate estimation of sediment load plays a vital role in the sediment management of existing and proposed reservoirs and run-of-the river hydropower schemes. However, the accurate estimation of sediment load is challenging under the influence of climate change and hysteresis phenomenon, where disproportional spatio-temporal trends between the sediment loads and flow discharges exist primary due to intra-annual shifts in flows at the Indus River. Based on the successful implementation of the ANN models for the estimation of sediment yield in the Dasu Hydropower Project [2], ANNs and conventionally used sediment rating curves (SRCs) were applied on occasionally collected suspended sediment concentration (SCC) samples for reconstruction of missing data of two gauge stations, Besham Qila and Partab Bridge. The Besham Qila gauge station is used to measure inflow and sediment load for the Tarbela dam, while Partab Bridge represents the whole glacier and snow melt catchment of the Upper Indus River. The SSC sampling frequency at both gauge stations were 22% and 17% of daily sampling, respectively.

The results showed a better performance of ANN models over the conventional sediment rating curves. However, the ANN was unable to adjust hysteresis phenomenon due to involved complexity related to the load availability and seasons or months of occurrence. As wavelet transform (WA) has the ability to adjust hysteresis phenomenon by splitting the information into time and frequency domain, more accurately estimate of SL on a daily time scale by coupling WA with ANNs can be obtained.

The results obtained using WA-ANN for daily SSL were NSE=0.85 compared to ANN NSE=0.81, and sediment rating curve NSE=0.48, respectively. The mean deviations in estimation (from 1696-2008) using these models were 13%, 18% and 36%, respectively. In addition WA-ANN and sediment rating curve results with sediments deposited in the Tarbela dam were also compared. The WA-ANN estimate for the mean annual mass deposited in the dam deviates only 12% from the hydrographic survey, compare to 43% deviation using sediment rating curve. In predicting cumulative deposits using sediment rating curve they were as high as 40% for the Tarbela dam over a mere 26 years. However, the variation over the same period were only at 12% using WA-ANN.

Based on the findings, the WA-ANN models can be used to more accurately detect the trends in sediment loads and can also contribute to the development of sediment management strategies for existing, under construction, and planned water related structures by setting more accurate boundary conditions.

Authors' contribution: Artificial neural networks (ANNS) and wavelet transform coupled with ANNs were developed and evaluated by Sardar Ateeq Ur Rehman under the guidance of Minh Duc Bui and Peter Rutschmann. Idea and concept of the article were formulated by Sardar Ateeq Ur Rehman with the help of Minh Duc Bui. Sardar Ateeq Ur Rehman prepared the manuscript with the support of Minh Duc Bui and Peter Rutschmann.

1.5.4 Detection of sediment load trends

In the following, the main findings of the publication "Variability and Trend Detection in the Sediment Load of the Upper Indus River" [4] are briefly summarized. The article was published in *Water* in 2018.

Main results: The fourth study was conducted to evaluate whether the past sediment load (SL) data without modifications can be used as sediment load boundary conditions for predictions of sedimentation in reservoirs. To do so, the temporal dynamics of suspended sediment loads (SSLs) and discharges were analyzed using suit of three non-parametric trend tests (i.e. Innovative trend test, Mann-Kendall test, and change point detection test) while the (trend) slope was identified using Sen's slope estimator. For the study WA-ANN reconstructed suspended sediment load series [3] and daily measured discharge flows for the meltwater-dominated zone up to the Partab Bridge and the whole Upper Indus Basin up to Besham Qila (used as gauge station for the Tarbela dam), which is additionally influence by monsoonal rainfall, were used.

The current study results show significant disproportional spatio-temporal trends between SSLs and discharges at both gauge stations caused primarily by intra-annual shifts in flows. The results also showed a substantial deposition of sediments in the river channel between Partab Bridge and Besham Qila gauge stations. This deposition process has also been causing a long-term decrease in suspended sediment loads at the Tarbela dam. In addition, the trends are also opposite to the flow volumes which have been showing a long-term increasing trends. Therefore, this disproportional behaviour and the significant trends strongly disconfirm the hypothesis that future inflows and SSLs are similar to the previous ones for reservoir sedimentation studies for the Upper Indus River.

Authors' contribution: Sardar Ateeq-Ur-Rehman designed the study, processed and analyzed the data, interpreted the results and wrote the paper. Minh Duc Bui and Peter Rutschmann contributed to the model development stage with theoretical considerations and practical guidance, assisted in the interpretations and integration of the results and helped in preparation of this paper with proof reading and corrections.

1.5.5   An innovative approach for modelling reservoir sedimentation

In the following, the main findings of the publication "An Innovative Approach to minimizing uncertainty in sediment load boundary conditions for Modelling Sedimentation in Reservoirs" [5] are briefly summarized. The article was published in *Water* in 2018.

Main results: The fifth study in this context of numerical modelling of the Tarbela dam was carried out using the cascade modelling approach, where more accurate WA-ANN reconstructed suspended sediment loads (SSLs) [3] were used as boundary condition in TELEMAC 2D model. In presence of statistically significant trends in flow discharges and SSLs [4], future flow discharges (2016-2030) calculated by [24] using hydrological model were used as boundary conditions. The corresponding future SSLs were estimated using WA-ANN model. The reservoir water levels from 2015-2030 were kept same as 2000-2015. To calibrate the model for hydro-morphodynamic calculations, an automatic hydrodynamic calibration algorithm was applied. This algorithm specifies bed roughness for each mesh node and subsequently enhance the performance of morphodynamic calculations by providing better hydrodynamic variables and total bed roughness for the calculations of sediment erosion, transport and deposit in the flow area.

The modelling results showed that the well calibration of hydrodynamic model using automatic calibration algorithm (which specified bed roughness for each mesh node) along-with more accurate sediment load boundary conditions (which better represent hysteresis phenomenon and hydrological variations) enabled the successive morphodynamic model to accurately predict the bed level changes in the Tarbela dam. The well calibrated hydrodynamic model has R^2=0.969, NSE=0.966, and morphodynamic model has R^2=0.97, and NSE=0.96. The model validated the sediment deposits in the Tarbela with R^2 =0.96 and NSE=0.95. Although the morphodynamic calculations were close to the measurement, the model also approximately 1% over-predicted sediment deposits due to omission of low flow months when water level is released form the dam. Interestingly, a desynchronization between the glacier melts and monsoonal rainfall due to warmer climate can cause a significant (up to 17%) decrease in sediment supply to the Tarbela dam, which can stabilize the delta development in the dam. Although the study findings contradict the previous clams of high reservoir sedimentation under climate change [52], the silting up rate of the Tarbela reservoir will be slower due to the desynchronization.

Authors' contribution: Sardar Ateeq-Ur-Rehman designed the study, processed and analysed the data, interpreted the results, and wrote the paper. Shabeh ul Hasson provided the hydrological model for future flow discharge predictions. Minh Duc Bui and Peter Rutschmann contributed to the model development stage with theoretical considerations and practical guidance, assisted in the interpretations and integration of the results, and helped in preparation of this paper with proof reading and corrections.

Chapter 2

Application of a 1D Numerical Model for Sediment Management in Dasu Hydropower Project

This chapter is published as:

Abstract: A one dimensional numerical model for the sediment study of the Dasu hydropower project (HPP), before constructing the Bhasha Diamer dam, is presented in this paper. Several formulae were used for sediment simulations under no flushing condition, maintaining reservoir water level at a full supply level (FSL) of 950 m asl. The preliminary assessment for both flushing methods, pressure flow flushing and free flow flushing was carried out. The validity of the model was checked with the Brune´s formula. The simulation result showed that without flushing, low level outlets and power intakes would be filled with the sediments between, 20-25 years. It was also observed that free low flushing, after minimum 15 years of dam commissioning, is more efficient compared to pressure flow flushing. It is recommended that without construction on any upstream reservoir, sedimentation is a severe problem for the Dasu HPP or any

downstream run-of-river power plant.

2.1 Introduction

Sedimentation is one of the most challenging carry-over problems in hydraulic engineering [68]. On a worldwide scale, dam reservoirs silt up at a rate of about 1% of their useful storage volume every year. With the same trend 25% of world reservoirs will be abolished in the coming 25 to 50 years [69]. Reservoir sedimentation causes various severe problems such as (1) decrease of active volume leading to both loss of energy production and water available for water supply and irrigation; (2) decrease of the retention volume in case of flood events; (3) endangerment of operating safety due to blockage of the outlet structures; and (4) increased turbine abrasion due to increasing specific suspended load concentration [70]. Similarly, Tarbela and Mangla reservoirs in Pakistan, are losing their storage capacities at the rate of 0.132 billion m^3/yr and 0.038 billion m^3/yr, respectively [71]. Same may happen with the Dasu hydroelectric power project (Pakistan) which has reservoir life of only 30 years, without flushing, due to sedimentation, along with 40% reduction in power generation due to ingress of sediments into the power inlets [6]. Warsak dam (Pakistan) also silted up just after thirty years of operation [72]. It is not possible to completely overcome the sedimentation problem but it can be reduced by flushing the reservoir regularly [73]. Venting of turbidity currents, efficiency also very much influenced by timing of gate opening and there arrangement in the dam body [74].

The sedimentation problem is more sever for Pakistan. The country is losing its existing storage capacities of the reservoirs due to sedimentation. This problem is affecting not only the water availability for agriculture but also the power generation in which it already faces crisis. The aim of this paper is to simulate the sedimentation patterns in the reservoir Dasu (1) without flushing, (2) under pressure flow flushing and free flow flushing, and (3) impact of sedimentation on downstream (d/s) run-of-river hydropower projects without any upstream (u/s) reservoir.

2.2 Site description

The Dasu Hydropower Project is located in the Indus River Basin, about 350 km north from the capital Islamabad, Pakistan. The proposed damsite is also 74 km downstream of the Diamer Bhasha damsite and 241 km upstream of the Tarbela dam, along the same river. The elevation at the damsite is 764 m asl. There are several tributaries between

the Bhasha dam and the Dasu HHP and of these, the prominent ones are the Daral River, Tangir River and Kandia River. These tributaries generally bring snowmelt flow to the Indus River with some fine to coarse sand. The catchment of the Indus River at the damsite is 158,800 km^2. The mean annual runoff at the damsite is 2,116 m^3/s and the lowest flow is 291 m^3/s. Total annual flows at Dasu is 66.7 billion m^3 and 90% of these flows come from melting of snow and glaciers. Hence nearly 80% of flows occur in summer months of June to September while October to May is known as the low flow season. Gross storage capacity of reservoir at elevation of 950 m asl is about 1.41 billion m^3 and operational storage capacity is 0.82 billion m^3.

2.3   Methodology

2.3.1   HEC-RAS program system

The Hydrologic Engineering Centre-River Analysis System (HEC-RAS) is a one-dimensional software, which is designed to perform steady flow water surface profile computations through natural rivers and full networks of natural and engineered channels, unsteady flow simulations, movable boundary sediment transport computations, and water quality analysis. A key element is that all these components will use a common geometric data representation and hydraulic computation routines. Sediment transport simulations are based on the calculations of one-dimensional movable material from the river bed causing scour or deposition over a certain modeling period of time. Generally, sediment transport through rivers, streams and channels occurs through two modes which depend on parameters such as the particle size, water velocity, and bed slope. The two modes are known as bed load and suspended load. The basic principle of evaluating sediment transport capacity within HEC-RAS is by computing sediment capacity associated with each cross section as a control volume and for all grain sizes in that particular case. For making such calculations, HEC-RAS requires boundary conditions for each type of data. These boundary conditions are required to obtain the solution to the set of differential equations describing the problem over the domain of interest. In HEC-RAS, there are several boundary conditions available for steady flow and sediments analysis computations. Boundary conditions can be either external specified at the ends of the network system (upstream or downstream) or internal used for connections to junctions. The background to the computational methods and equations used for modeling sediment transport can be found in [75].

2.3.2   Model setup

Based on observed data, a rating curve of suspended sediment load per day Q_s (tons/day) was developed (Eq. 2.1 and 2.2), and used as the upper boundary condition of the Dasu reservoir.

$$Q_s = 4.99 \times 10^{-14} Q^4, \text{ for } Q < 448 m^3/s \qquad 2.1$$

$$Q_s = 7.61 \times 10^{-8} Q^{2.52}, \text{ for } Q > 448 m^3/s \qquad 2.2$$

Where Q_s = suspended sediment load with respect to flow discharge Q. Furthermore, bed load was also added as 10% of the suspended load. The sampling for the river bed material within the Dasu reservoir was carried out (Tab. 2.1) and used as initial grain size distribution in the model.

Table 2.1: Gradation of river bed material in Indus River.

Size (mm)	3.5 km d/s of damsite (%fine)	56 km u/s of damsite at Shatial Bridge (%finer)
0.075	2.9	2.7
0.16	10.2	10.4
0.30	51.6	52.6
0.60	99.5	100
1.20	100	-

Daily inflow discharge over 47 years from 1962 to 2008 were given as upper boundary conditions and reservoir water levels (RWL) as downstream boundary conditions on daily basis. For the sediment simulation and management study in the Tarbela dam in 1998 [65], the Ackers-White transport formula has been intensively adopted in view of much sand fraction than finer materials. [76] also suggested the use of the Ackers-White formula, for total load transport capacity of sand-sized fraction is appropriate tool. Hence, in the present study this formula is used again.

In general pressurized and free flow flushing are used for venting of sediments from the dam. Hydraulic features of pressure flushing includes (i) less velocity in reservoir and less tractive force along the river bed due to high water depth (ii) development of scour cone around inlet of the Low Level Outlet (LLO) due to rapid flow towards LLO inlet in radial direction and (iii) higher trapped sediment in the reservoir due to less flushing efficiency. Reversely hydraulic features of free flow flushing includes (i) higher velocity in the reservoir and higher tractive force along river bed due to shallow water depth and (ii)

less trapped sediment in the reservoir due to high flushing efficiency. In order to evaluate applicability of both flushing methods to the Dasu reservoir, the flushing simulation by using HEC-RAS is carried out.

2.4 Results and discussions

To assess and clarify the accuracy of transport formula selected, the preliminary simulation sedimentation study was carried out by using the Ackers-White, Laursen-Copeland and Yang formulas under no flushing conditions, maintaining RWL at a FSL of 950 m asl. Up-to 17 years, there was not much difference in the results of both formulas, such as reduction of storage volume, annual sediment inflow and outflow, trapped efficiency and accumulated sediment volume in the reservoir. However, after 17 years the accumulated sediment volumes by the Laursen-Copeland formula and the Yang formula showed the higher amounts than Ackers-White due to change of profile delta. It was also justified that the Ackers-White formula gives safer results than that of the Laursen-Copeland and Yang's formulas. Fig. 2.1 shows the calculated results of annual sediment inflow, outflow and trapped sediment in the reservoir during no flushing. It was observed that the trapped sediment volume using the HEC-RAS model (58% of sediment inflow) was well coincided with the trap efficiency obtained by Brune's curve (61%).
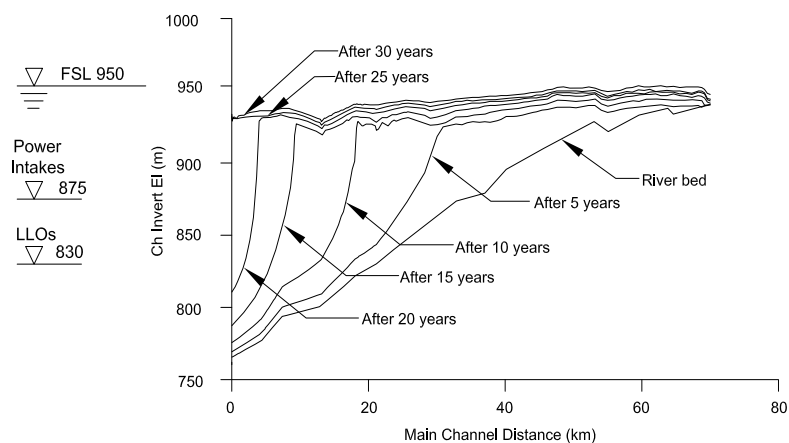
Figure 2.1: Sediment profile by maintaining RWL at FWL (no flushing).

In order to grasp sedimentation in the reservoir for certain operation period, the scour and deposition were analyzed using computer simulation basis that the reservoir water level was maintained at a FSL of 950 m asl. without flushing operation. The results suggested the following points (Fig. 2.1): (1) From the longitudinal profiles of

sedimentation delta in each 5-year interval, it was expected that the inlets for LLOs and power intake would be filled with the sediment between 20-25 years. (2) At 15 years elapsed period after Commercial Operation Date (COD) of Phase-1, the foot of sedimentation delta was developed up to 780 m asl. at about 9 km upstream of the dam and its top was accumulated up to 910 m asl. Satisfying the stable slope of 5.3 m/km shown in the guideline of the Tarbela reservoir. (3) It was likely that the sedimentation delta will rapidly approach to the dam exceeding the stable slope. This might bring the sudden collapse of delta and will result in the blockage of LLO inlet. The inlet facilities for LLO and power intake might be filled with the sediment within 25 years after commissioning of Phase-1.

Every year flushing since impounding of reservoir in the month of June at low level outlets EL. 830 m asl. and LLOs discharge capacity of 6,600 m^3/s under free flow flushing suggests the following results (Fig. 2.2):

1. In case that the one month flushing is started immediately after the impounding, the reservoir life is extended to 40 years.

2. Drawdown flushing in the month of June will allow filling of the reservoir immediately, after termination of flushing, in the following months of high flows during the monsoon season. Rapidly filling the reservoir in the following months will also provide greater opportunity of power generation in the rest monsoon period.
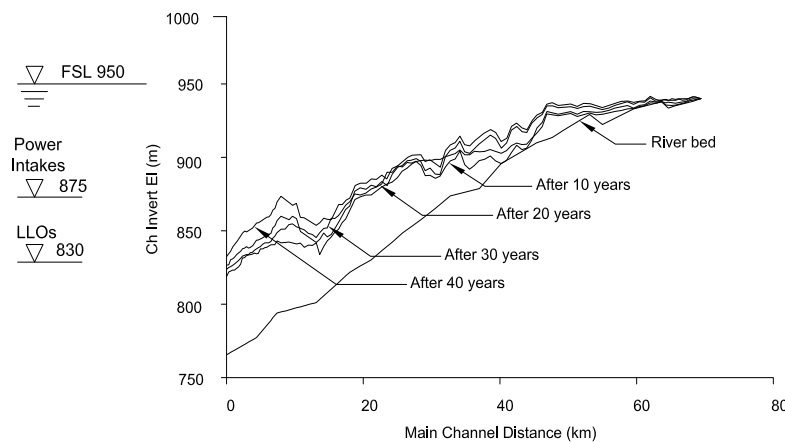
Figure 2.2: Sediment profile under free flow flushing.

The preliminary assessment for both flushing methods, pressure flow flushing and free flow flushing were checked and clarified by the tractive force and critical friction velocity

based on the backwater calculation. Under the pressure flow flushing having discharges varying from 1,000 to 6,000 m^3/s, maintaining RWL at FSL. 950 m asl., whole wash loads below 0.0625 mm were mobilized and trapped in the reservoir section over 15 km u/s of dam. Part of wash loads was expected to be flushed out through LLOs and turbine under pressure flow. The velocity in the reservoir was ranged from 0.02 to 0.14 m/s near the damsite. Under the free flow flushing having discharges of 6,000 m^3/s, and RWL at 853.92 m asl., the suspended loads with 0.2 to 0.6 mm were mobilized and trapped in the reservoir section over 15 km u/s of dam. Particles below 0.2 mm were flushed out through LLOs during flushing operations under the free flow. The velocity in the reservoir was ranged from 0.39 to 0.44 m/s near the damsite.

2.5   Conclusions

It is evident that the period of non-flushing operation for the Dasu reservoir should be limited to 15 years if it is at the status of "Pre-Bhasha". This operation would contribute not only for the maximization of annual energy during construction phases of the Dasu project but also for the mitigation of annual sediment inflow to the Tarbela reservoir and the extension of the reservoir life for the Tarbela project. If "Post-Bhasha" is achieved, the flushing operation is not required further than 30 years since the Bhasha dam has enough storage capacity. From the above initial flushing operation study, it is concluded that the free flow flushing is more appropriate and expected to show higher efficiency of sediment evacuation due to shallow water level near the dam. It is further concluded that an upstream reservoir is necessary for sustainable operation of run-of-river hydropower project on the Indus River in Pakistan.

Chapter 3

Estimation of Sediment Yield for Dasu Hydropower Project Using Artificial Neural Networks

This chapter is published as:

Abstract: Reservoir sedimentation of Dasu Hydropower Project (DHP) was analysed by developing three ANN architectures of data driven method. The inputs of the ANN model were daily data of the river inflow into the reservoir, river outflow from the reservoir and change in reservoir storage capacity, while the output of the model was the daily amount of sediment retention in the reservoir ponding area. For ANN model inputs, hydrological data of forty years were used in this study (70% for training, 15% for validation, and remaining 15% for testing). The target of the model was estimated by using the HEC-RAS 1-D numerical model. The ANN architectures were created with the multilayer perceptron (MLP) using Marquardt Levenberg training method. In well performed ANN architectures, the transfer function in the hidden layers was 'logsig', while 'purelin' was used as transfer function in the output layer. Among well performed ANN architectures, ANN (4-14-1) performed well in the three layers neural network, ANN (4-8-10-1) performed well in the four layers neural network architecture while ANN (4-5-4-5-1)

performed well in the five layers neural network architecture. The results showed that the ANN models selected captured the process of reservoir sedimentation very well in both ways, daily volume of sediment deposition and daily volume of sediment venting out of the reservoir during wettest and driest hydrological cycles. The results also showed that with an increase the length of data set of shorter intervals, the efficiency of the model can be improved. It was also noticed that the length of artificial neural network did not affect the statistical performance of the model when employing short-interval observational data of long period. It was concluded that the artificial neural network is a good tool for the estimation of reservoir sedimentation in the Dasu Hydropower Project.

3.1   Introduction

The challenge of reservoir sedimentation is depleting per capita availability of water in Pakistan. That is not only affecting agriculture crop water requirement only but also power generation, which it's already facing severe crisis. Per capita water availability in Pakistan has decreased from 5,000 in 1951 to 1,100 cubic meter per annum in 2006. The increasing gap between water supply and demand has led to severe water shortage, in almost all sectors, [77]. The present facts are just above the level of 1,000 mtextsuperscript3 per capita per annum [78], the internationally recognized water scarcity rate. In Pakistan, water shortfall between requirement and availability will be 12% in 2025 [79]. At the moment, the country has only 30 days water storage capacity [80]. Around 92% of the country's area is classified as semi-arid to arid, facing extreme shortage of precipitation [81]. Under this scenario, the construction of mega multi-purpose storage dams is assuming highest priority to sustain irrigated agriculture which is the backbone of Pakistan's economy and to meet the growing power need of the country [82].

Prediction of sedimentation is not an easy task due to its high complexity and non-linearity. In recent past, the artificial neural network (ANN) technique, is gaining popularity among the hydrologic community due to its ability to identify a relationship from given patterns to solve large scale complex problems such as pattern recognition, non-linear modelling and classification [83, 84]. ANN provided many promising results in the field of hydraulic and civil engineering. For example its working style like human nervous system, to learn from data samples presented, proved it a highly tolerated against data simple errors [85]. Compared to regression analysis with conventional stochastic dynamic programming, ANN showed superiority to tackle the nonlinearity problems as well as superior simulation model in deriving the operating policy for reservoir systems

[86]. [87] made a comparison between suspended sediment rating curves and artificial neural network (ANN) for EI Kebir catchment in Algeria. Daily water discharge and daily suspended sediment data from the gauging station of Ain Assel were used as input and output parameter. The model was based on the cascade-forward and feed- forward back propagation using Levenberg-Marquardt and Bayesian regulation algorithms. It was found that ANN model efficiency to produce the daily sediment load and global annual sediment yield was the highest. [88] developed an artificial neural network (ANN) for reservoir sedimentation of Gobindsagar Reservoir at Bhakra Dam on Satluj River in India which is a tributary of Indus River Basin System. In the model, 32 years data of annual rainfall, annual inflow and annual capacity were used as input parameters. The pattern of sediment retained in the reservoir was well captured by the multi-layer perceptron (3-5-1) ANN model using back propagation algorithm with sigmoidal activation function. It was found that ANN estimated the reservoir sedimentation with better accuracy compared to conventional methods. [89] developed an artificial neural network to study the relationship between sediment yield and Indus river runoff during high flows for Tarbela Dam utilizing Besham Qila's gauge station data. In the three layers neural network with back propagation algorithm, weekly time series data of discharge and sediment load of 20 years was used as an input and output parameter, respectively. The correlation of 0.56 was found in observed and computed sediments for the ANN model. ANN model is also a very efficient tool for water level prediction especially when the duration of quick response components of individual events is less than 6 hours [90].

In the present study, an ANN model has been developed by using 40 years hydrological data for the estimation of sediment load at the under constructed Dasu Hydropower Project. The input parameters such as river discharge into the reservoir, outflows from reservoir and reservoir capacity were decided on the basis of their influence in sedimentation process and sediment load retained in the dam ponding area was considered as the output parameter.

3.2   Study area and methodology

Dasu dam is a gravity dam currently being constructed on the Indus River near Dasu town in Khyber Pakhtunkhwa province of Pakistan (Fig. 3.1). Its design discharge is of 2,670 m^3/s [6] and one of the series of hydropower development projects included in the vision programme developed by Water and Power Development Authority of Pakistan. In feasibility studies of Dasu HPP, it was decided to construct after completion of an

upstream Diamer Bhasha reservoir to provide regulated flows for energy generation and also to control downstream proposed projects reservoir sedimentation [57]. Later, a detailed design of the project was conducted without considering any upstream reservoir which will definitely cause huge sedimentation within Dasu reservoir storage area and may be a danger for dam components [1]. Catchment area of Indus River at the damsite is 158,800 km^2. Mean annual runoff at dam site is 2,116 m^3/s with lowest river flow of 291 m^3/s. Annual flow volume at Dasu dam site is 66.7 billion m^3, 90% of these flows are generated from melting snow and glaciers. Hence nearly 80% of flows occur in summer months from June to September while from October to May is known as the low flow season. Gross storage capacity of reservoir at elevation of 950 masl is about 1.41 billion m^3 and operational storage capacity is 0.82 billion m^3 [7] The project is going to be constructed with the help of World Bank funding and will operate under Water and Power Development Authority (WAPDA) Pakistan [7]. WAPDA is also controlling authority of Pakistan reservoirs, conduct reservoir thalweg surveys regularly to measure actual sediment deposited in the reservoirs. The Indus River originates from Tibetan plateau, to the North of Manasarowar Lake, at an elevation of about 5,500 masl. Operational Mete-Hydrological data stations along Indus River till Dasu site and nearby downstream are at Partab Bridge, Dasu Bridge, Kandia Bridge, Pattan, and Besham Qila.

3.2.1   Method

The ANN model developed by using simple mass balance equation for the estimation of sediment retained within the reservoir area;

$$\Delta s = q_{w(in)} - q_{w(out)} + q_{s(in)} - q_{s(out)} \qquad 3.1$$

$$\Delta s = q_{w(in)} - q_{w(out)} + q_{s(R)} \qquad 3.2$$

$$q_{s(R)} = \Delta s + q_{w(out)} - q_{w(in)} \qquad 3.3$$

$$\Delta s = s_t - s_{t-1} \qquad 3.4$$

where, Δs = change in reservoir capacity (m^3), $q_{w(in)}$ = water inflow into reservoir (m^3), $q_{w(out)}$ = water outflow from reservoir (m^3), $q_{s(in)}$ = sediment incoming in reservoir (m^3), $q_{s(out)}$ = sediment outgoing from reservoir (m^3), $q_{s(R)}$ = sediment retained in the reservoir

(m^3)
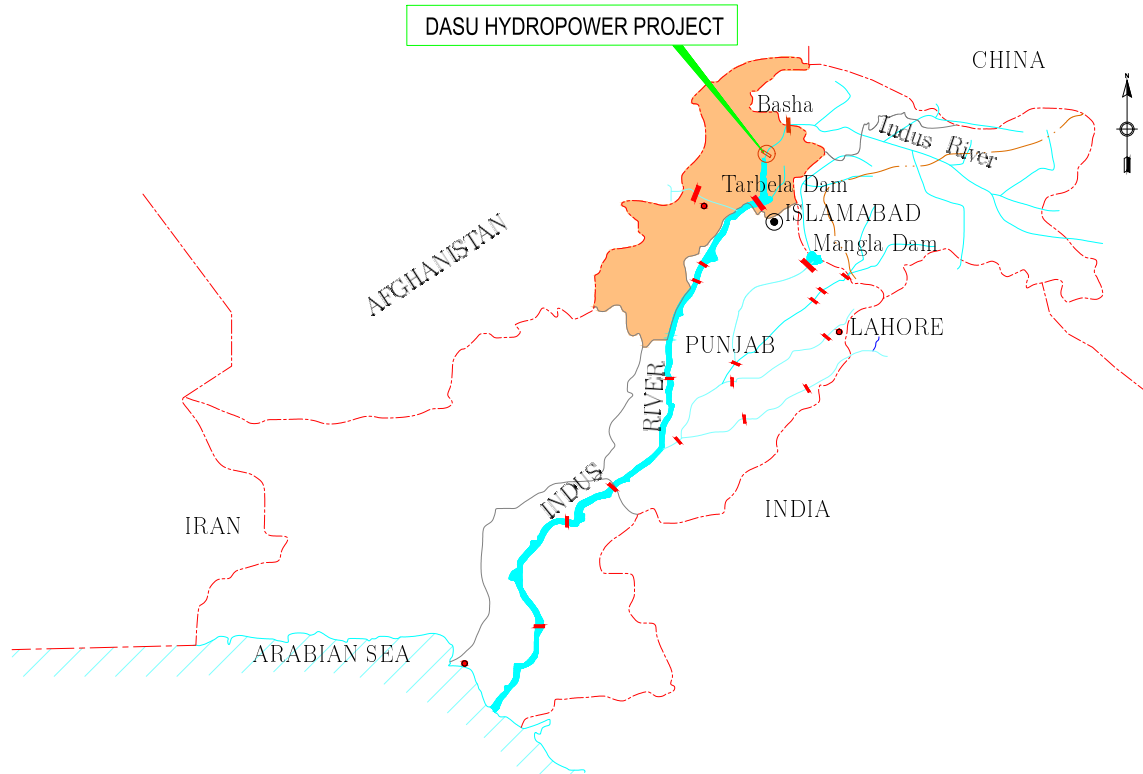
Figure 3.1: A Location map of the study area, Dasu Hydropower Project on Indus River, Pakistan [7]

Assuming similar hydro-metrological conditions, daily river inflow at dam site from 1969-2008 was used as input parameter in the model for the period 2027-2066. In the inflow data, the moderate hydrological season was 1999 with peak daily discharge of 7.07×10^8 m^3/day (Fig. 3.2). Just one year later, 2000 was the driest season with a peak daily discharge of 5.06×10^8 m^3/day. The year 2006 was the wettest season with a peak daily discharge of 9.04×10^8 m^3/day. The difference between peak flows of the wettest and driest season was 3.97×10^8 m^3/day. River outflow from the reservoir was calculated based on reservoir operation guidelines of Dasu Hydropower Project. In the outflow hydrograph, 2057 was the moderate hydrological season (Fig. 3.3). In the outflow hydrograph the wettest seasons were 2064, 2043, 2040, 2059, 2031, and 2038. The peak outflow discharge in 2064 was 9.04×10^8 m^3/day. The driest season in outflow hydrograph was 2058 with a peak outflow discharge of 4.8×10^8 m^3/day. The outflow of 4.8×10^8 mtextsuperscript3/day is comparatively lower than the inflow at the same period, i.e. 5.06×10^8 m^3/day. The difference in inflow and outflow hydrograph was due to filling of the dam to its full supply level after finishing the free flow flushing operation in monsoon at that period.
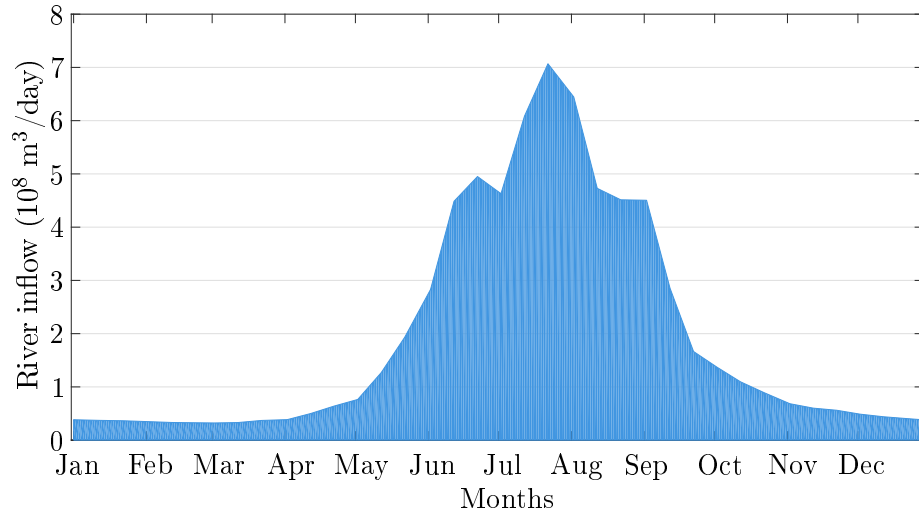
Figure 3.2: ANN input, daily inflow hydrograph of moderate hydrological year (1999)

The reservoir capacity was calculated from the area-capacity and elevation curve of the reservoir operation (Fig. 3.4). Target for subject ANN model was sediment retained in the reservoir ponding area during 2027-2066, which was estimated by using HEC-RAS-1D numerical model. In HEC-RAS model, daily inflow discharges and reservoir water levels (RWL) were used as upper and lower boundary conditions, respectively. Acker-White sediment transport formula was used for sediment simulations in this model. Acker-White sediment transport formula showed better results for Dasu Hydropower Project, in previous studies conducted by [1]. [91] evaluated total load sediment transport formulas using ANN technique and it was found that ANN model is a reliable and uncomplicated method to predict total sediment transport rate of total bed material load transport rate. It was also found that the accuracy of Ackers and White (1973) sediment transport formula showed some preference in the study results [91]. In constructed sediment retention graph (Fig. 3.5), the year 2038 was among the wettest seasons along with longer duration of high flows. In 2038, the monsoon started from the mid of April and ended in August. In normal years, the rotation of monsoon starts in the June and ended in August. The effect of longer duration high predicted more flushing of sediments from the dam (Fig. 3.5). The year 2066 showed highest peak of outflow but its duration of high flow event was only 20 days in June. Therefore, in 2066 the flushing of sediments out of the dam body was an average as of the other years. The flushing operation in the starting years of the project was planned for the shorter time due to less accumulation of sediments in the dam.

The combination of both ANN and HEC-RAS models is shown in Fig. 3.6. The input and output parameters of both models were correspond to the same period. The HEC-RAS model output of volume of sediment retained in the reservoir was used as target in

the ANN model. The aim of using HEC-RAS output as target in ANN model was to observe the efficiency of ANN model to predict reservoir sedimentation.
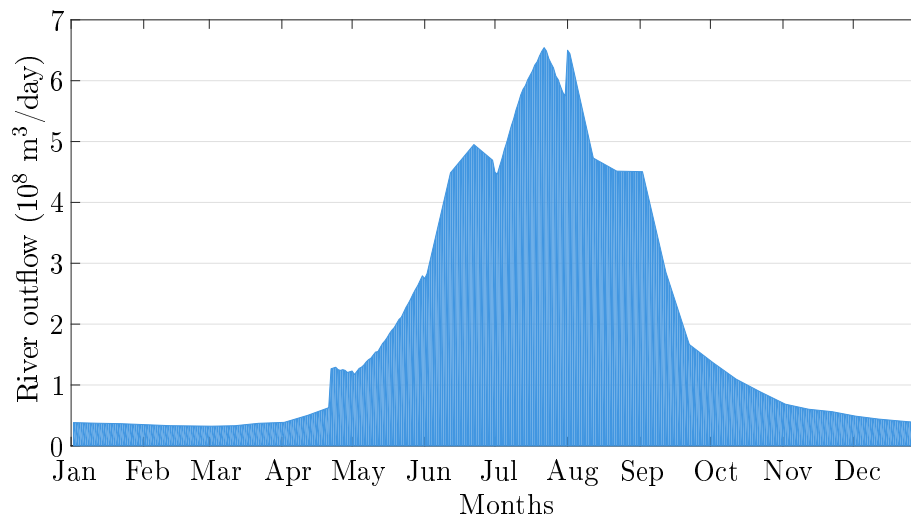
Figure 3.3: ANN input, planned daily outflow hydrograph of moderate hydrological year (2057)
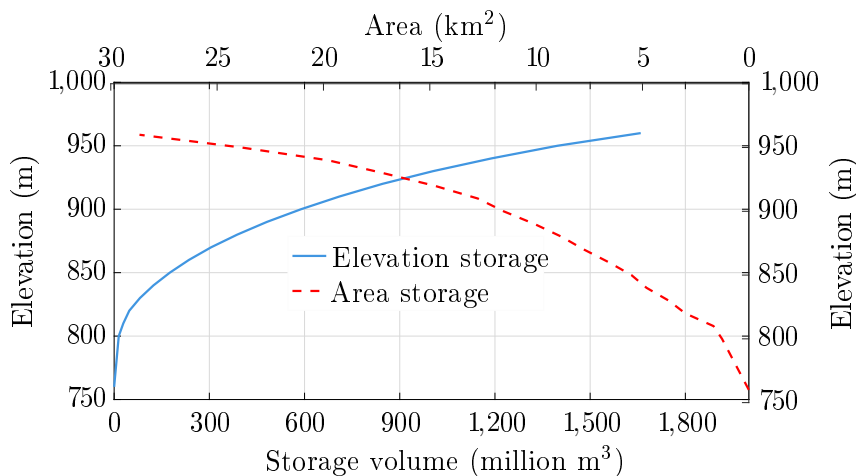
Figure 3.4: Area-elevation-storage curve of Dasu HPP [7]

3.2.2   ANN model development

The most commonly used artificial neural network in hydrological studies is feed forward neural network with back propagation [92]. There is no fixed rule for the development of an ANN model, even though a general framework can be followed based on previous successful applications in engineering [88]. In the present study of Dasu HPP, three types of multilayers perceptron (MLP) of ANN model architecture were developed to estimate

reservoir sedimentation using 40 year's data. Trial and error method was used to select an appropriate ANN architecture. Input parameters such as river inflow, river outflow, and change in storage capacity of the reservoir, for the model, were decided on the basis of available data and possible factors which can affect sediment retention (Eq. 3.4). Number of hidden layers and size of hidden layers were selected on trial and error basis. The number and size of hidden layers affect the performance of ANN, significantly. Random, Levenberg-Marquardt 'trainlm', and means squared error functions were used for data division, training and performance of ANN algorithms. The 'trainlm' training function was used as training function in the developed ANN architectures. Permutations of logsig, tansig, radbas and purelin transfer functions in hidden and output layers were used to obtain the best possible solution.
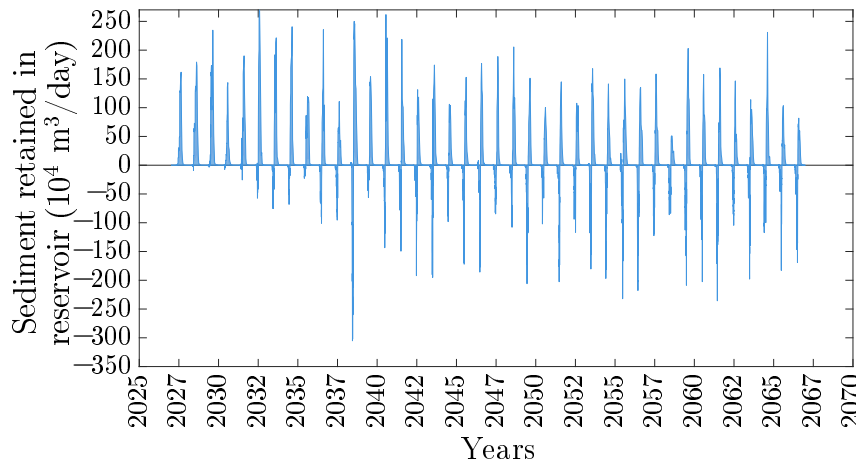
Figure 3.5: ANN target, daily sediment retained in the reservoir ponding area (2027-2066)
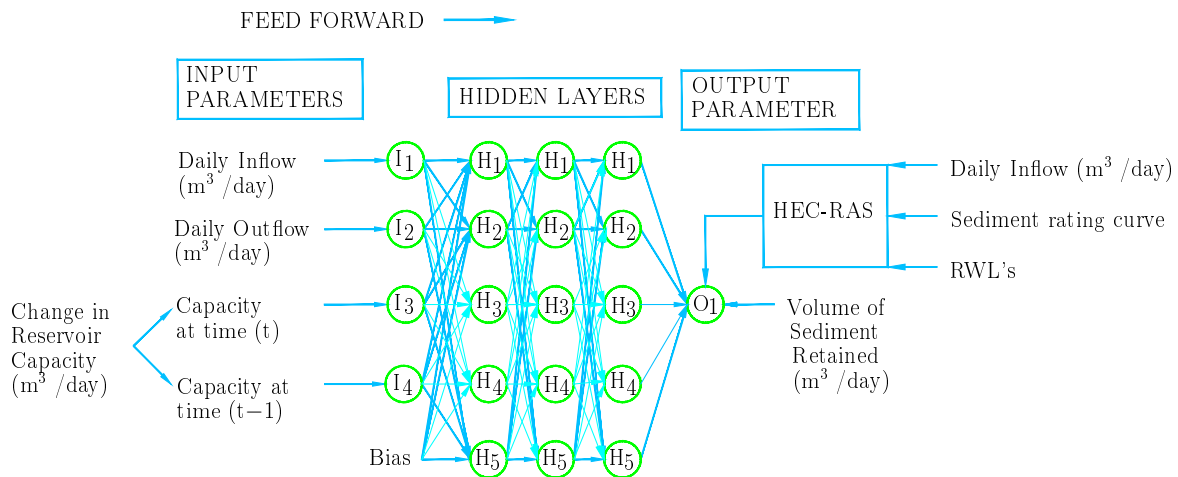
Figure 3.6: ANN (4-5-4-5-1) architecture used in present study, with HEC-RAS output as target parameter.

3.2.2.1   Training and validation of an ANN

In multilayer perceptron, artificial neural network, connections exist between different nodes of different layers and there is no connection exists within the same layer. The inputs are fed through the input layer and the output layer produced output after going through different training, testing functions in the input, hidden and the output layers. Between different layers there is a connection which is updated during the learning process by bias and synaptic weights. At initially, networks use small random values for training. In gradient decent algorithm, learning process stops when network attained to a steepest decent approach. Once the training process is satisfactory completed, the network was saved, the test and validation data set recalled and values predicted by the model were compared with the targeted data. When a comparison is within the satisfied limit, the network than the network is considered to be a well-trained network. For training purposes Levenberg-Marquardt algorithm was used as it has been widely used in approximating a complicated non-linear function [93]. In the present study, the model was used to test the statistical indicators of coefficient of regression (R), root mean-square error (RMSE) and mean absolute error (MAE). The RMSE of the training period was the deciding parameter for the selection of corresponding performance parameters and ANN architecture (Fig. 3.7). Block diagram of 3-D array ANN architecture with three hidden layers as an example with the input and the output parameters is as shown in Fig. 3.7. Furthermore, ANN model sediment estimation error, per km^2 of the catchment area was estimated by using error to catchment area relationship:

3.2.2.2   Model setup

Multilayer perceptron of artificial neural network architectures were developed by using MATLAB tool. Three feedforward network architectures of ANN having one, two and three hidden layers were tested for the current simulations. Input data was allocated to the model according to default, i.e. in random basis. 70% of the data set (Δs , $q_{w(in)}$ and $q_{w(out)}$) was used for training, 15% for testing and the remaining 15% was used for validation. Trial and error method was used for selection of appropriate ANN architecture and number of neuron in the hidden layers. The one-hidden-layer ANN architecture was tested 100 times with 1 to 20 neurons in the hidden layer, the two-hidden-layers ANN architecture was tested 10 times with 1 to 10 neurons in the hidden layers, and the three-hidden-layers ANN architecture was tested 5 times with 1 to 5 neurons in the hidden layers, respectively. The output for each simulation was daily volume of sediment retained in

the reservoir. After specifying the whole arrangement, the programme was simulated to find out the best combinations of different performance statistics (R, RMSE & MAE). Statistical performance of respective ANN architectures output and used functions were stored after each simulation and best results were sorted out after finishing the whole simulation process as an example of the four layers ANN algorithm is shown in Fig. 3.7. To get visualization of the model performance, a comparison was made between the best performed ANN architecture for predicting the sediment retained.

$$\text{Sediment estimation error, per } km^2 \text{ of cathment area} = \frac{Error}{\text{Catchment area}} \qquad 3.5$$
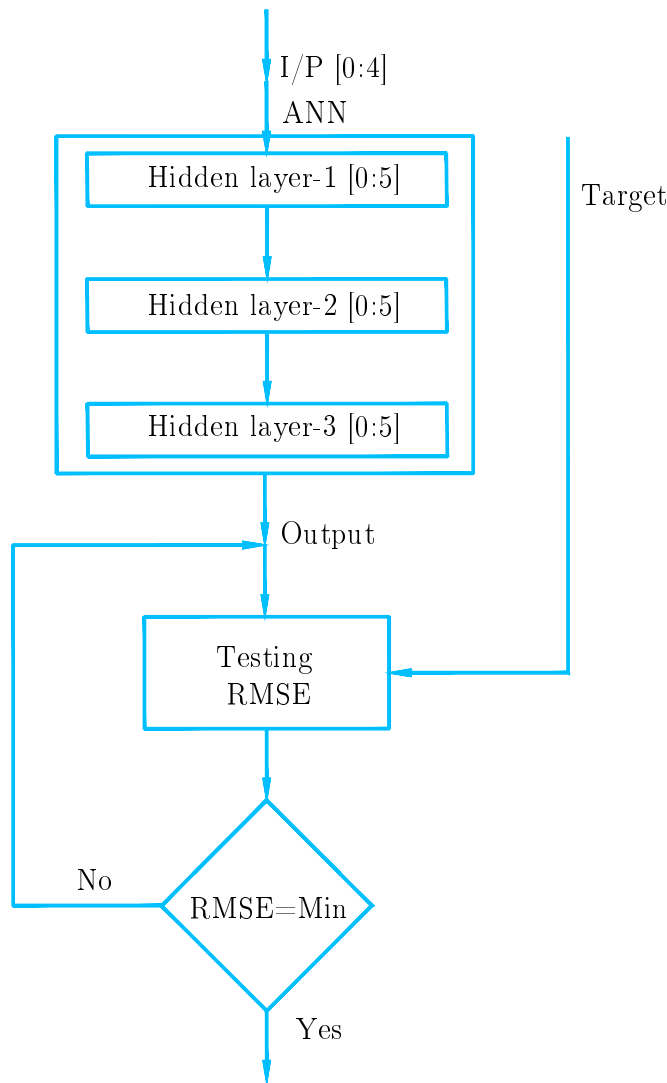
Figure 3.7: ANN algorithm for correlation, RMSE and MAE.

3.3 Results and discussions

The results of the three tested architectural cases were categorised on the basis of number of layers in each architecture. Case-I contains the one-hidden-layer ANN architecture results, case-II contains the two-hidden-layers ANN architecture results, and case-III contains the three-hidden-layers ANN architecture results.

3.3.1 Case-I

The one-hidden-layer neural network architecture was tested with four permutations of 'logsig', 'tansig', 'radbas', and 'purelin' transfer functions in the hidden and the output layers. RMSE in the testing period was the deciding factor of selecting the suitable ANN architecture. For this case, the minimum RMSE was found by using 'logsig' and 'purelin' transfer functions in the hidden and the output layers, i.e. 1.86×10^5 m^3. The value of RMSE 1.86×10^5 m^3 was comparatively lower than the value of RMSE by using 'tansig' and 'radbas' transfer functions in the hidden layers. The 'tansig' and 'logsig' transfer functions showed maximum RMSE, i.e. 2.7×10^5 m^3. Similarly 'logsig' transfer function in both, hidden and output layers also showed higher RMSE, i.e. 2.3×10^5 m^3. Number of neurons in the hidden layer of the best performed ANN architecture were 14. This ANN provided correlations of 0.92 and 0.90 for the testing and training data set, respectively.

3.3.2 Case-II

The same procedure was repeated for the two hidden layers neural network and it was tested with permutation of 'logsig', 'tansig', 'radbas' and 'purelin' transfer functions in the hidden and the output layers. In this case using transfer functions of 'tansig', in both hidden layers and 'purelin' in the output layer predicted efficient results for RMSE of testing, i.e. 1.88×10^5 m^3. In this ANN architecture combination, number of neurons in two hidden layers were 8 and 10. The correlation coefficients for testing and training periods were 0.92 and 0.91, respectively.

3.3.3 Case-III

The three hidden layers ANN architecture was simulated with 30 different combinations of transfer functions of 'logsig', 'tansig', 'radbas' and 'purelin'. The minimum RMSE of

the testing period for case-III was obtained with 'logsig' transfer function in all three hidden layers and 'purelin' transfer function in the output layers ($1.86{\times}10^5$ m^3). The numbers of neurons in the respective hidden layers were 5, 4, and 5. For the testing and training period, the correlation coefficients were 0.92 and 0.91, respectively.

In efficiently performed ANN architectures, the most common factor among all the results was the transfer functions (Tab. 3.1). The 'purelin' transfer function in output layers predicted efficient results of RMSE of testing in the three layers neural architecture ANN (4-14-1), four layers neural architecture ANN (4-8-10-1), and the five layer neural network ANN (4-5-4-5-1): i.e. $1.86{\times}10^5$ m^3, $1.88{\times}10^5$ m^3, and $1.86{\times}10^5$ m^3. The ANN (4-14-1) and the ANN (4-5-4-5-1) architecture used 'logsig' transfer functions in all hidden layers. Thus the RMSE of testing of these architectures is almost similar. The RMSE of three layers neural network with 'logsig' transfer function in both hidden layers and 'purelin' transfer function in the output layer was $1.93{\times}10^5$ m^3. That is higher than RMSE with 'tansig' transfer function in the both hidden layers and 'purelin' transfer function in the output layer, i.e. $1.88{\times}10^5$ m^3. Therefore, in four layers neural network, the best transfer function in hidden layer was 'tansig' while the best transfer function in three and five layers neural network was 'logsig'. Among the performance parameters of RMSE for testing and validation periods, ANN (4-14-1) performed better. Again, in MAE of training, ANN (4-14-1) performed better. ANN (4-5-4-5-1) performed better in MAE of testing, i.e. $8.17{\times}10^4$ m^3. Although, RMSE of training as well as MAE of testing and validation were not the deciding parameters of selecting the appropriate neural network structure, these parameters reveal the performance of selected architectures. Among the best three selected architectures, ANN (4-14-1) performed better and ANN (4-8-10-1) was at the last in performance statistics. It may be possible that neural network architectures with one hidden layer and 1 to 20 neurons in the hidden layer were tested and recorded 100 times to get best results. The neural network architectures with two hidden layers and 1 to 10 neurons in the hidden layers were tested and recorded 10 times to get the best results. The neural network architectures with three hidden layers and 1 to 5 neurons in the hidden layers were tested and recorded only 5 times to get the best results. Thus, the two and the three hidden layers neural network predicted best results by utilizing the maximum allowed number of neurons, i.e. 8, 10 in the two hidden layers neural network and 5, 4, 5 in the three hidden layers neural network. Therefore, it could be possible that by increasing the number of neurons in the hidden layers of three and four layers neural network may improve the efficiency of these ANN architectures. However, increasing the number of neurons or size of neural networks utilize more power, time, and memory. In current simulations of three and four hidden layers neural network, the elapsed time was

7,322 and 17,238 seconds. Thus, selection of appropriate neural network architectures always require a compromise between cost and efficiency.

Table 3.1: Summary of performance statistics of efficient ANN architectures

ANN architecture	Transfer function				Performance parameters					
	HL[1]-1	HL-2	HL-3	Output layer	R test	R val[2]	RMSE test (10^5 m^3)	RMSE val (10^5 m^3)	MAE test (10^4 m^3)	MAE val (10^4 m^3)
ANN(4-14-1)	logsig	-	-	purelin	0.926	0.905	1.860	2.146	8.224	9.259
ANN(4-8-10-1)	tansig	tansig	-	purelin	0.924	0.909	1.884	2.159	8.299	9.347
ANN(4-5-4-5-1)	logsig	logsig	logsig	purelin	0.923	0.908	1.863	2.229	8.177	10.061

The study on reservoir sedimentation estimation by using the artificial neural network was conducted [88] for the Gobindsagar Reservoir on the Satluj River in India. The Satluj River is a tributary of the Indus River Basin System [94]. [88] employed annual rainfall, inflow, and reservoir capacity of 1971 to 2003, as an input parameters in ANN (3-5-1) model and determining the volume of sediment retained in the reservoir was the target and the output of the model. The study results showed that the RMSE and MAE of the testing periods of ANN (3-5-1) for the Gobindsagar Dam, with a catchment area of 56,876 km^2, were 3.51×10^6 m^3 and 3.14×10^6 m^3, respectively. Per square kilometre catchment area RMSE and MAE of testing periods, for the Gobindsagar reservoir were about 61.76 m^3 and 55.26 m^3. In the present study of Dasu HPP, RMSE and MAE of the testing periods of ANN (4-14-1) were 1.86×10^5 m3 and 8.22×10^4 m^3. Similarly, catchment area sedimentation estimation error per km^2 during the testing period, for RMSE and MAE were 1.17 m^3/km^2 and 0.51 m^3/km^2, respectively (Tab. 3.2).

Table 3.2: Comparison of ANN performance statistics of the Dasu HPP with the Gobindsagar Dam

Dam	RMSE test (million m^3)	MAE test (million m^3)	CA[3] (km^2)	RMSE test/CA (m^3/km^2)	MAE test/CA (m^3/km^2)
Dasu	0.186	0.082	158,800	1.17	0.51
Gobindsagar	3.51	3.14	56,876	61.76	55.26

The model predictions of ANN (4-14-1) for Dasu Hydropower Project showed statistical preferences over ANN (3-5-1) model predictions of existing Gobindsagar Dam. It may possible due to differences in input parameters and time duration of input data sets. In Gobindsagar Dam [88] annual rainfall, annual inflow and annual capacity was used as input parameter while in the present study daily data of inflow, outflow and capacity was

[1]hidden layer
[2]validation
[3]catchment area

used as input parameter. The length of data sets in Gobindsagar Dam and Dasu HPP were 32 years and 40 years, respectively. The catchment area of Dasu is almost 2.8 times more than Gobindsagar Dam's catchment area. Therefore, it seems that the interval of data set and catchment area effects the efficiency of ANN.

A comparison of optimal performed ANN architecture predictions with target sediment volume retained in the reservoir ponding area showed that the model prediction in all three best ANN architectures, i.e. ANN (4-14-1), ANN (4-8-10-1) and ANN (4-5-4-5-1), captured well the sediment retention and flushing in the dam ponding. Comparison of targeted and best performed ANN (4-14-1) network model estimation for the testing period is shown in Fig. 3.8. At the beginning, ANN model deviated from the target sediment retention. The possible reason behind deviated trend may be the training of ANN. The ANN model was trained with input data on randomly basis. Furthermore, there was no flushing operation planned in the initial five years of the project, the only sediment flushing was due to high flows in the river during monsoon period. After five years the flushing operation was repeated every year in the dam. After training well, the ANN predicted well the sediment retention and flushing operations in the dam as showed in both testing and all periods of Fig. 3.8a and Fig. 3.8b. To visualize the sediment retention trend of ANN (4-14-1) model predictions in wettest and moderate hydrological seasons, a comparison of results is made in Fig. 3.9. It was noticed that ANN (4-14-1) captured well the overall trend of sediment retention in the reservoir and flushing out of the reservoir (Fig. 3.9a). The year 2057 was the moderate hydrological year and in sectional view of Fig. 3.9b, the model predicted well both processes of sediment flushing and sediment retention during the filling of the reservoir. Similarly, the year 2064 was the wettest season with highest peak of discharge of 20 days, that high event was also well captured by the model as shown in Fig. 3.9c. The year 2038 was also wettest season with longer peaks of high flows due to pre start of monsoon and that trend was also captured well in the model. During these year more flushing was predicted both in target and ANN (4-14-1) as shown in Fig. 3.9d.

3.4 Conclusions

The developed artificial neural network could well capture the pattern of the volumes of sediment deposited in the reservoir and flushed out of the reservoir on a daily basis for Dasu Hydropower Project (DHP). The best MPL of ANN (4-14-1) was with 'logsig' transfer function in the hidden layer and 'purelin' transfer function in the output layer.

This ANN also captured well the events of sedimentation in wettest and driest hydrological seasons of the Project. It was observed that with longer length of data set of shorter intervals could improve the efficiency of the ANN model. Furthermore, the catchment area of the watershed also influenced the performance parameters of the model outcome. It was also observed that increasing the size of neural network for long duration data set of shorter intervals did not affect the statistical performance of the model. It was concluded that the artificial neural network is a good tool for the estimation of sediment deposition within the reservoir ponding area and estimation of sediment flushing out of the reservoir for the Dasu Hydropower Project.

(a) Testing data points   (b) All data points
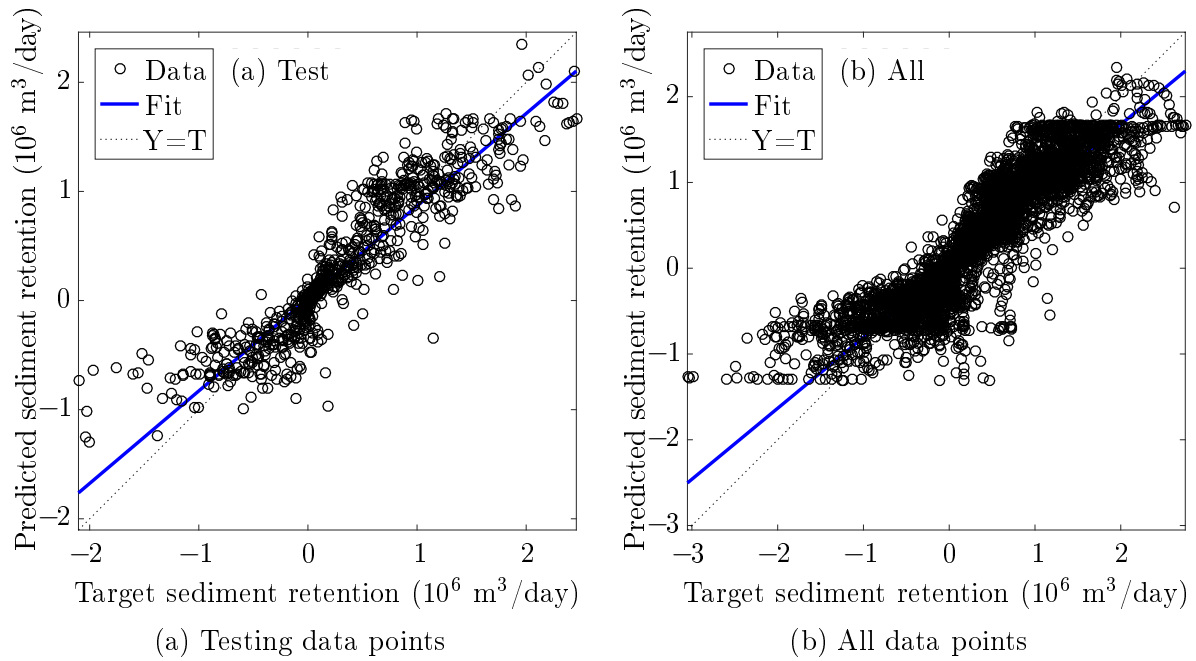
Figure 3.8: Comparison of sediment estimation by ANN (4-14-1) model with the targeted data

(a) All years

(b) Moderate year

(c) Wettest year

(d) Wettest with long duration year
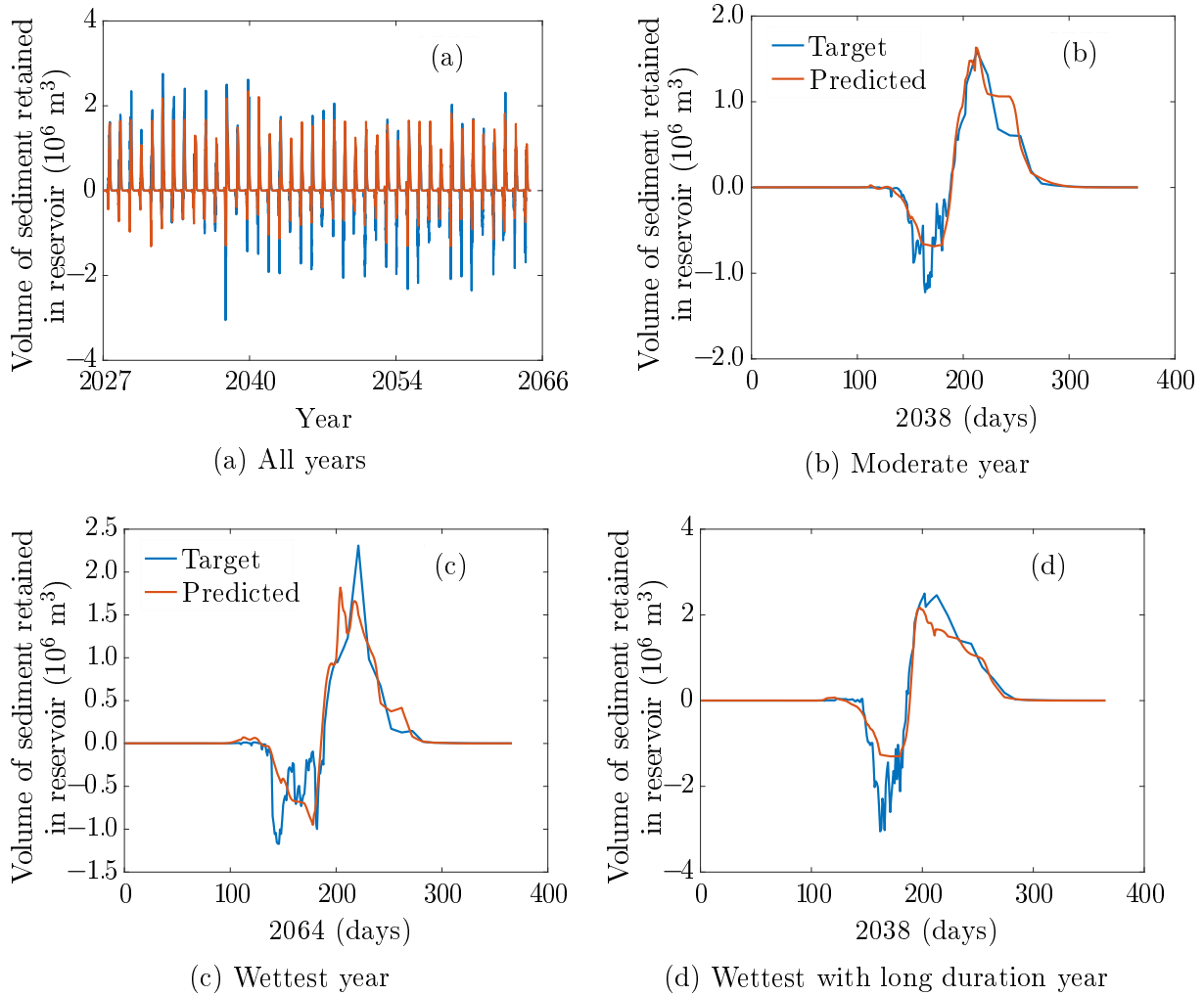
Figure 3.9: Comparison of sediment estimation by ANN (4-14-1) model with the targeted data in (Fig. 3.9a) all, (Fig. 3.9b) moderate, (Fig. 3.9c) wettest with high peak, and (Fig. 3.9d) wettest with long duration, hydrological cycles.

Chapter 4

Development of a Wavelet-ANN Model for Estimating Suspended Sediment Load in the Upper Indus River

This chapter is submitted for publishing as:

Abstract: The precise estimate of sediment load plays a vital role in the sediment management of existing and proposed reservoirs and run-of-the-river hydropower schemes. In this study, missing suspended sediment load (SSL) at Besham Qila was estimated using three different modelling approaches. Comparison of the results estimated by these models and observations showed that a standard artificial neural network (ANN) and discrete wavelet transform coupled with neural network (WA-ANN) estimated SSL more accurately than the conventional sediment rating curves (SRC). The results obtained using WA-ANN for daily SSLs were NSE=0.85 compared to ANN NSE=0.81 and SRC NSE=0.48, respectively. In addition, the mean deviations during the whole study period (38 years) were 13%, 18% and 36% using WA-ANN, ANN and SRC models, respectively. Moreover, the WA-ANN estimate for the mean annual mass deposited in the Tarbela dam deviates only 12% from the hydrographic survey, compare to a 43% deviation using SRC. Exceptional events were more accurately estimated using the WA-ANN model. The results therefore indicate that coupled wavelet-neural network models can be applied for more precise estimation of suspended sediment load for rivers subjected to strong

hysteresis phenomena, disproportional spatio-temporal trends between discharges and SSLs, as well as parallel processes of landslide degradation and aggradation. Our study shows that the method can be used for setting correct sediment load boundary conditions of sedimentation models for 14,000 MW planned hydraulic structures and detection of sediment load trends in the upper Indus River and similar environments.

4.1 Introduction

The deposition of sediment load in reservoirs reduces their life span. Due to sedimentation, in Asia alone, 80% of the useful storage capacity for hydropower production will be lost by 2035, and 70% of the storage volumes used for irrigation purposes will be lost by 2025 [53]. Even construction of new storage reservoirs will only replace already lost storage capacity. The most common conventional method for sediment load estimation is the sediment rating curve (SRC), which is a relatively simple relationship between flow discharge and sediment concentration. However, in a real time scenario, multiple variable act on the given circumstances of the sampled data, which is why SRC mostly results over or under estimate the sediment load [8]. A number of reservoirs have silted up earlier than expected due to underestimation or are inefficient due to overestimation of sediment load. Examples include the Warsak and Mangla dams in Pakistan [9, 10]. The cause of this problem might be the significant variance in SSL estimates on which the design and operation of these hydraulic structures were based. For example, the variance in SSL estimates at Besham Qila gauge station of the upper Indus River ranges from 200 Mt yr^{-1} to 675 Mt yr^{-1} (Tab. 4.1). Such variance can lead to a circular error in the design and operation of planned and existing infrastructures. The circular error starts from poor sediment load estimation and subsequently affects the boundary conditions of the modelling process, which results in the poor quality operation rules that ultimately contribute to the structure's life cycle. Thus, the accuracy of an estimate plays a decisive role in setting the correct boundary conditions for sediment studies and can improve the quality of hydraulic designs. However, minor consideration has been paid to quantifying the uncertainty associated with sediment load estimates in the model forecasts. Therefore, it is necessary to improve the sediment load estimation techniques in order to manage the rapid decline of the reservoir's storage capabilities [95].

SSL estimation has become vastly more challenging, in particular under the influence of climate change, where disproportional spatio-temporal trends between SSLs and discharges exist primarily due to intra-annual shifts in flows [20, 37, 4]. This highlights the

need for sediment models which operate in real time and are able to provide a better estimation of sediment load for the planning of new reservoirs or better management of existing ones. This specifically applies to the upper Indus River, where the presence of complex sediment transport processes related to the hysteresis phenomena and marked hydrological variations, such as: (a) the fluvial erosion and transport processes which interact with other sediment producing processes, (b) temporary sediment storage in the main river channel [22], (c) aggradation and degradation phases of landslides [23], (d) on average 5-10 high flow waves of an average 10-12 days duration during the monsoon period, and (e) different transit times of discharge and sediment and their different lag times from several sources to the gauge stations, all pose a challenge in precise SSL estimation process.

Table 4.1: Estimates published on the Indus River sediment yield

Suspended sediment yield (Mt yr^{-1})	References
480	[11]
400	[12]
475	[13]
446	[96]
200	[14]
675	[16]
300	[17]
200	[97]
197	[19]
200	[6]

In addition, hydro-morphological processes are highly nonlinear in nature and, in many cases, modelling these variables with conceptual models may be limited by a poor understanding of the complex interactions involved. In such cases, artificial neural networks (ANNs) are often viewed as an appealing alternative, as they have the ability to extract a nonlinear relationship from data without requiring an in depth knowledge of the physics occurring within the system [25]. Application of wavelet transformation (WT) has been found to be effective in dealing with the issue of non-stationary data. WT is a mathematical tool that may improve the performance of ANN models by simultaneously considering both the spectral and the temporal information contained in the input data. WT decomposes the main time series data into its sub-components. ANN models developed using input data processed by the WT instead of using data in its raw form are known as wavelet neural network (WA-ANN) models. These models afford improved performance by using multi-scale input data and capturing useful information concealed

in the main time series data in its raw form [98].

ANN and WA-ANNs have been performing well over the last decades of estimating and forecasting of sediment loads [26, 27]. WA-ANNs can decompose the data time series up to several levels in time, space and frequency domain and reveal the information from a give data scenario [28]. This decomposition of data is required where the sediment transport process is subjected to temporary sediment storage, strong hysteresis phenomena and parallel aggradation and degradation of landslides. Data decomposition beyond level one can lead to low efficiency [29], however, the concept of appropriate decomposition levels of data for rivers with temporary substantial sediment load storage is still not understood for sediment load estimation. ANNs sediment load estimation abilities with semimonthly sediment loads, using simple ANN structures have only been tested for that rivers have small catchments [30]. Moreover, WA-ANNs have not been tested for filling the gaps between intermittent suspended sediment concentration (SSC) samples; in the state-of-the-art techniques [26, 31], they have only been applied on continuous (daily) data time series.

In granting the importance to hydraulic structures as non-renewable resources, it is important to quantitatively and qualitatively evaluate the performance (and uncertainties originating using) of these (SRC, ANN and WA-ANN) methods for the rivers with complex sediment transport processes. To our knowledge, this is the first study to apply an ANN and a WA-ANN models using different architectures, incorporating four different training methods, transfer functions and wavelets (up to 8 level of decompositions) for suspended sediment load time series in the upper Indus River. In order to evaluate model performance and to analyse the capabilities of the models in terms of daily, yearly and cumulative sediment load predictions, we compare our results using these models with those obtained by measurements. The study also explores the capabilities of these models to reconstruct the missing daily SSL which plays a vital role in setting correct boundary conditions for reservoir sedimentation studies and detection of sediment load trends for rivers which have intermittent SSC samples.

4.2 Study area and data

The Indus River is one of the largest rivers in south Asia with a total length of 2,880 km and a drainage area of 912,000 km^2 starting in China, running through India and then across the whole of Pakistan. There are 17 operational climatological and hydrological gauge stations along the Indus River before the Besham Qila gauge station. Besham Qila

is located approximately 65 km upstream of the Tarbela dam (Fig. 4.1), which is one of the largest earth filled dams in the world. Run-off from the upper Indus Basin above Besham Qila forms the greater part of the flow entering the Tarbela dam. The specific sediment yield with drainage area along the Indus River at Besham Qila is approximately 1,197 Mt km^{2}yr^{-1}. This high sediment yield is due to the large number of small and relatively steep catchments discharging straight into the Indus River. 80 to 85% of the annual sediment load is transported by the Indus River in July and August (monsoon months). In the monsoon period, the flow discharge can vary significantly over a few days with an immediate and large increase in the sediment concentration [67]. The contribution of rainfall, glacier and snow melt to the total flow at Tarbela dam is 33% in July and 55% in August. This makes the Indus River the most melt water dependent river in the world [21, 46].
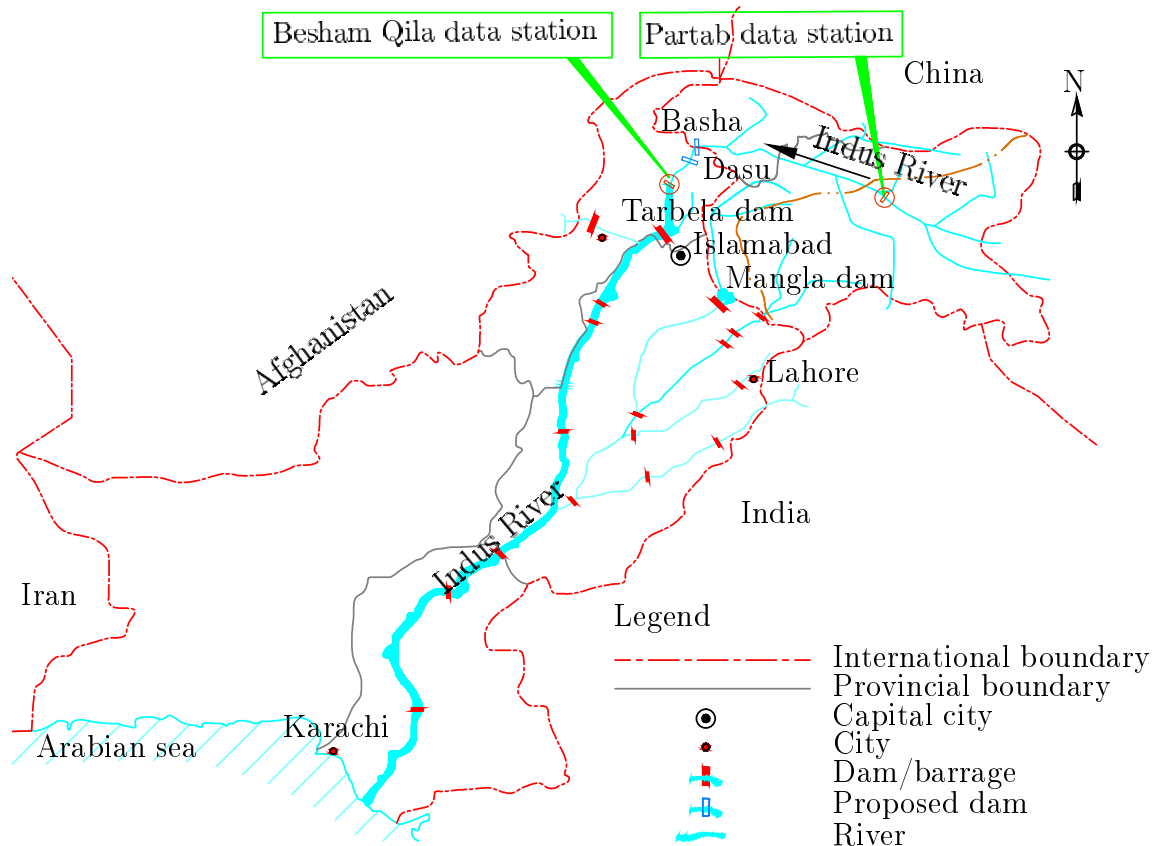
Figure 4.1: Location map of study area and gauge stations in the study area, developed by [6]

The data used in this study include daily flow discharges and distinct sediment samples over 40 years (1969-2008) at Besham Qila. As the suspended sediment concentration (SSC) data from 1978 and 1979 (along-with some samples in other years e.g. 1981) were not calendrically documented, these two years were excluded from model construction.

However, for convenient representation, the data calendar is defined as 1969-2008. The sediment sampling was carried out twice a week in summer (high flow season) and once a week in winter (low flow season) as per availability of resources (labour) and sampling feasibility (weather) following the U.S. Geological Survey (USGS) procedures [99, 100, 101]. Additional SSC sampling was also conducted during high flood and extreme events. Moreover, the sampling was not conducted on a fixed day in a week, which also covers a broad range of variations in SSC. The flow discharge at gauge stations on the Indus River was measured using an AA current meter following the USGS method. The total number of suspended sediment samples taken at Besham Qila from 1969 to 2008 was 3,213. The sampling frequency is an average 80 samples per year, which is high (22%) and covers a broad range of events. The outliers in sediment data samples were excluded by examining the general behaviour of the river and river catchment. The catchment of the Indus River at Besham Qila is around 164,867 km^2 [102]. Given this immense catchment area, the changes within the discharge and sediment concentration are not as rapid as changes in small river catchments. This makes excluding the outliers easier owing to the relatively small variation in the behaviour of the river. Another reason for removing the outliers through manual examination was the distinct nature of SSC samples, which hindered the employment of statistical methods. The total size of data samples was reduced by about 4.2% after excluding outliers.

The hydrological and sedimentological data showed great variance in distribution of sediment load and discharge over the time period concerned (Tab. 4.2). The standard deviation (SD) of sediment load and discharge indicated a wide spread of hydrological events for the Indus River. The highest exceptional flow years were 1973, 1988, and 1994 with a total volume of $9.9{\times}10^{10}$ m^3, $9.5{\times}10^{10}$ m^3 and $9.4{\times}10^{10}$ m^3, respectively. The highest peak flow year was 1984 with a volume of $8.9{\times}10^{10}$ m^3. By contrast, 1982 was an extreme low flow year with a volume of $6.1{\times}10^{10}$ m^3. The mean annual volume of flow at Besham Qila in last 40 years was $7.6{\times}10^{10}$ m^3. Based on these flow patterns, low flow and high flow seasons can be traced. For example, 1974-1977 was a low flow season (dry season) with an average annual volume of $7.0{\times}10^{10}$ m^3. On the other hand, 1988-1992 was a high flow season (wet season) with an average annual flow volume of $8.5{\times}10^{10}$ m^3. There was also a lag time in discharge and sediment concentration peaks, which may have been the result of the immense catchment area before Besham Qila gauge station (i.e. 164,867 km^2). The 10,000 years and 100 years return period floods at Dasu damsite were 21,218 m^3/s and 15,078 m^3/s, respectively [6]. Dasu damsite is located about 95 km upstream of Besham Qila gauge station (Fig. 4.1).

Table 4.2: Hydrological and sedimentological data characteristics at Besham Qila gauge station

Parameter	Discharge (m^3/s)	Sediment concentration (ppm)
Duration	1969-08 (daily)	1969-08 (samples)
Max discharge	13,910	3,770 (at Q$_{max}$)
Min discharge	325	132 (at Q$_{min}$)
Max sediment	12,401	8,660
Min sediment	456	1
Mean sediment	-	1,071
SD of sediment	-	1,456
Mean discharge	3,000	-
SD of discharge	2,923	-
Q$_{-10,000}$ at Dasu damsite	21,218	-
Q$_{-100}$ at Dasu damsite	15,078	-

The average grain size distribution of suspended load in the Indus is 45.7% sand, 39.9% silt and 14.4% clay [57]. More than 90% of the annual sediment load reaches Besham Qila in the summer months from May to September. This is mainly due to glacial melting in summer and erosion of rocks and steep slopes in the basin area [103]. More details on data collection, data quality and period of records for the Indus River can be found in [19].

4.3 Methodology

4.3.1 Sediment rating curves (SRC)

SRC empirically relates the water discharge with sediment discharge for a given stream [104, 74]. The SRC method is simple and easily applicable. However, its accuracy is limited. In some cases, SRC provides relatively poor load estimates [105, 106, 30]. Despite the uncertainty of obtaining a useful water-discharge sediment relation, SRC may nevertheless provide a satisfactory relation in the form of a linear or non-linear correlation coefficient (Eq. 4.1)

$$Q_s = \alpha Q^\beta \qquad\qquad 4.1$$

Where Q$_s$ is the sediment discharge, Q is the river/stream flow discharge, α and β are the coefficients. For more accurate SRC, the equation can be based on low and high flows. Additionally the fraction rate of corresponding discharges to inflow discharge are derived

from the sediment measurement data [107, 6]. Usually, rating curves are developed on the premise that the relationship between sediment concentration and discharge is stable. Although estimates are highly variable, SRC is still widely used [19, 108, 15, 6, 33, 1, 2].

Based on the distinct SSC measurements from 1969-2008 [6] developed two sediment rating curves using the SSL-discharge relationship. The first curve (Eq. 4.2) is based on low and high flow seasons in the winter and summer months, respectively, while the second (Eq. 4.3) is based on the relationship of overall flow with SSL.

$$Q_s = \begin{cases} 1.4774 \times 10^{-8} \times Q^{2.632}, & \text{if } Q > 17,000 \; ft^3/s. \\ 1.4865 \times 10^{-63} \times Q^{15.625}, & \text{otherwise.} \end{cases} \qquad 4.2$$

$$Q_s = 6.835 \times 10^{-09} \times Q^{2.695} \; , \quad (single \; equation) \qquad 4.3$$

Where Q_s is the sediment discharge in short ton/day, Q is the flow discharge in ft^3/s.

4.3.2 Artificial neural networks (ANN)

ANN is a computational model inspired by biological neural systems and it can be defined as a set of simple processing units (called neurons) working as a parallel distributed processor [109]. These neurons are responsible for acquiring and storing experiential knowledge and making it available for use. Different types of ANNs that are able to perform various tasks. Among others, Multi-Layer-Perceptron (MLP) using a training algorithm of the feed-forward of the input information and the backpropagation of error is one of the most common ANNs applied to solving various engineering problems. Such an MLP network consists of an input layer, an output layer and one or more hidden layers between its input and output layer. Each layer consists of certain number of neurons. Every neuron in a layer is connected to all neurons in the adjacent layers using synaptic or connection weights but the information flows only in one direction, i.e. from the input side to the output side. Further, each neuron applies an activation (or a transfer) function to its net input (sum of weighted input signals) to determine its output. The behaviour of the ANN depends on both the weights and the activation function that is specified for the neuron. More importantly, each layer has its own transfer function. Some examples of common activation functions are the step function, sign function, sigmoid function and linear function. Applying a backpropagation algorithm, the network learns a pre-defined set of input-output training pairs by using a two phase propagate-adapt cycle. The applied input pattern to the first layer propagates through each upper layer until an output pattern is generated. An error indicating the difference between the predicted and observed outputs is computed. This error is back-propagated through the network to each

neuron, and the connection weights are correspondingly adjusted. This training process is performed by minimizing the error function representing the square of the errors. A validation process can be used during training in order to prevent over fitting. Once the network has been trained to simulate the best response to input data, the configuration of the network is fixed and a test process is conducted to evaluate the performance of the ANN as a predictive tool.

A neural network is characterized by: (1) its pattern of connections between the neurons (called its architecture), (2) its activation or transfer function, and (3) the training method for determining the weights on the connections. It is worth mentioning here that the performance of an ANN model is significantly related to the number of hidden layer nodes. Less neurons in the hidden layer may affect the learning process in terms of a network under fitting problem while more neurons in the hidden layer restrict the efficiency in terms of computational time. The increase of neurons may also cause a network over fit problem. [110] suggested that the neurons for optimal generalization should be in a range from $2\sqrt{N_I} + N_O$ to the value $2N_I + 1$, where N_I and N_O represents the number of input and output nodes, respectively. More details about ANN approaches with these methods can be found in [109].

4.3.3   Wavelet transform (WT)

Wavelet transform (WT) is a mathematical tool that converts time domain signals into time-frequency domain signals [111]. As there are many good books and articles introducing the wavelet transform (e.g. [112, 113, 111]), only the main concepts of the transform are presented in this paper.

In a time series $f(t)$, the two basic parameters used for time-frequency representations are a frequency and b position in the signal. The continuous wavelet transform (CWT) of this time series is defined as follows:

$$W_{a,b} = \frac{1}{\sqrt{a}} \int\limits_{-\infty}^{\infty} f(t) \Psi^* \left(\frac{t-b}{a} \right) dt \qquad\qquad 4.4$$

Where $\Psi(t)$ is the transforming function also called the mother wavelet and " $*$ " denotes the complex conjugate. CWT searches for correlations between the signal and wavelet function. This calculation is done at different scales of a, and locally around the time of b. The result is a wavelet coefficient $W_{a,b}$ contour map. However, computing the

wavelet coefficients at every possible scale (resolution level) necessitates a large amount of data and computation time.

If one chooses the scales and the positions based on the powers of two (dyadic scales and positions), the analysis will be much more efficient and more accurate. This transform is refereed to as the discrete wavelet transform (DWT). For a discrete time series f_i, the discrete wavelet transform becomes:

$$W_{m,n} = 2^{-\frac{m}{n}} \sum_{i=0}^{N-1} f_i \psi^* \left(2^{-m}i - 1\right)$$
\hfill 4.5

Where i is integer time steps ($i = 0, 1, 2, ..., N-1$ and $N = 2^M$); m and n are integers that control, respectively, the scale and time; $W_{m,n}$ is wavelet coefficient for the scale factor $a = 2^m$ and the time factor $b = 2^m n$. The original signal can be reconstructed using the inverse discrete wavelet transform as follows:

$$f_i = A_{M,i} + \sum_{m=1}^{M} \sum_{n=0}^{2^{M-m}-1} W_{m,n} 2^{\frac{-m}{n}} \Psi \left(2^{-m}i - n\right)$$
\hfill 4.6

or in a simple form as:

$$f_i = A_{M,i} + \sum_{m=1}^{M} D_{m,i}$$
\hfill 4.7

Where $A_{M,i}$ is referred to as an approximation sub-signal at level M, and $D_{m,i}$ are detailed sub-signals at levels $m = 1, 2, ..., M$. The approximation coefficient $A_{M,i}$ represents the high scale low frequency component of the signal, while the detailed coefficients $D_{m,i}$ represent the low scale high frequency component of the signal. The low frequency component of the signal is important because it contains the most significant and most detailed information. Similarly, the high frequency component is important since it contains the information on the edges and abrupt changes in the signal. The detailed signals can capture trivial attributes of interpretational value in the data while the approximation shows the background information on the data [114]. There is a variety of mother wavelets, such as the Haar wavelet, Daubechies wavelet, Coiflet wavelet and Biorthogonal wavelet. The selection of an appropriate mother wavelet depends on the type of application and data characteristics. Normally, Daubechies performs better in sediment transport processes due to its ability to detect time localization information. Time localization information is useful in handling the seasonality and hysteresis phenomena in flow discharge and sediment load processes. The Coiflet wavelet is more symmetrical than Daubechies. The Biorthogonal wavelet has the property of linear phase, which is needed for signal reconstruction [29].

4.3.4   Wavelet neural network (WA-ANN)

Before applying an ANN, the input data time series is decomposed into detailed and approximated coefficients up to different (desired) levels using wavelet transform functions. The maximum possible number of levels depends on the temporal length of the data. The values corresponding in time to the output are extracted from the decomposed data series (fi). The extracted time series data is used as input for the ANN. The ANN architecture uses data time series decomposed by the WT is designated by WA-ANN (Fig. 4.2). The number of input nodes in the WA-ANN model depends on the level of decomposition, based on which appropriate neurons in the hidden layers are selected. The selection of hidden layer and hidden neurons in the model are important for maximizing the efficiency of the model.

PSfrag replacements
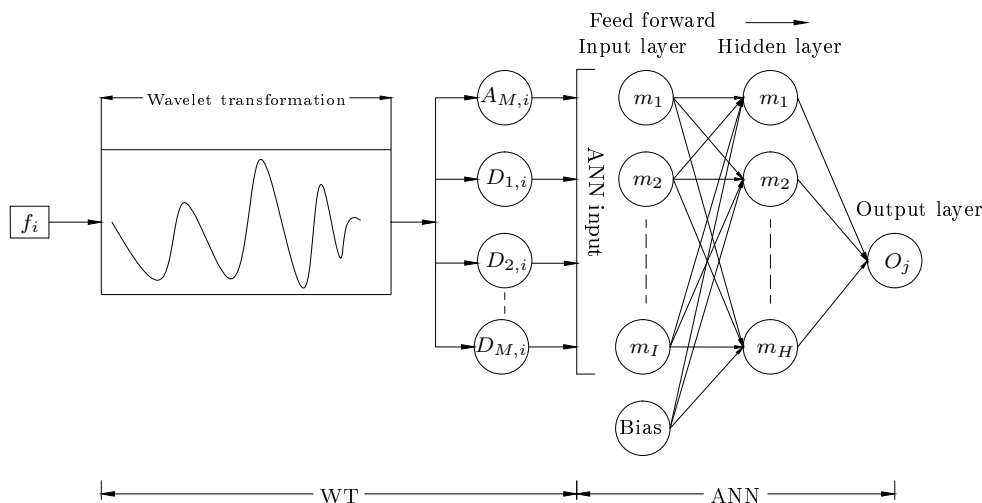
Figure 4.2: Schematic diagram of WA-ANN model

4.3.5   Performance measures for model evaluation

The performance of models is commonly assessed by computing a number of measures of performance or goodness-of-fit statistics. These measures can be characterised as absolute (i.e. expressed in the units of the output variable) or relative (i.e. dimensionless).

In the present study, two absolute metrics were chosen: the root mean square error (RMSE) and the mean absolute error (MAE), which provide an idea of the absolute differences between observed and modelled values in their original unit measures, and are

non-negative metrics:

$$RMSE = \sqrt{\frac{1}{P}\sum_{i=1}^{P}(Q_{si}^{obs} - Q_{si}^{sim})^2} \qquad 4.8$$

$$MAE = \frac{1}{P}\sum_{i=1}^{P}|Q_{si}^{obs} - Q_{si}^{sim}| \qquad 4.9$$

Where Q_{si}^{obs} is observed sediment load, Q_{si}^{sim} is predicted sediment load and P is the number of observations/predictions. These two non-negative metrics have no upper limit where 0 indicates a perfect fit between the observed and predicted values. Unlike MAE, the RMSE is weighted towards higher or lower magnitude events. As the differences between the observed and predicted values are squared, the RMSE measure penalises prediction errors in high flow events compared to low flows, as high flows are generally where the greatest error in model prediction occurs. The RMSE tends to be slightly larger than the MAE, where the magnitude of this difference can also be used to indicate the extent of outliers in the data.

Further, two indices of relative differences were also chosen: the coefficient of determination/Pearson correlation coefficient (R^2) and the Nash-Sutcliffe coefficient of efficiency (NSE), which compare the errors from the selected model with respect to those from a reference model. Both use different benchmark models for comparison, i.e. the mean and persistence.

$$R^2 = \left(\frac{\sum_{i=1}^{P}(Q_{si}^{obs} - \bar{Q}_{si}^{obs})(Q_{si}^{sim} - \bar{Q}_{si}^{sim})}{\sqrt{\sum_{i=1}^{P}(Q_{si}^{obs} - \bar{Q}_{si}^{obs})^2 \sum_{i=1}^{P}(Q_{si}^{sim} - \bar{Q}_{si}^{sim})^2}}\right)^2 \qquad 4.10$$

$$NSE = 1 - \frac{\sum_{i=1}^{P}(Q_{si}^{obs} - Q_{si}^{sim})^2}{\sum_{i=1}^{P}(Q_{si}^{obs} - \bar{Q}_{si}^{obs})^2} \qquad 4.11$$

Where $\bar{Q}_{si}^{obs}$ and $\bar{Q}_{si}^{sim}$ are the mean values of observed and simulated sediment loads. The values of these relative measures are upper bounded to one. A value of 1 represents a perfect match between predicted and observed sediment load. The NSE generally ranges from 0 to 1 although negative values are possible. NSE = 0 indicates that the model is no

better than simply forecasting the mean value. The closer the NSE value to 1, the better the model's performance. The simulated results are normally referred as good when the NSE is higher than 0.75 and satisfactory when it lies between 0.36 to 0.75 [115].

4.4 Model development

It is known that major factors such as data processing, determination of adequate model inputs, choice of suitable network architecture, careful selection of some internal parameters that control the optimization method, stopping criteria, and model validation may affect the performance of ANN models. Hence, these factors were considered during design of the models used in this paper. The ANN and WA-ANN models were developed using the MATLAB tool.

4.4.1 Design of ANN model

Data processing is usually required before it is applied to the neural network models when the neurons have a transfer function with bounded range. The original data are processed through two steps: data normalization and data set partition. In the first step, data are rescaled to a certain interval. The reasons for scaling of the data can be described to ensure that each variable is treated equally in a model and to improve the interpretability of network weights. Following this, the normalised data are usually divided into a training sub-set, a validation sub-set and a testing sub-set. The representativeness of the data sets used for training should be considered, because networks trained with a data set that represents the characteristics of the hydrologic patterns will achieve higher generalizability. In this study, the following data sub-sets are applied (Tab. 4.3):

1. 60, 70 and 80% of the training data sub-set is randomly selected from the entire available data for the network. The remaining 40, 30, and 20% of the data is used for testing and validation.

2. Data from the earlier periods are used for training, and data from later periods for testing and validation.

Based on preliminary results, it was found that the ANN model could perform well using (70%, 15%, and 15%) data on a random basis and (1969-1995, 1996-2002, and 2003-2008) data on a systematic basis for the training, testing and validation, respectively. It

also shows that the selected training data length covers all hydrological variations for the study period (1969-2008) at Besham Qila and it is sufficient for training the ANN model. In the following sections, we present only the calculated results based on the randomly selected sub-set, referred to above.

Table 4.3: Data used for model design

Data sub-sets	Training	Testing	Validation
Randomly selected from the whole data set	60%	20%	20%
	70%	15%	15%
	80%	10%	10%
Based on the time series data	1969-1995	1996-2002	2003-2008
	1969-1990	1991-2000	2001-2008
	1969-2000	2001-2004	2005-2008

Using flow discharge, precipitation, temperature and pan evaporation as input parameter, we found that the flow discharge is one of the most important factors influencing suspended sediment concentration at Besham Qila. It is most likely that at Besham Qila flow discharge alone implicitly represents these hydrometeorological parameters of the upper Indus basin in the modelling process. [8] suggest that in sediment load estimation for the Indus River, a discharge-SSC relationship performs better than a discharge-SSL relationship. If the model output $S_{(t)}$ presents sediment concentration at time t, whose unit is a day, and water discharge at the same time is $Q_{(t)}$, the five following input combinations are evaluated using ANN to identify the best relation between sediment and water discharge:

(a) $Q_{(t)}$

(b) $Q_{(t)}$, $Q_{(t-1)}$

(c) $Q_{(t)}$, $Q_{(t-1)}$, $Q_{(t-2)}$

(d) $Q_{(t-1)}$ $Q_{(t-2)}$ $Q_{(t-3)}$

(e) $Q_{(t)}$, $Q_{(t-1)}$, $Q_{(t-2)}$, $Q_{(t-3)}$

The last four input-combinations examine the time lag between the water discharge and sediment load, which is based on the observed data with a lag time of up to three days at Besham Qila. This lag time also occurred at other upper gauge stations.

Many studies have shown that an MLP with one hidden layer is capable of approximating any finite nonlinear function with very high accuracy. The MLP used in the present study consists of one hidden layer. Following Fletcher and Goss' (1993), the number of neurons in the hidden layer varies from 3 to 9. The primary purpose of activation functions for the hidden units, in contrast to linear transfer functions, is to introduce a non-linearity into the neural network. In this paper, we test the model architecture with *logsig*, *tansig*, *purelin* and *radbas* transfer functions. The networks are trained using four different algorithms, namely Levenberg-Marquardt (*trainlm*), scaled conjugate gradient backpropagation (*trainscg*), gradient decent backpropagation (*traingd*) and Bayesian regularization backpropagation (*trainbr*).

Since there is no special rule for ANN model development, trial and error method is usually employed to choose an appropriate ANN model. In developing the most accurate training model architecture, the individual cases are first ranked according to the magnitude of two absolute metrics (RMSE, MAE) and two indices of relative differences (R^2, NSE). The best individual model has the minimum (RMSE, MAE) and the maximum (R^2, NSE). Tab. 4.4 shows the best MLP architectures with their performance indices. It can be seen from the table that the network trained by Levenberg-Marquardt's approach performs best with the input combination ($Q_{(t)}$, $Q_{(t-1)}$, $Q_{(t-2)}$) which comprises seven hidden neurons using a non-linear *tansig* transfer function and linear activation function for the output. In Tab. 4.4, the best statistical values for this network are highlighted in bold.

Table 4.4: Performance parameters of the best ANN architectures using different learning methods

Training method	Model inputs	Neurons	Transfer function		R^2		RMSE (ppm)		NSE	
			First	Output	Train	Test	Train	Test	Train	Test
	a	3	radbas	purelin	0.767	0.759	680.8	709.5	0.768	0.759
	b	5	tansig	purelin	0.770	0.759	668.2	715.4	0.77	0.759
LM	**c**	**7**	**tansig**	**purelin**	**0.773**	**0.794**	**676.6**	**615.1**	**0.773**	**0.793**
	d	5	tansig	purelin	0.767	0.773	675.9	665.4	0.767	0.773
	e	6	tansig	purelin	0.774	0.740	667.6	729.1	0.775	0.739
	a	3	tansig	tansig	0.694	0.704	1000.9	960.8	0.516	0.532
	b	4	tansig	tansig	0.607	0.635	894.8	850.4	0.618	0.608
SCG	c	5	tansig	tansig	0.721	0.740	786	725.9	0.708	0.727
	d	6	logsig	purelin	0.721	0.718	832.3	840.3	0.657	0.652
	e	6	logsig	purelin	0.724	0.728	855.1	914.1	0.638	0.628
	a	3	logsig	tansig	0.764	0.741	692.9	754	0.763	0.739
	b	4	tansig	purelin	0.767	0.766	684	713.3	0.767	0.764
GDS	c	7	tansig	purelin	0.769	0.796	681	613	0.77	0.794
	d	6	tansig	tansig	0.766	0.720	690.9	712.4	0.765	0.706
	e	7	logsig	tansig	0.769	0.738	673.4	672.3	0.769	0.728
	a	3	tansig	purelin	0.764	0.730	685.7	795.3	0.764	0.729
	b	5	tansig	tansig	0.770	0.752	676.5	756.1	0.772	0.749
BR	c	6	logsig	tansig	0.778	0.764	676.9	683.3	0.778	0.761
	d	7	tansig	purelin	0.771	0.733	676.8	782.8	0.772	0.73
	e	9	tansig	tansig	0.785	0.734	661.8	742.7	0.785	0.733

4.4.2 Design of WA-ANN model

The proposed WA-NN models consist of a three layer feed forward perceptron structure so that the first layer is the wavelet neurons unit with the inputs of time series sub-signals obtained via a wavelet transform. This means the flow discharge signals are firstly decomposed into sub-signals with different scales, i.e. one large-scale sub-signal and N small-scale sub-signals (depending on the decomposition level) in order to obtain temporal characteristics of the input time series. The number of neurons in the input layer is then determined with $N + 1$. This study deals with some irregular mother wavelets such as $db1$ (Daubechies wavelet of order 1), $bio3.5$ (biorthogonal wavelet of order 3.5) and $coif1$ (coiflet wavelet of order 1). These wavelets are used to decompose the five input combinations up to eight levels (2-4-8-16-32-64-128-256 days). The eight levels are selected to encounter the effects of sediment deposition post monsoon in the channel of the Indus River. The excess amount of sediment transported during the rising water discharge is eroded from the material deposited in the river channel during a preceding flood situation [22]. These types of effects in SSL not only depend on the water availability and river transport capacity but also load availability, which is complexly related to the seasons of occurrence [26]. This means that the sediment transport is not only dependent upon the momentary discharge but also its history.

Fig. 4.3 shows the variation of the coefficients R^2 and NSE by applying different input combinations decomposed into different levels with the three mother wavelets mentioned above. It can be seen that the overall performance of $db1$ wavelet is the best compared to $bio3.5$ and $coif1$ wavelets. Tab. 4.5 summarizes the performance parameters of the best WA-ANN architecture using the $bd1$ wavelet mother function. It can also be seen from this table that the WA-ANN performed best with the input combinations (c): ($Q_{(t)}$, $Q_{(t-1)}$, $Q_{(t-2)}$) decomposed into 7 levels (128 days) using 24 neurons with a $tansig$ transfer function for the hidden layer and a linear activation function for the output layer. The decomposition of data from approximately half year (7 levels) to extract important information from the past indicates a complex nonlinear behaviour of sediment transport process at the upper Indus River.

The three models, SRC, optimum ANN, and optimum WA-ANN models were used to estimate SSC for the days when SSC sampling was performed. The estimated SSC was statistically evaluated and compared with the measured mean annual, cumulative and distinct daily SSC samples. In order to obtain daily SSC time series data, the best statistically performing model was used to estimate SSC data for the dates when sediment sampling was not performed, i.e. for the dates when SSC is missing. The newly developed daily SSC time series data composed of measured and simulated values was used to obtained annual sediment load for the Besham Qila gauge station. The annual sediment load for Besham Qila was also compared with Tarbela dam's annual hydrographic survey.
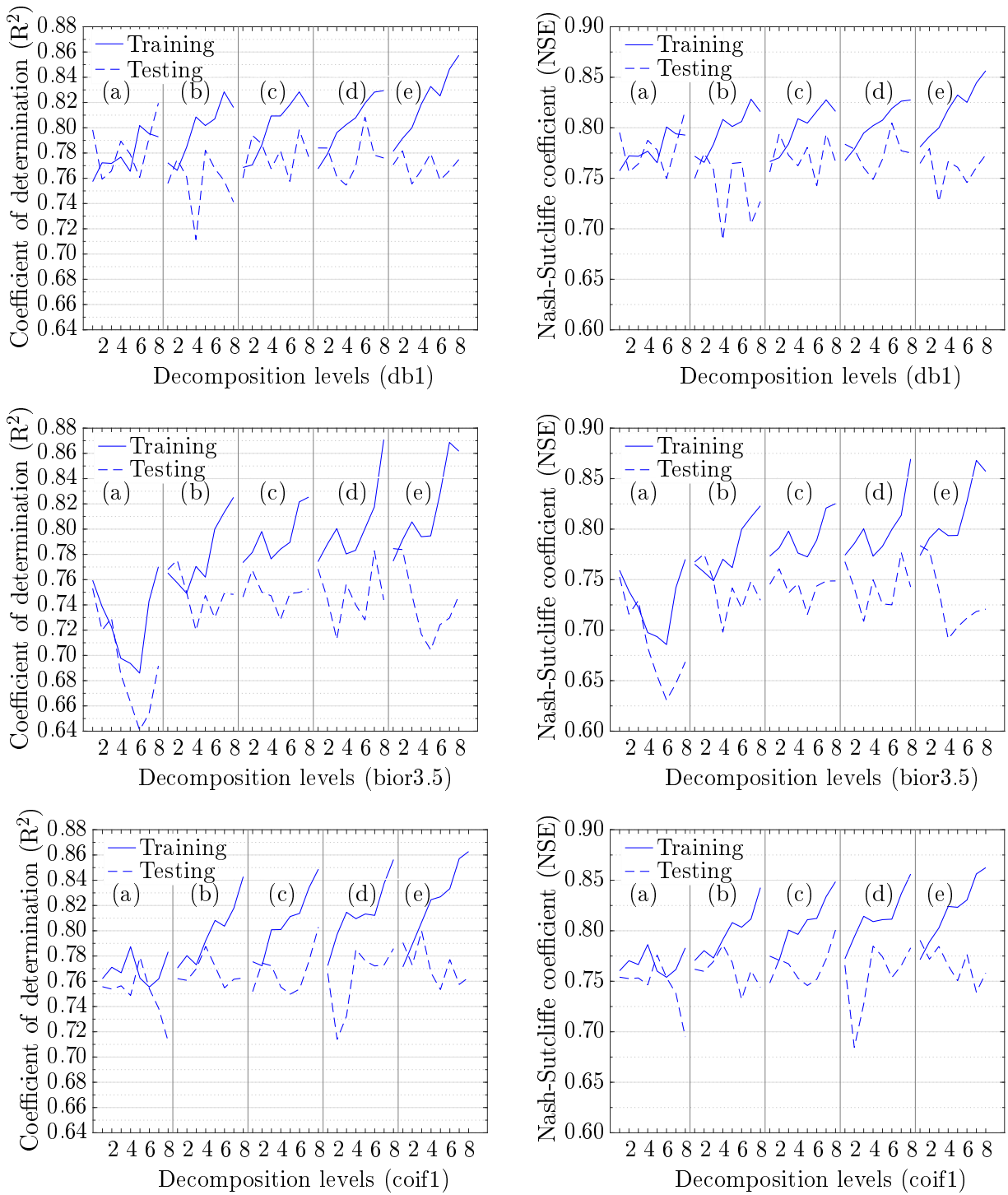
Figure 4.3: Variation of coefficient of determination (R^2), left, and Nash-Sutcliffe efficiency (NSE) coefficients, right, using three different wavelet functions

Table 4.5: Performance indices of the best WA-ANN model using Daubechies ($db1$) wavelets

Model inputs	Decomposition level	Neurons	Transfer function		R^2		RMSE (ppm)		NSE	
			First	Output	Train	Test	Train	Test	Train	Test
c	7	24	tansig	purelin	0.828	0.792	604.4	615.4	0.83	0.79

4.5 Results and discussion

4.5.1 Time series of suspended sediment concentration and suspended sediment load

To evaluate the performance of the designed models in predicting time series of SSC in the study domain, we compare the results obtained from these three models with the measurements.

Tab. 4.6 illustrates the correlation for these prediction methods with the statistical performance indices between predicted results and observed data in the whole data set. It is obvious that the two-equation SRC model (Eq. 4.2), which fitted the data by separating SSC for low and high flows, provided slightly better results than the single-equation SRC (Eq. 4.3). However, there was no significant difference in the statistical parameters between these two SRC models. Using the designed ANN model we achieved a better agreement between predicted and observed SSC at Besham Qila. More particularly, among all models the designed WA-ANN produced the best predictions. In the following, we try to explain the possible reasons for difference in the model performance.

Table 4.6: Statistical performance indices of the SRC, ANN and WA-ANN models for computing the SSC

Model	R^2	RMSE (ppm)	MAE (ppm)	NSE
SRC-1	0.706	1005.3	495.4	0.50
SRC-2	0.706	964.6	509.0	0.54
ANN	0.757	698.4	373.2	0.76
WA-ANN	0.81	625.2	356.3	0.81

As can be seen from Tab. 4.1 and Tab. 4.2, the observed SSC as well as the annual sediment load estimated by conventional methods vary widely. Comparison of the observed data in the high flow years shows a sudden decrease of SSC during the floods period (May, June and August) in 1983 at Besham Qila (Fig. 4.4). These enormous variations

could be explained by the magnitude of complexity in sediment transport processes in the Indus River. This complexity in transport processes may be caused by hydrological variations and the hysteresis phenomena, where, for example, the same discharges can produce different SSC at different times. Different factors can be associated with the hysteresis phenomena in the Indus, such as: (1) The fluvial erosion and transport processes interacting with some other sediment producing process; (2) Temporary sediment storage in the main river channel [22]; (3) Aggradation and degradation phases of land slides [23]; (4) An average 5-10 high flow waves of an average 10-12 days during the monsoon period; (5) Different transit times of discharge and sediment and their different travel time from several sources to the gauge stations. In addition to the flow discharge magnitude, these factors may influence the SSC at Besham Qila. Unfortunately, applying simple relationships between water flow discharge and sediment concentration, the SRC models are unable to adjust and model these impact factors. Consequently, in long term sediment load estimates, SRC models are unable to supply good results for sediment variability scenarios.

As remarked on by [116], factors that exert influence on sediment transport processes are highly variable in hydraulic and hydrological conditions of stream flows and patterns associated with river nature. In contrast to SRC methods, ANNs do not need to make assumptions about the relationships among inputs and outputs. ANNs learn from data examples presented to them in order to capture the subtle functional relationships among the data. ANNs are thus well suited to modelling the complex behaviour of sediment transports which, by their very nature, exhibit extreme variability. Using a suitable input combination, the ANN model is able to handle the hydrological variations in sediment transport load at Besham Qila. These variations consist of alternative cycles of wet and dry seasons. Normally, in a dry season, SSC is low due to less run-off and size of area as well as time covered by the run off. In wet seasons, the contrary holds. The hydrological variation patterns behave in a systematic way and the ANN has the ability to recognise these systematic patterns.

Although the estimation efficiency of the ANN is better than SRC, it might be that the ANN alone is still not good enough to model the hysteresis phenomena in the study domain, which consists of the upper glacierized sub-basin, lower sub-basin and lower reached sub-basin [19]. When flows in these three sub-basins are not well synchronized, especially during monsoon seasons, it causes strong hysteresis with many peaks in discharge. In this case, using WT techniques, the decomposed time series of the observed data present different periodic components. Each of the wavelet components makes a distinct con-

tribution to the original time series. These series are employed as inputs to constitute the WA-ANN model for SSC forecasting. Based on the performance of SRC, ANN and WA-ANN models in terms of R^2, RMSE, MAE and NSE, it is clear from Tab. 4.6 that the statistical performance of WA-ANN is best with $R^2 = 0.81$, RMSE = 625 ppm, MAE = 356 ppm, and NSE = 0.81 for SSC. In addition, a temporal resolution of approximately half year (7 levels of data decomposition) with a lag time of two days for a gauge station (Besham Qila) located down stream of these sub-basin can reduce the variations in SSL reconstruction. The reconstruction variations increase when conventional methods (SRC and ANN) do not include the temporary sediment storage in the main river channel and different transit times of discharges and sediment from their sources to the gauge in the modelling process. Therefore, the quality of hydraulic design based on poor estimation ultimately can affect the accuracy and subsequent studies along-with associated benefits.

As mentioned above, measurements of SSC were not conducted daily. However, applying SRC, ANN and WA-ANN models we were able to create the whole data set for the daily SSL over 38 years (1969-2008). To estimate the accuracy of each model we compared the available daily observed SSL data with the calculated results. It is clear from Tab. 4.7 that the best statistical indices, $R^2 = 0.85$, RMSE = 34,900 ton/day, MAE = 17,500 ton/day, and NSE = 0.85, for the daily SSL were obtained using WA-ANN model. Further, Fig. 4.4 shows an exemplary comparison between the SSL observations and the WA-ANN results in the years 1983 (year with the exceptional sediment transport) and 1984 (year with the longest monsoon period). Due to the lack of data after flooding, although the variation between observation and calculation is still large, values for the coefficient of determination $R^2 = 0.68$ (for the year 1983) and $R^2 = 0.91$ (for the year 1984) indicate that the WA-ANN model was able to simulate the hydrological variations and handle the hysteresis phenomena at Besham Qila quite well.

Table 4.7: Statistical performance indices of the SRC, ANN and WA-ANN models for computing the daily SSL

Model	R^2	RMSE (ton/day)	MAE (ton/day)	NSE
SRC-1	0.760	7.80×10^5	3.04×10^5	0.402
SRC-2	0.766	7.38×10^5	2.92×10^5	0.480
ANN	0.814	4.45×10^5	1.96×10^5	0.814
WA-ANN	0.852	3.94×10^5	1.75×10^5	0.852
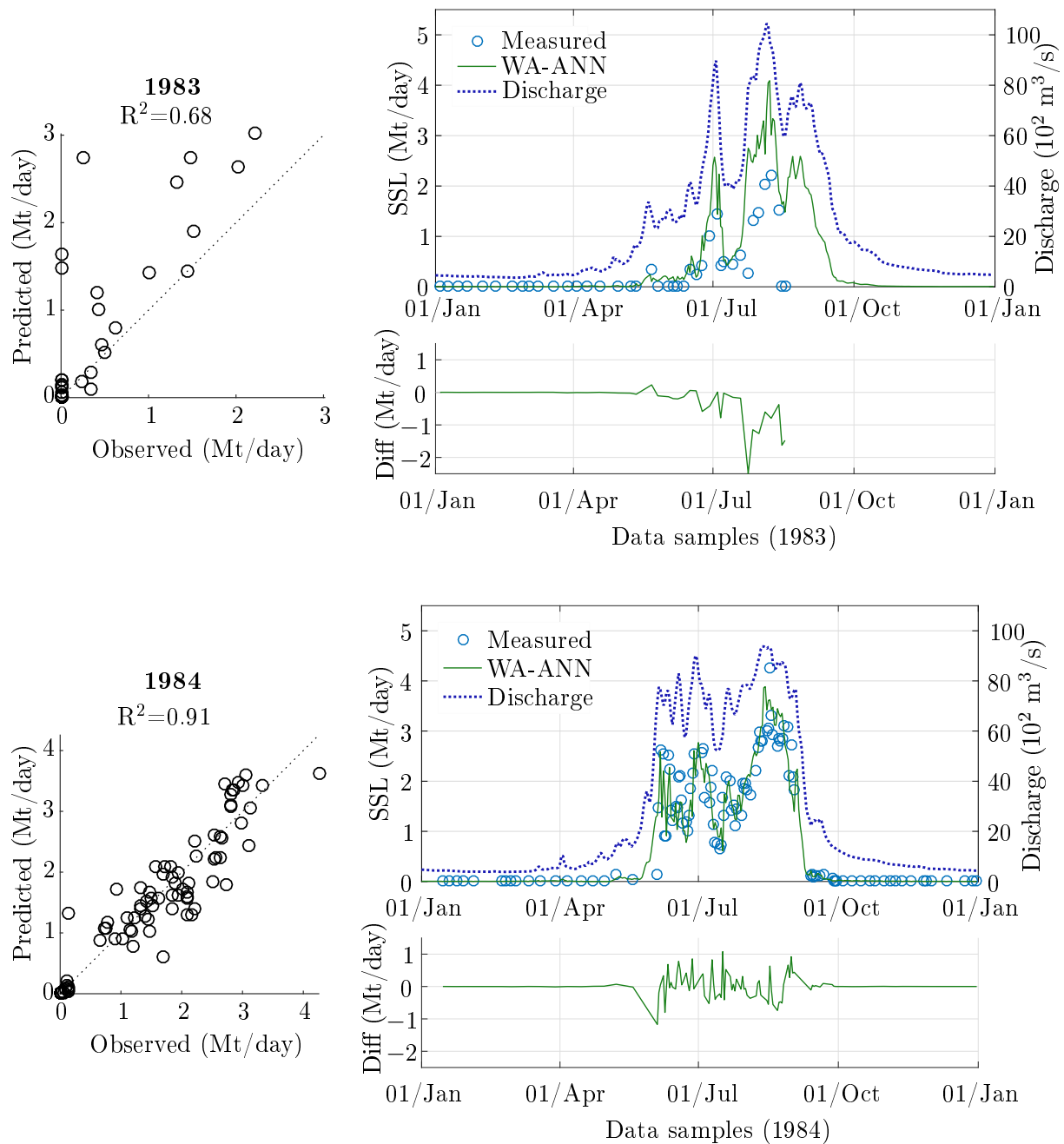
Figure 4.4: Comparison of the daily observed SSL and calculated results of the WA-ANN model in the years 1983 and 1984. 1984 was a longest monsoon year of the analyzed record, whereas in 1983 sediment load was blocked by a landslide upstream of the gauge station.

From the observed data of flow discharge and SSC, we estimated the total mass of suspended sediment sampled annually. Fig. 4.5 presents a comparison between these masses and the calculated results in the considered time period. Overall, the ANN and

WA-ANN models provide better results than the SRC. However, all three models failed to yield reliable outcomes for several exceptional events. Maximal deviation between samples and calculations is observed in the year 1983, where the mass calculated by WA-ANN is overestimated by 90%. The ANN overestimated the mass value by 98% and SRC by up to 155%. It should be emphasized that due to scarce data collected in this year (see Fig. 4.4) both the ANN and WA-ANN were not trained well for such exceptional events. However, it would be possible to resolve the issue by using more data to design the whole nets or developing another net for exceptional events.

Considering the whole time period of 38 years, the mean deviations are 13%, 18% and 36% respectively for WA-ANN, ANN and SRC. Following [117], the typical cumulative measurement errors associated with discharge and SSC should remain in the range of 10 to 15%. The models with an error in the mentioned range should be considered as reliable [31]. For this reason, the designed WA-ANN proved to be the best model among those tested for SSL in the study domain.

4.5.2 Sedimentation in Tarbela reservoir

Sediment load (consisting of SSL and bed load) from the upper Indus basin passes through Besham Qila before entering in Tarbela dam. In the period from 1980 to 2005, the hydrographic survey in the reservoir was conducted annually with systematic sounding method along the range lines [118]. Based on the geometrical change, we were able to estimate the mass of deposited sediments in the ponding area. Further, the bed load at Besham Qila is considered equal to 10% of the SSL [57]. Following [19], on average, 90% of the annual sediment load was trapped in the reservoir, which is approximately equal to amount of the incoming SSL from Besham Qila. Based on this assumption, the developed models can also estimate the annual and cumulative masses of the deposited sediment in the reservoir. The estimated results were also compared with the surveyed data. It is obvious from Fig. 4.6 that the WA-ANN model provides better agreement with the survey than the conventional SRC model. Using the SRC model, the mean variations amount to 43% and 40% respectively for the annual and cumulative deposited sediment. Applying WA-ANN, these variations reduced to 12% and 7%.
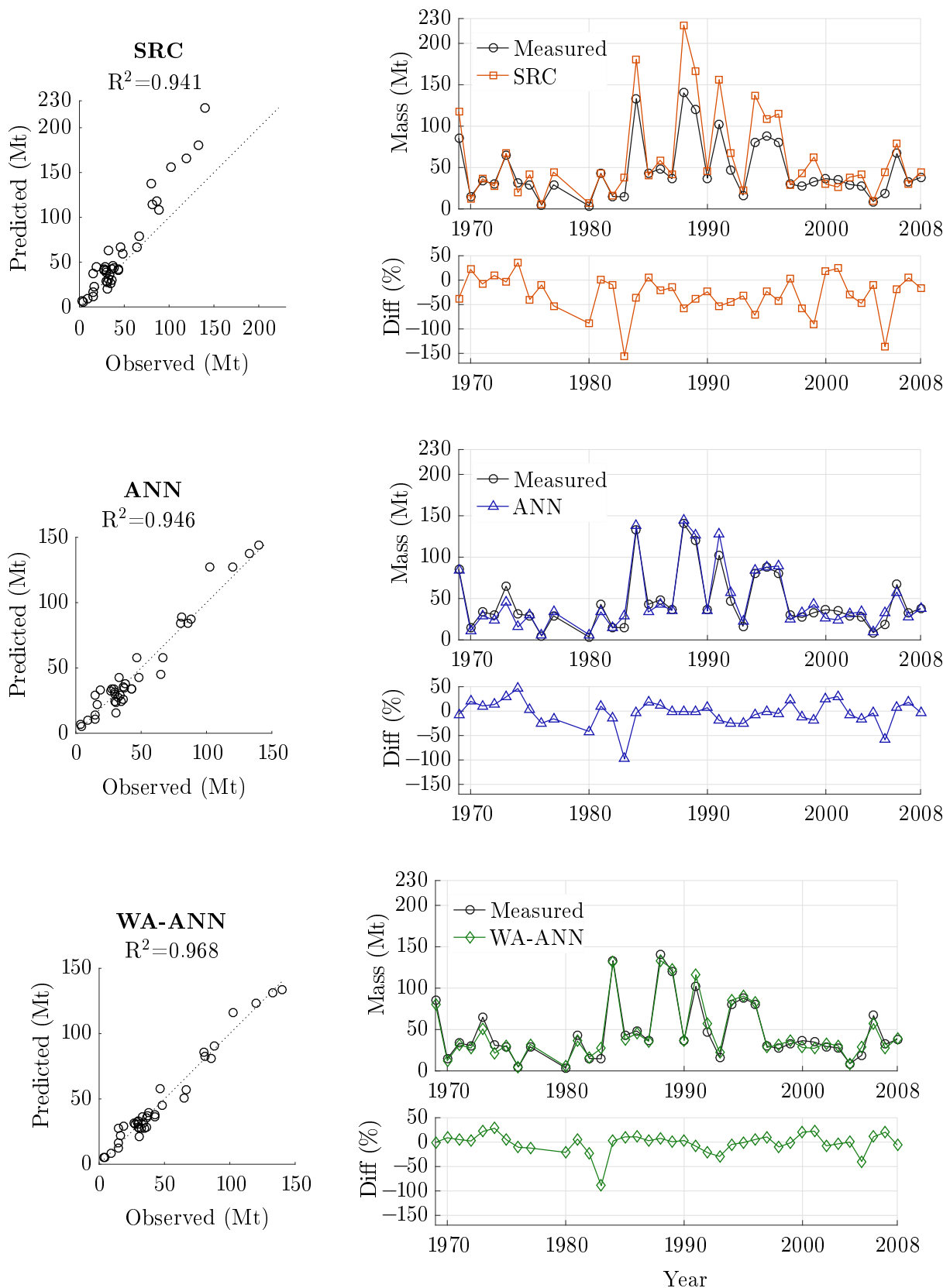
Figure 4.5: Comparison between the mass of suspended sediment sampled annually and computed results using the SRC, ANN, and WA-ANN models

Using WA-ANN, a curve for annual suspended sediment load and a power trendline were reconstructed for the time period (1969-2008). It can be seen from Fig. 4.7 that the calculated annual SSLs vary over the time in a range from 90 Mt to 270 Mt depending on hydromorphological conditions. The mean value of annual SSL at Besham Qila using the WA-ANN model amounts to approximately 160 Mt, which is much smaller than the values estimated by other authors (see Tab. 4.1). The reasons for the decreasing trend in sediment load over time at Besham Qila may be: (1) decrease in sediment erosion in catchment area; (2) a continuous substantial sediment storage in the relatively flat Tibetan Plateau and the Indus valley between Partab Bridge and Shatial (Shatial is about 150 km upstream of Besham Qila) [19]: (3) good catchment management practices [119]. In addition there are neither hydraulic structures at the upper Indus River/basin, nor land use changes that might have affected the situation. With regard to the planned hydraulic structures in the study area, the parametrically decreasing trend in sediment load urges against using unmodified past sediment load data as the boundary condition for future reservoir sediment studies.
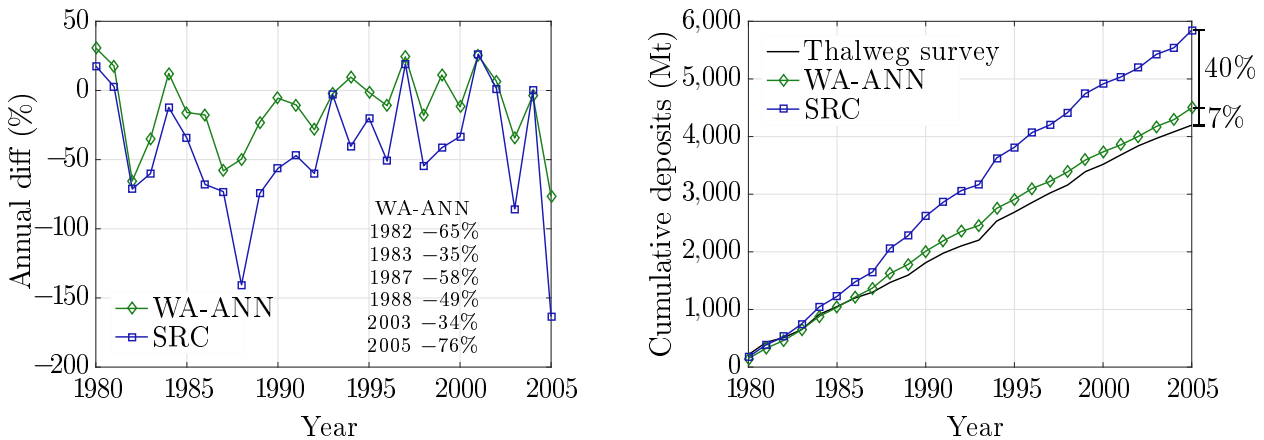
Figure 4.6: Comparison of the calculated results with hydrographic survey of Tarbela dam

4.6 Conclusion

We found that WA-ANN can precisely predict the sediment load time series with a temporal resolution of more than one level for the Indus, which has a complex sediment transport process due to temporary sediment storage, strong hysteresis phenomena and landslides. The new estimate of only 160 Mt yr^{-1} at Besham Qila is close to real time. The annual yield of sediment load at Besham Qila is lower than the published estimates, and can be attributed to the substantial sediment storage in the relatively flat Tibetan Plateau

and the Indus River Valley between Partab Bridge and Besham Qila. Consequently, it suggests that the past sediment load series cannot simply (without modification) be reapplied to arrive at sedimentation predictions in the upper Indus River. Therefore, our study may contribute to the development of sediment management strategies for existing, under construction, and planned water related structures by setting precise sediment load boundary conditions. This particularly applies in Pakistan, where approximately 14,000 MW hydropower schemes are under construction on the Indus River. The existing reservoirs are also endangered due to sedimentation problems, which may need new reservoir operational rules.
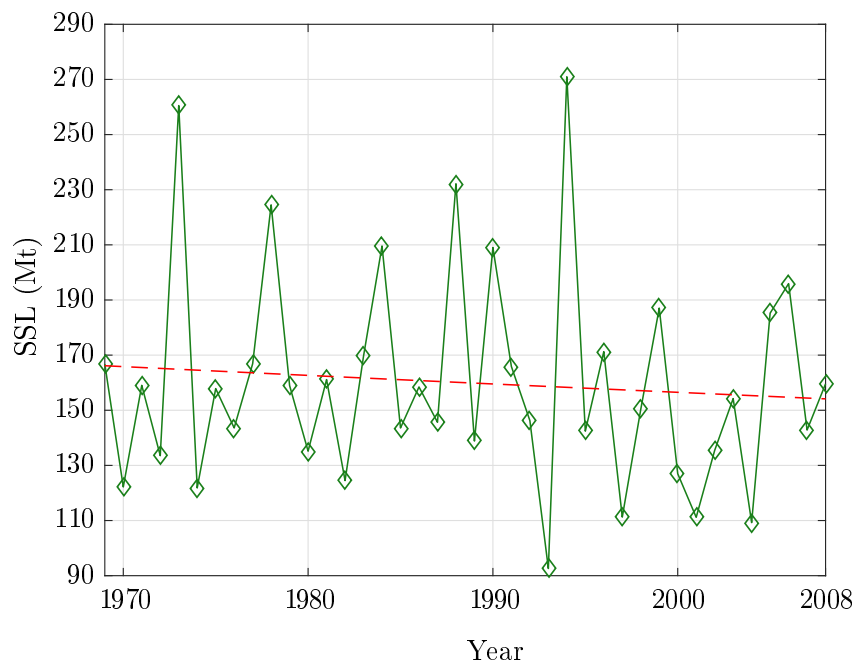
Figure 4.7: Annual suspended sediment load calculated by the WA-ANN model for Besham Qila and its power trendline

Chapter 5

Variability and Trend Detection in the Sediment Load of the Upper Indus River

Abstract: Water reservoirs planned or constructed to meet the burgeoning energy and irrigation demands in Pakistan face a significant loss of storage capacity due to heavy sediment load from the upper Indus basin (UIB). Given their importance and the huge investment, assessments of current UIB sediment load and possible future changes are crucial for informed decisions on planning of optimal dams' operation and ensuring their prolonged lifespan. In this regard, the daily suspended sediment loads (SSLs) and their changes are analyzed for the meltwater-dominated zone up to the Partab Bridge and the whole UIB up to Besham Qila, which is additionally influenced by monsoonal rainfall. The gaps between intermittent suspended sediment concentration (SSC) samples are filled by wavelet neural networks (WA-ANNs) using discharges for each site. The temporal dynamics of SSLs and discharges are analyzed using a suite of three non-parametric trend tests while the slope is identified using Sen's slope estimator. We found disproportional spatio-temporal trends between SSLs and discharges caused primarily by intra-annual shifts in flows, which can lead to increased trap efficiency in planned reservoirs, especially upstream of Besham Qila. Moreover, a discernible increase in SSLs recorded at Partab

Bridge during summer is being deposited downstream in the river channel. This is due to a decrease in river transport capacity in the monsoonal zone. These findings will not only help to identify these morphological problems, but also accurately anticipate the spatio-temporal changes in the sediment budget of the upper Indus River. Our results will help improve reservoir operational rules and sediment management strategies for existing and 30,000-MW planned dams in the UIB.

5.1   Introduction

Estimation of the suspended sediment loads (SSLs) is important in the design and operation of water structures and in the planning of sediment management (yield reduction, routing and removal) to preserve their live storage capacities [32, 6, 33, 34, 35]. The temporal variations and changes in SSLs are also an important indicator of the effectiveness of existing watershed management practices or tectonic and land-sliding activities in the catchment area. Being a water stressed country amongst the top ten most climate-affected countries [55, 56], Pakistan has a total water storage capacity of only 30 days (equal to 10% of the annual available water), which has been depleting due to heavy sedimentation transported through the Indus River system from the young Hindukush-Karakoram-Himalaya (HKH) ranges [45]. For example, amongst three big reservoirs, the Tarbela dam has lost 35% of its storage capacity since 1974 due to trapping of approximately 8 km^3 of sediment in the reservoir ponding area [108]. The Warsak dam constructed on Kabul River has filled with 60 Mt of SSL annually in the 30 years after its construction, and no structural or non-structural remedies can reverse its depleting storage capacity [10]. Mangla dam, the second largest Pakistani water storing facility, had an initial storage of 7.1 billion m^3 (BCM), which was reduced to 5.6 BCM in 2005 due to sedimentation. In 2009, an additional 9 m rise of the dam increased the storage to 9.1 BCM, which cost one billion USD over five years. However, the rise created technical problems such as an increase of seepage through the dam embankment in addition to the displacement of 45,000 people living in the vicinity of the dam [120]. In view of the transboundary nature of the source of water, such a decrease in water storage capacity in Pakistan exacerbates the instability and geopolitical tensions of the region [46]. Hence, the assessment of prevalent sediment patterns and their projected changes are vital for the optimization of sediment management processes to ensure the water and food security in the country and to regulate the transboundary water availability pressures.

Although there are many studies assessing the climate-induced adverse impacts on

the UIB river flow patterns [20, 36, 37, 38, 21, 39, 40], few have investigated the impact of flow pattern changes on the sediment load capacity [41, 42]. Furthermore, the studies conducted in this regard differ widely in their suggested estimates. For instance, the SSL to Tarbela Dam (the country's largest) or at the immediately upstream Besham Qila discharge gauge is reported to range from 200 Mt y^{-1}–675 Mt y^{-1} over the past 50 years (Tab. 5.1). Such uncertainty leads to poor design quality of the operating rules for existing dams and those under construction. Moreover, the studies have generally estimated the SSL by using empirically-developed sediment rating curves (SRCs), whose accuracy is limited as they oversimplify the relationship between the suspended sediment concentration (SSC) samples and the observed discharges [104, 8, 74].

Table 5.1: Estimates published on the suspended sediment load (SSL) of the upper Indus River.

Suspended Sediment Yield (Mt yr^{-1})	Estimated by
480	[11]
400	[12]
475	[13]
200	[14] reported by [15]
675	[16]
300	[17]
200	[18]
197[1]	[19]
138[2]	[19]
200	[6]

The accuracy of SRCs is also limited since it does not model the complex sediment transport processes related to hysteresis phenomena and marked hydrological variations within the UIB, such as: (a) the fluvial erosion and transport processes, which interact with other sediment-producing processes; (b) temporary sediment storage in the main river channel [22]; (c) aggradation and degradation phases of landslides [23]; (d) on average, 5–10 high flow waves of an average 10–12-day duration during the monsoon period; (e) different transit times of discharge and sediment and their different lag times from several sources to the gauge stations. Given that SRCs are employed in the estimation process, there may be a marked compromise in the design quality of reservoir sedimentation prevention measures, as apparent from the current sedimentation rate of the Tarbela and Mangla dams. Since the assessment of the SSL patterns is important for the management of water-related structures, watershed management practices and the sediment

[1]Besham Qila
[2]Partab Bridge

budget of the Indus, it is necessary to detect the temporal changes in sediment transport, which are influenced by the river discharge responses and hysteresis phenomena, requiring frequent discharge and SSC observations.

As opposed to the discharge time-series typically available on a daily resolution, the SSCs are intermittently sampled, which can affect the trend outcome needed to reconstruct the non-observed days. However, to deal with the non-linear nature of the time series, the wavelet transform coupled artificial neural networks (WA-ANNs) outperform SRCs, since they are able to model theoretically any kind of relationship between the dependent and independent variables without having to know their physical relationship [105, 117, 30, 29, 121, 122]. The wavelet transform decomposes the data time series up-to J levels in the time, space and frequency domains and reveals the information from a given data scenario [28]. The temporal scale of the decomposition provides information on temporary storage, aggradation and degradation phases, high flow waves and transit time of the sediment load in the detail coefficients. Given these details, i.e., the detail coefficients along with the approximation coefficient, ANN precisely models the hysteresis phenomena. WA-ANNs have been used successfully over the last decade for reconstructing the missing data by adjusting the hysteresis phenomena in sediment load processes [123, 124, 88, 125].

In assessing temporal dynamics of SSLs and discharges, non-parametric tests are assumed to be more robust as compared to their parametric counterparts, in view of the fact that the sediment load data are not normally distributed, owing to the highly nonlinear nature of the sediment transport processes. However, several non-parametric tests may also result in distinct estimates, which requires employing a suite of successful non-parametric methods and then quantifying their associated uncertainty to build more confidence in the results.

Analyzing discharges and SSCs at two different sites over the past 50 years, this study for the first time shows how changes in the flow patterns are affecting the sediment transport capacity of the UIB for the meltwater-dominated zone (up to Partab Bridge site) and for the whole UIB (up to Besham Qila), which is additionally influenced by the summer monsoonal rainfall regime. The gaps between intermittently sampled SSCs are filled using the wavelet transforms coupled with the artificial neural networks (WA-ANNs). The temporal discharge and SSL dynamics are robustly assessed using a suite of three widely-used non-parametric approaches, including: (1) the innovative trend analysis (ITA), which can analyze the trends in low, medium and high annual SSLs without

requiring any assumptions, such as serial correlation, non-normality, sample numbers and others [47]; (2) the Mann–Kendall (MK) and the seasonal Kendall (SK) tests together with Sen's slope method; the MK test detects a trend in a time series without requiring normally-distributed input data [48, 49]; Sen's slope method estimates its true slope, while SK analyzes annual trends by removing the seasonal cycles in a time series; (3) a change point detection test, which reveals the changing tendency in the SSL series on monthly and annual scales [50, 51]; (4) mean monthly variations, which detect monthly changes based on differences from the (a) first and last decades and (b) monthly regression equations of the analyzed records.

5.2 Study area and data description

With a total length of 2,880 km and a drainage area of 912,000 km^2, the Indus River is one of the largest in south Asia. It starts from China and then travels through India and across the whole of Pakistan, finally draining into the Arabian Sea. The drainage of the Indus River is divided into upper and lower parts, typically at the Besham Qila discharge gauge or around 65 km downstream at, so far, its only reservoir, Tarbela, which is one of the largest earth-filled dams in the world (Fig. 5.1). The Besham Qila site located at an elevation of 580 masl drains the mostly high-altitude area of 165,515 km^2, 12% of which is covered with the Hindukush-Karakoram-Himalaya (HKH) glaciers and permanent ice, while the seasonal snow cover varies between 3 and 67% [126, 39, 127]. Mean annual discharge of the UIB at Besham Qila is 2,405 m^3/s, which constitutes roughly half of the annual surface water availability in Pakistan [39, 127]. More than 70–80% of such discharge is generated from the melting of snow and glaciers, making the Indus River amongst the most melt-water-dependent rivers in the world [46].

The second study site at Partab Bridge is located at an elevation of 1250 masl about 300 km upstream of Besham Qila, draining around 95% of the cryospheric region and contributing around 75% of the Besham Qila flows. The rest of the Besham Qila flows are mostly received from the monsoonal rainfall from July–September. This 300-km river reach, Partab Bridge to Besham Qila, has gained in importance due to the many planned hydraulic structures. For example, the tenders for three major hydropower projects, Bunji 7100 MW (190 m high), Bhasha dam 4500 MW (272 m) and Dasu 5400 MW (242 m), have been completed for construction located downstream of the Partab Bridge gauge [128]. In addition, the river reach contains huge sediment deposits due to landslides and tectonic activities.
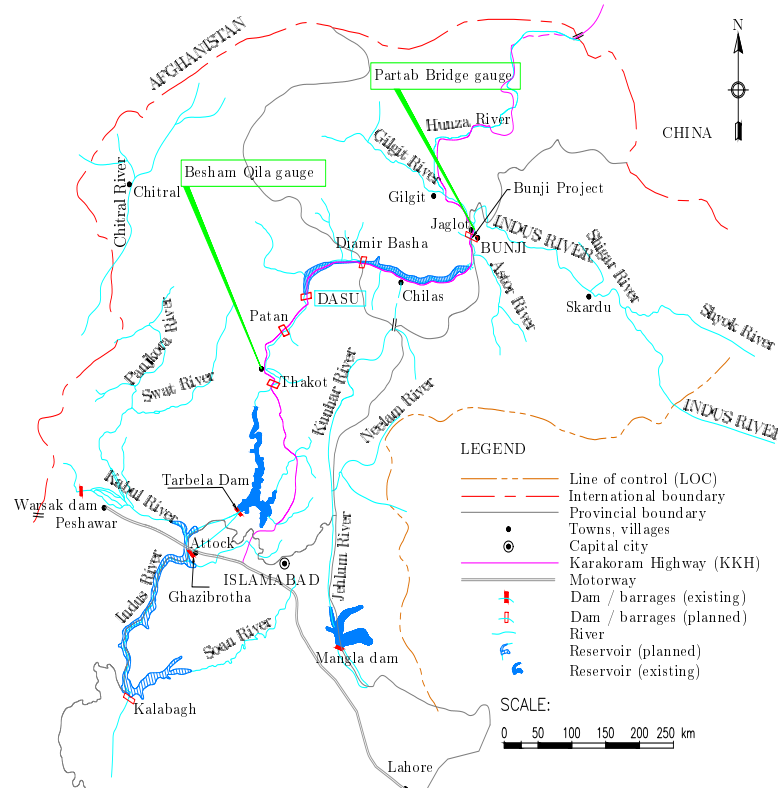
Figure 5.1: Locations of study gauges in the study area. Modified from [6].

Since both gauges feature large drainage areas, overall variations in their discharges
and SSCs are not as abrupt as in the small catchments, but such variations are still large
(Tab. 5.2), indicating the occurrence of frequent hydrological events within the UIB. For
instance, 1973, 1988 and 1994 were the exceptional flow years at Besham Qila with a
total volume of 98.95, 95.31 and 94.88 billion m^3 (BCM), respectively (Fig. 5.2). The
year with the highest peak flow was 1984 with a volume of 89.33 BCM. In contrast, only
a 61.54 BCM flow volume was observed in 1982, distinguishing it as an extremely low
flow year. For Partab Bridge, the exceptional flow years were 1973, 1994 and 1990 with a
total volume of 76.5, 69.7 and 69.6 BCM, respectively. On the other hand, 1965 and 1982,
with a volume of 42.16 and 46.8 BCM, respectively, were the extremely low flow years.
Based on flow patterns, the UIB can be classified into a low flow cycle of 1974–1977 (dry
period) and a high flow cycle of 1988–1992 (wet period) with their annual average volume
being 71 and 85 BCM, respectively. In drought years, with wet winter and dry summer,
the share of glacier melt increases, maintaining the water supply to the Indus River [46].

The specific suspended sediment load (SSL) from the drainage area of the Indus at
Besham Qila is estimated to be 1,197 Mt km^{-2} y^{-1}, more than 90% of which reaches the
Partab Bridge and Besham Qila during the high flow period that spans May–September.

Such a heavy sediment load is mainly due to glacial bedrock erosion from a large number of small, but steep catchments that directly discharge into the Indus [103]. Generally, the peak SSL correlates well with the peak discharge with a short time lag, particularly for Besham Qila during the monsoon season when discharge varies significantly within a short span of a few days, accompanied by an immediate and large increase in the sediment concentration [67]. The SSC average grain size distribution for the UIB is about 45.7% sand, 39.9% silt and 14.4% clay [6].

Table 5.2: Hydrological and sedimentological characteristics at the Besham Qila and the Partab Bridge gauges.

Parameter	Besham Qila		Partab Bridge	
	Q (m^3/s)	SSC (ppm)	Q (m^3/s)	SSC (ppm)
Duration	1969–08 (daily)	1969–08 (samples)	1962–08 (daily)	1962–08 (samples)
Max discharge	13,910	3770 (at Q$_{max}$)	9599	5780 (at Q$_{max}$)
Min discharge	325	132 (at Q$_{min}$)	168	221 (at Q$_{min}$)
Max sediment	12,401	8660	1101	25,040
Min sediment	456	1	1200	1
Mean sediment	-	1071	-	1947
SD of sediment	-	1456	-	2847
Mean discharge	3000	-	2231	-
SD of discharge	2923	-	2191	-
Q$_{-10,000}$ at Dasu damsite [6]	21,218	-	-	-
Q$_{-100}$ at Dasu damsite [6]	15,078	-	-	-
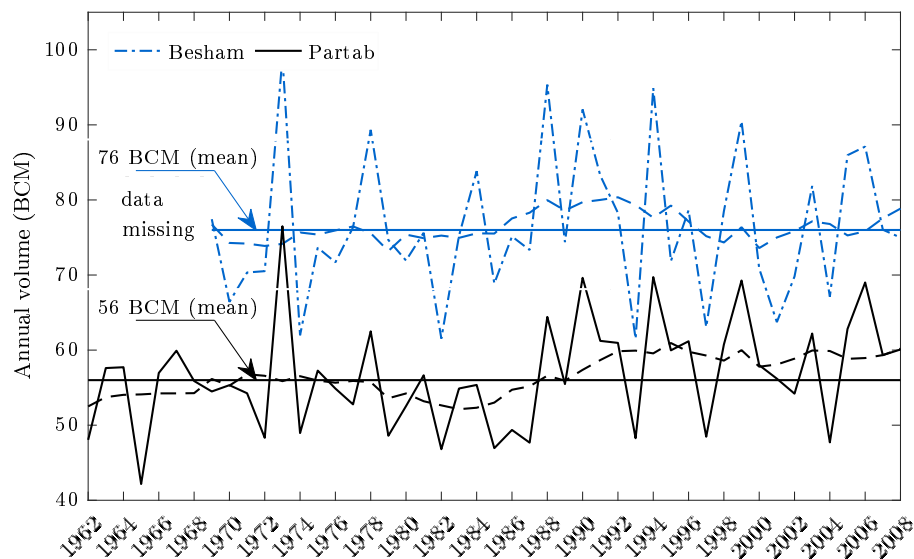
Figure 5.2: Hydrograph showing actual and smoothed flows with 10-year moving average (dashed lines) in billion m^3 (BCM).

The daily discharges and the discontinuous suspended sediment concentration (SSC) samples were collected for Partab Bridge over the period 1962–2008 and for Besham

Qila over the period 1969–2008. Following the U.S. Geological Survey (USGS) guidelines, discharges at these gauges are measured using AAcurrent meter, while the SSC samples are taken once a week in winter and twice a week in summer, depending on the availability of labor and sampling feasibility [99, 100, 101]. The total SSC samples within the collection periods on record were 3,213 and 2,117, representing around 22% and 14% of the daily time series for the Besham Qila and the Partab Bridge sites respectively. Due to low sampling frequency at Partab Bridge, we decided to use all available data samples. The long length of these samples improves the learning of the WA-ANN model, which in turn leads to better reconstruction of missing SSLs. The outliers in sediment data samples were excluded by examining the general behavior of the river and river catchment. More details on data collection, data quality and period of records for the Indus River can be found in [19].

5.3 Methods

We analyze how changes in the flow patterns are affecting the sediment transport capacity of the UIB specifically for the meltwater-dominated zone (up to the Partab Bridge site) and for the whole UIB (up to the Besham Qila), which is additionally influenced by the summer monsoonal rainfall regime. In order to do this, we analyze the observed discharges and SSCs over the past 50 years. Since the SSCs are intermittently sampled and thus represent only a fraction of the daily discharge series of the study gauges, we reconstructed the SSCs for the non-observed days using the wavelet transforms coupled with the artificial neural networks (WA-ANNs). We then employ three non-parametric statistical approaches to analyze the monthly-to-annual scale temporal dynamics of the reconstructed SSLs and observed discharges. These methods include: (1) innovative trend analysis; (2) Mann–Kendall (and seasonal-Kendall) trend test and Sen's slope method; (3) the Pettitt change point test. We also analyzed temporal dynamics by performing decadal and regressional comparisons.

5.3.1 Wavelet neural network

Artificial neural networks are widely used in hydrology and water resources studies for data optimization, reconstruction of missing sediment load and prediction of sediment load trends. The ANN architecture acts as an information processing system containing several non-linear and interconnected elements in the form of layers connected via weights. The

multi-layer perceptron (MLP) is a typical ANN, which consists of a number of nodes that are organized according to a particular arrangement. The layers process the information from the input layer to the hidden layer and further the hidden layer to the output layer for the generation of results. Generally, the hidden layers contain non-linear transfer functions to process the non-linear or linear information in order to build a relation between input and output variables. The output layer normally contains a linear transfer function to produce the output outside of the range of -1–1. Moreover, the hidden layers can also vary from single to multiple layers using different numbers of neurons. The size of a hidden layer and neurons within the hidden layer also affect the model performance. Less neurons in the hidden layer may affect the learning process, while more neurons in the hidden layer or the number of hidden layers restrict the efficiency in terms of computational time. The increase of neurons may also cause a network over fitting problem. The work in [110] suggested that the neurons for optimal generalization should be in the range from $\sqrt{2n} + m$ to the value $2n + 1$, where n and m represent the number of input and output nodes, respectively.

Wavelet transform (WT) decomposes signals into successive wavelet components corresponding to a time-domain signal within a frequency range. The original signal can be represented in terms of a wavelet expansion that utilizes the coefficients of the wavelet functions. Several wavelets can be constructed from a function $\psi(t)$ known as a "mother wavelet", which is confined in a finite interval. That is, WT decomposes a given signal into frequency bands and then analyses them in time. WT are broadly classified into continuous wavelet transform (CWT) and discrete wavelet transform (DWT). CWT is defined as the sum over all time of the signal to be analyzed multiplied by the scaled and shifted versions of the transforming function ψ. The CWT of a signal $f(t)$ is defined as follows:

$$W_{a,b} = \frac{1}{\sqrt{a}} \int_{-\infty}^{\infty} f(t)\Psi^* \left(\frac{t - b}{a} \right) dt \qquad\qquad 5.1$$

where '*' denotes the complex conjugate. CWT searches for correlations between the signal and wavelet function. This calculation is done at different scales of a and locally around the time of b. The result is a wavelet coefficient $W_{a,b}$ contour map. However, computing the wavelet coefficients at every possible scale (resolution level) necessitates a large amount of data and computation time. DWT analyzes a given signal with different resolutions for different frequency ranges. This is done by decomposing the signal into coarse approximation and detail coefficients. For this, the scaling and wavelet functions are employed. Choosing the scales a and the positions b based on the powers of two

(dyadic scales and positions), DWT for a discrete time series f_i becomes:

$$W_{m,n} = 2^{-\frac{m}{2}} \sum_{i=0}^{N-1} f_i \Psi^* \left(2^{-m}i - n\right) \qquad 5.2$$

where i is integer time steps ($i = 0, 1, 2, ..., N-1$ and $N = 2^M$); m and n are integers that control, respectively, the scale and time; $W_{m,n}$ is the wavelet coefficient for the scale factor $a = 2^m$ and the time factor $b = 2^m n$. The original signal can be reconstructed using the inverse discrete wavelet transform as follows:

$$f_i = A_{M,i} + \sum_{m=1}^{M} \sum_{n=0}^{(2^{M-m}-1)} W_{m,n} 2^{\frac{m}{2}} \Psi \left(2^{-m}i - n\right) \qquad 5.3$$

or in a simple form as:

$$f_i = A_{M,i} + \sum_{m=1}^{M} D_{m,i} \qquad 5.4$$

where $A_{M,i}$ is called an approximation sub-signal at level M and $D_{m,i}$ are detail sub-signals at levels $m = 1, 2, ..., M$. The approximation coefficient $A_{M,i}$ represents the high scale low frequency component of the signal, while the detail coefficients $D_{m,i}$ represent the low scale high frequency component of the signal.

There is a variety of mother wavelets such as the Haar wavelet, Daubechies wavelet, Coiflet wavelet and biorthogonal wavelet. Normally, the Daubechies wavelet, which also belongs to the Haar wavelet, has been performing better in sediment transport processes due to its ability to detect time localization information. Time localization information is useful in handling the seasonality and hysteresis phenomenon in flow discharge and sediment load processes. The Coiflet wavelet is more symmetrical than the Daubechies wavelet. Similarly, the biorthogonal wavelet has the property of a linear phase, which is needed for signal reconstruction [129]. The selection of an appropriate mother wavelet depends on the type of application and data characteristics.

Before applying an ANN, the input discharge time series are decomposed using pre-selected wavelets. After data decomposition, a portion of the signal associated with certain frequency bands need to be eliminated if there is a poor correlation between the decomposed signal and the observation data. Only the decomposed signals that have significant correlation with the observation signal are used in the forecast model. Furthermore, on decomposed signals, the permutation of the *logsig, tansig, radbas* and *purelin* transfer functions was tested for the hidden and output layers. The Levenberg–Marquardt algorithm was used to train the networks due to its simplicity. The neurons in the hidden layer were selected based on the criteria described by [110]. The stopping criteria of the models was a maximum of 1,000 epochs. The final networks were saved for later use to reconstruct the missing SSCs in the daily time series. Due to the different

data time series at both gauges, we developed two different WA-ANN models. Fig. 5.3 shows the methodology of coupling WT with ANN for forecasting SSC in the study area.

PSfrag replacements
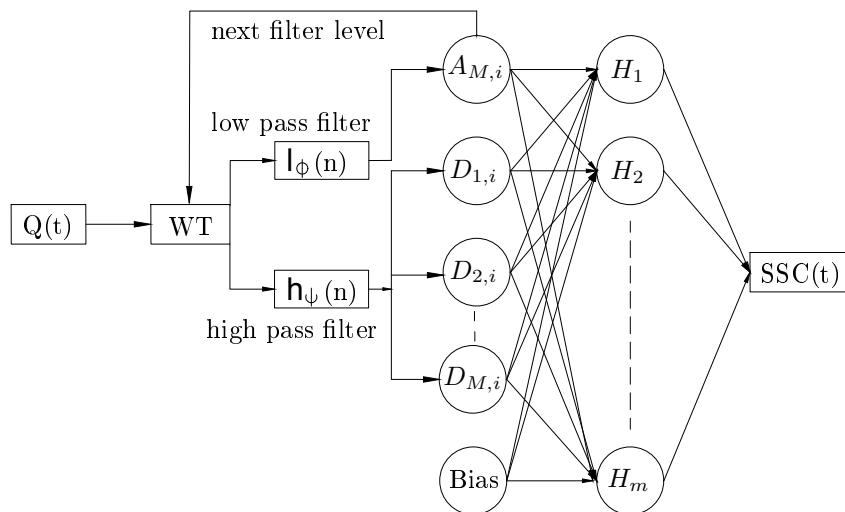
Figure 5.3: Schematic diagram of a wavelet transform coupled to an artificial neural network (WA-ANN). SSC; suspended sediment concentration.

The performance of the model was assessed employing the correlation coefficient (R), root mean square error (RMSE), mean absolute error (MAE) and the Nash–Sutcliffe efficiency (NSE). The correlation coefficient indicates a perfect fit at 1 and otherwise at 0. Similarly, RMSE and MAE indicate the best model performance when close to 0. The NSE ranges from $-\infty$–1, where 1 represents a perfect match and 0 indicates that the model is no better than simply representing the mean value. The simulated results are normally considered 'good' when the NSE is higher than 0.75 and 'satisfactory' when it lies between 0.36 and 0.75 [115].

5.3.2 Trend analyses

5.3.2.1 Innovative trend test

The innovative trend analysis (ITA) [47] divides a time series into two halves, where the latter half is plotted against the first, after being sorted in ascending order. Given both halves are identical to each other, the plot shows a scatter of points along a 1:1 (45°) line on the Cartesian plane. The scatter of points falling above (below) the 1:1 line indicates a monotonically-increasing (decreasing) trend. ITA does not require pre-whitening, a specific sample size, a serial correlation structure of the time series or a normal probability distribution. ITA can easily identify the variations and trends in the

lower, medium or higher hydrological processes [130, 131]

5.3.2.2 Mann–Kendall test

The Mann–Kendall (MK; [132, 133]) test can detect a trend in a time series without being affected by the outliers. With the use of normal approximation, the MK test statistic S is calculated as follows:

$$S = \sum_{i=1}^{n-1} \sum_{j=i+1}^{n} sgn(X_j - X_i) \qquad 5.5$$

where X_i and X_j are the adjacent data values, S is the sum of positive or negative signs, n is the number of observations and:

$$sgn(X_j - X_i) = \begin{cases} +1 & (X_j - X_i) > 0 \\ 0 & if \ (X_j - X_i) = 0 \\ -1 & (X_j - X_i) < 0 \end{cases} \qquad 5.6$$

The two important parameters of the MK test are the significance level and the slope. The former indicates the strength, while the latter indicates the magnitude and direction of a trend. If there are many tied data values, then the method specified for the number of data values greater than 40 is used ([133], as reported by [134]). The variance of S (Eq. 5.7) takes into account these ties, where q is the number of tied groups and t_p is the number of data in the p group.

$$VAR(S) = \frac{1}{18}\Big[n(n-1)(2n+5) - \sum_{p=1}^{q} t_p(t_p - 1)(2t_p + 5)\Big] \qquad 5.7$$

After calculating S and its variance, an MK statistic Z is computed using Eq. 5.8. A positive value of Z indicates an upward tend, whereas its negative value indicates a downward trend. If there is no detectable trend, then the MK statistic Z has a standard normal distribution.

$$Z = \begin{cases} \frac{S-1}{\sqrt{VAR(S)}} & S > 0 \\ 0 & if \ S = 0 \\ \frac{S+1}{\sqrt{VAR(S)}} & S < 0 \end{cases} \qquad 5.8$$

To detect the season-wise monotonic trends, a slightly modified version of the MK test, namely seasonal Kendall (SK), is used, which runs the original MK test on each season (k) separately, where k can refer to any period of time within a year (e.g., months or four quarters of a year). The overall S statistic is then computed by adding each SK statistic (S_k) for m number of seasons, and the statistical significance of the trend can be

assessed using the outcome of Eq. 5.10 and 5.11 in Eq. 5.8.

$$S_k = \sum_{i=1}^{n_k-1} \sum_{j=i+1}^{n_k} sgn(X_{k,j} - X_{k,i}) \tag{5.9}$$

$$S = \sum_{i=k}^{m} S_k \tag{5.10}$$

and:

$$VAR(S) = \sum_{k=1}^{m} VAR(S_k) \tag{5.11}$$

Based on sets of Monte Carlo simulations, [135] show that the presence of a positive serial correlation increases the variance of the distribution of S and thus increases the possibility of rejecting the null hypothesis of no trend; the same was also found by [136]. By contrast, negative serial correlation diminishes the variance of the distribution and results in underestimation of the significant trend detection probability. To limit the influence of serial correlation, we applied a correction factor, described by [137] in Eq. 5.8, as follows;

$$Z^* = \frac{Z}{\sqrt{\eta^k}} \tag{5.12}$$

$$\eta^k = \begin{cases} 1 + \frac{m}{2} \sum\limits_{i=1}^{m-1} (m-j)\rho_j & \text{for } j>1 \\ 1 + 2\frac{\rho_1^{m+1} - m\rho_1^2 + (m-1)\rho_1}{m(\rho_1-1)^2} & \text{for } j=1 \end{cases} \tag{5.13}$$

Normally, the population serial correlation coefficient ρ_j is replaced with the sample serial correlation coefficient r_j;

$$r_j = \frac{\frac{1}{m-j}\sum\limits_{i=1}^{m-j}(X_i - \bar{X})(X_{i+j} - \bar{X})}{\frac{1}{m}\sum\limits_{i=1}^{m}(X_i - \bar{X})^2} \qquad \text{where } j = 2, 3, .., m-1. \tag{5.14}$$

$$\bar{X} = \frac{1}{m} \sum_{i=1}^{m} X_i \tag{5.15}$$

The correction factor η^k shrinks (expands) the MK statistics in the presence of positive (negative) serial correlation.

An estimate of trend magnitude, which is closely related to the MK test procedure, is known as Sen's slope estimator [138]. The slope estimates of N_k pairs of data of the k-season are first computed by:

$$P_{k,l} = \frac{X_{k,j} - X_{k,i}}{j - i} \tag{5.16}$$

for all $1 \leq i \leq j \leq n_k$ and $1 \leq l \leq N_k$. The median of these $P_{k,l}$ values is Sen's slope

estimator P_k:

$$P_k = \begin{cases} P_{k,\left(\frac{N_k+1}{2}\right)} & \text{if } N_k \text{ is odd} \\ \frac{1}{2}\left[P_{k,\left(\frac{N_k}{2}\right)} + P_{k,\left(\frac{N_k}{2}+1\right)}\right] & \text{if } N_k \text{ is even} \end{cases} \qquad 5.17$$

Finally, P_k is tested by a two-sided test at the $(1-\alpha) \times 100\%$ confidence interval, and the true slope can be obtained. More details about the Mann–Kendall and Sen's slope tests can be found in [134] and [139].

5.3.2.3   Change point detection

We used the Pettitt test [50] to detect the qualitative and quantitative changes in SSL and discharge series. The Pettitt change point test is non-parametric and based on a version of the Mann-Whitney statistics $U_{j,n}$ as follows:

$$U_{j,n} = U_{j-1,n} + \sum_{i=1}^{n} sgn(X_j - X_i) \qquad \text{where } j = 2, 3, .., n \qquad 5.18$$

whereas X_i and X_j are the adjacent data values, n is the number of observations and sgn can be quantified using Eq. 5.6. The statistics K_j and corresponding significance testing are given by:

$$K_{j,n} = Max|U_{j,n}| \text{ where } 1 \leq j \leq n \qquad 5.19$$

and:

$$p \cong 2exp\left[\frac{-6(K_{j,n})^2}{(n^3 + n^2)}\right] \qquad 5.20$$

If $p \leq 0.05$, a significant change point exist.

5.3.2.4   Decadal analyses and linear regressions

Similar to the innovative trend method of [47], we divided the suspended sediment load (SSL) and discharge data into two time series of one decade each. The first time series consists of the initial decade of the dataset, and the second time series consists of the last decade of the dataset. To determine the mean annual and mean monthly changes, we compared the SSL and discharge shares of pre-selected spatial resolution for both gauges.

At the upper Indus River, the effect of high discharge events is influential; they transport a considerable amount of SSL [103]. Therefore, we also explored the mean monthly changes in most effective discharges during the initial and last decades of the datasets. The work in [140] defined the most effective discharge as the midpoint of the range of

flows, which over a certain period can transport a considerable proportion of the SSL. The effective discharge can be computed using sediment transport formulae and regional flow duration curves. In the present study, we used the effective discharge (Q/Q_{avg}) of 2.0-times the average discharge (Q_{avg}) for Besham Qila and 5.0-times the average discharge (Q_{avg}) for the Partab Bridge gauge as per the classifications formulated by [67].

To obtain the linear changes in each month during past 50 years, we developed linear regression equations of the reconstructed SSLs and observed discharges. Using these equations, we also quantitatively and qualitatively analyzed the changes.

5.4 Results

To analyze the trends in suspended sediment loads (SSLs) of the upper Indus River, we reconstructed the missing SSC data using wavelet neural networks (WA-ANNs) and then estimated corresponding SSLs using measured discharges, i.e., SSC × Q. The reconstructed daily data series in the form of monthly and annual SSLs were used in four different trend analysis techniques, namely: (1) innovative trend test; (2) Mann–Kendall and Sen slope tests; (3) Pettitt change point test; (4) decadal analyses and linear regressions. The study findings are described below.

5.4.1 Reconstruction of daily sediment load time series

Based on several preliminary simulations for both gauges, we eventually trained both networks using 70% of the data for the training, 15% for testing and 15% for validation on a random basis. In a similar way, we also decomposed Q_t, Q_{t-1}, Q_{t-2}, for Besham Qila and Q_t, Q_{t-1} for Partab Bridge up to seven levels using the Daubechies (db1) wavelet. The best performing WA-ANN architectures reconstructed SSLs with a correlation coefficient R = 0.92 for both sites (Tab. 5.3). The RMSE and MAE for Partab Bridge were approximately two times more than Besham Qila; likewise, the standard deviation (SD) and mean in the actual SSC samples (Tab. 5.2). This difference shows the complexity in the transport process in the glacier influence zone of the upper Indus River at the Partab Bridge gauge. The NSE, which is used to analyze the model performance, was 0.85 for both stations. Therefore, we consider the WA-ANNs reconstructed suspended sediment load (SSL) series good as the NSE is higher than 0.75 [115, 29, 141]. In addition, both WA-ANN models reconstructed SSLs with a cumulative difference of ±1% with the measurements. Thus, according to another comparison criterion, the models that led to an

error between $\pm10\%$ and $\pm15\%$ are considered as accurate models [117]. A comparison between the mass of suspended sediment sampled daily and computed results using WA-ANN models is also shown in Fig. S1 of the Supplementary material.

The reconstructed results showed a higher mean annual SSL of 171 Mt for Partab Bridge compared to 160 Mt at the downstream Besham Qila site (Fig. 5.4). Moreover, the annual SSLs appear to have been rising at Partab Bridge since 1993 and causing the 10-year moving average to increase. In contrast, the annual SSLs have been decreasing at Besham Qila since 1993 (Fig. 5.4). The similar changes in SSLs are also shown in linear and quadratic trends for both gauges (Fig. 5.5). The statistical parameters of linear and quadratic line fittings are shown in Tab. S1 (Supplementary material).

Table 5.3: Statistics of the best performing WA-ANN architectures for the Besham Qila and the Partab Bridge sites.

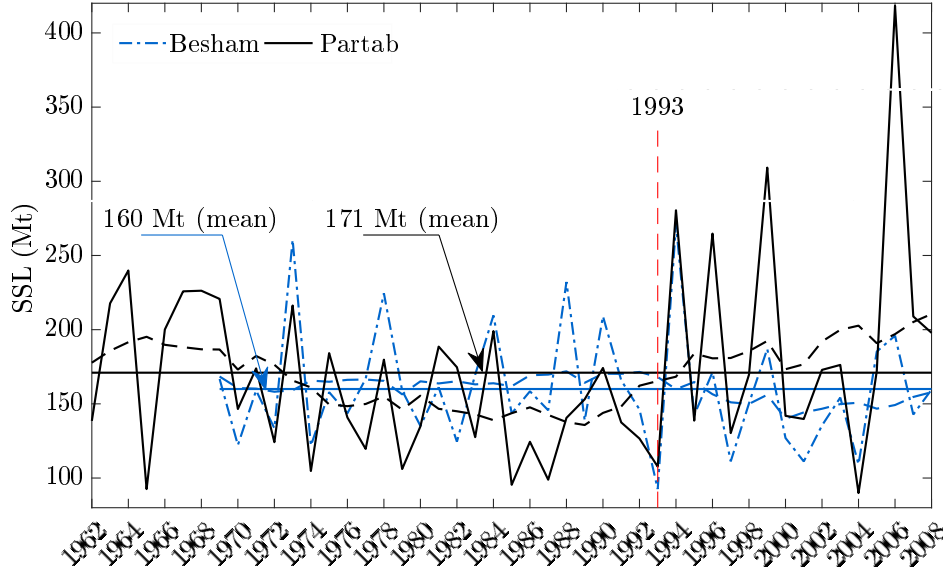| Location	Neurons	Transfer Function		R	RMSE (ton/day)	MAE (ton/day)	NSE
		First	Output				
Besham Qila	24	*tansig*	*purelin*	0.92	3.94×10^5	1.75×10^5	0.85
Partab Bridge	30	*logsig*	*tansig*	0.92	6.12×10^5	2.87×10^5	0.85

PSfrag replacements

Figure 5.4: WA-ANN reconstructed annual suspended sediment loads (SSLs) for Besham Qila and Partab Bridge gauge stations showing an increase after 1993 at Partab Bridge (the dashed lines represent the 10-year moving average).
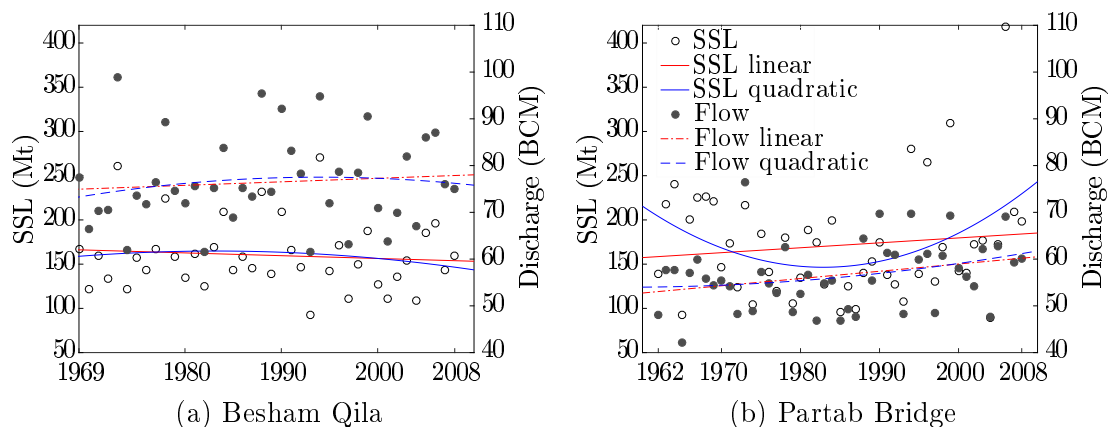
Figure 5.5: Linear and quadratic annual trends of reconstructed SSLs and observed discharges (legends for Fig. 5.5b also apply for Fig. 5.5a).

5.4.2 Innovative trend test for annual loads

The innovative trend test (ITA) shows a decreasing trend in low annual SSLs at Besham Qila against an increasing trend in high annual SSLs at the Partab Bridge site (Fig. 5.6a and 5.6b). The frequencies have been increasing at both gauge sites. On the other hand, the overall annual flows at Partab Bridge show an increasing trend, while there are diverse trends at Besham Qila, where, apart from medium annual flows, the low and high flows have no discernible trend (Fig. 5.6a and 5.6b). Contrary to Besham Qila, the increase in flows has also been causing an increase in SSLs at Partab Bridge. However, in the absence of hydraulic structures, urbanization or industrialization along the upper Indus River or within the UIB, this increase in annual SSLs noticed at the Partab Bridge did not appear at the downstream gauge, i.e., Besham Qila (Fig. 5.6).

5.4.3 MK test for annual and monthly loads

The MK trend analyses show that the annual SSLs at Besham Qila have been decreasing at a rate of 0.634 Mt y^{-1} (Tab. 5.4). Calculating according to the same rate, this indicates a maximum decrease of 34 Mt from the estimate made by [14] (reported by [15]) for the Tarbela dam in 1982 (Tab. 5.1). Due to a negative slope of 0.634 Mt y^{-1}, it is possible that the estimates published in 1970s and 1980s show higher sediment loads compared to our estimate (160 Mt y^{-1}) at Besham Qila. In contrast to the results of the MK test, the seasonal Kendall (SK) test showed an annual statistically-significant increasing trend at the Besham Qila ($Z = 3.2$) and Partab Bridge ($Z = 4.1$) gauges. This contrast in both tests results arises due to the addition of each season's trend in the SK test (Eq. 5.10

(a) Besham Qila (b) Partab Bridge
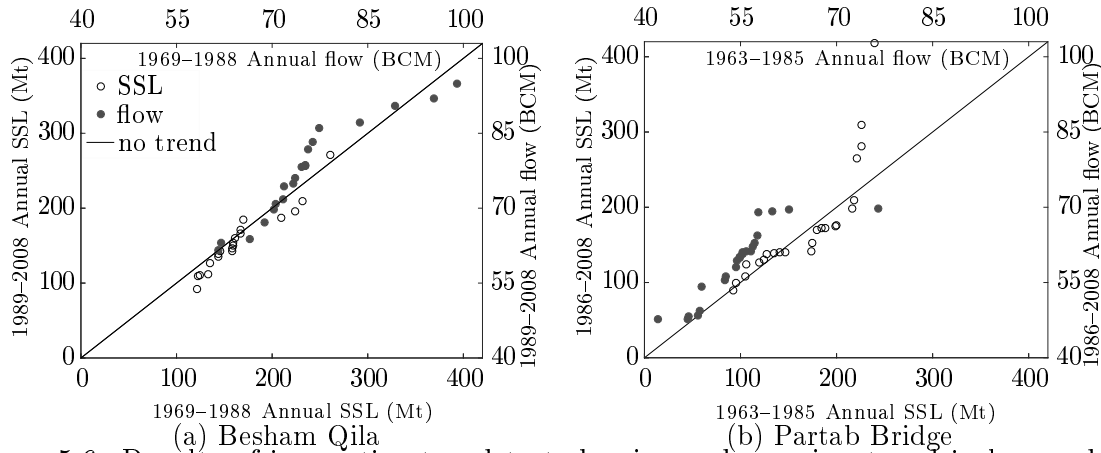
Figure 5.6: Results of innovative trend test showing a decreasing trend in low and high annual SSLs and flows at the Besham Qila and an increasing trend in high annual SSLs at Partab Bridge, along with an increase in all flows (legends for Fig. 5.6a also apply for Fig. 5.6b).

and 5.11). In addition, the results of the SK test are similar either using seasons as four quarters of a year (December–February, March–May, June–August and September–November) or each month as a season.

The monthly SSLs show a significant increasing trend in the winter months (November–February) at Besham Qila with a cumulative magnitude of 0.004 Mt y^{-1}. This is a slight cumulative magnitude, which is unbalanced by the decreasing trend of -0.24 Mt y^{-1} alone in August (Tab. 5.4). Surprisingly, sandwiching increasing trends, April at Besham Qila shows a declining trend only in SSLs. The monthly SSLs at Partab Bridge, in contrast to Besham Qila, show a declining trend of 0.33 Mt y^{-1} only in August. This trend is balanced by 0.36 Mt y^{-1} rise in June and September (Tab. 5.4). Despite the diversified trends at both gauges, May showed a statistically increasing and August a statistically decreasing trend, whereas in summer, only August at Besham Qila and June, August and September at Partab Bridge show any trends. However, their contribution (33% and 83%) is still higher than the magnitudes of the trends in the remaining months of the year. In summer (July–September), the mean SSL recorded at Partab Bridge is 141 Mt y^{-1}, while during the same period or even until October, only 125 Mt passed through the Besham Qila gauge; this apparently indicates a durable deposition of SSLs between both gauges in summer.

5.4.4 Change point detection test

The test results show discernible change points in the monthly SSLs after 1982, whereas no change point was detected in annual SSLs at both gauges (Fig. 5.7). Therefore, it might be possible that the peaks in annual SSLs recorded after 1993 at Partab Bridge gauge in Fig. 5.4 in the absence of an increase in corresponding discharges may have been caused by degradation of landslides, which may have previously blocked the sediments [23]. On the other hand, the interventions of landslides are marginal for river flow due to a mean discharge of about 2,600 m^3/s. Thus, the change points in monthly discharges are similar at both gauge stations (Tab. 5.5). As the Besham Qila site is located in a monsoon rainfall and snowmelt zone, no change in annual flows indicates a decrease in contribution from these sources (Tab. 5.5).

Table 5.4: Mann–Kendall's (MK) annual and monthly SSL and discharge trends for the Besham Qila and the Partab Bridge sites. The minus symbol for the MK statistics indicates a downward trend, whereas the (-) symbol without numbers means no trend.

Period	SSL			Discharge		
	MK Statistic [3]	Sen's Slope (Mt y^{-1})	Average SSL (Mt y^{-1})	MK Statistic	Sen's Slope (BCM y^{-1})	Average Flow (BCM y^{-1})
Besham Qila						
Annual	−1.21	−0.6345	160	-	-	76.41
January	2.74	0.0011	0.16	5.60	0.0081	1.25
February	2.76	0.0016	0.12	4.71	0.0068	1.08
March	1.08	0.0020	0.22	2.39	0.0061	1.40
April	−1.14	−0.00280	0.48	-	-	2.25
May	2.66	0.0769	4.61	2.60	0.0471	5.98
June	-	-	28.04	-	-	13.21
July	-	-	61.55	-	-	19.69
August	−1.00	−0.2414	53.80	-	-	17.53
September	-	-	9.90	-	-	7.77
October	-	-	0.74	1.55	0.0067	3.01
November	2.16	0.0013	0.22	3.51	0.0075	1.80
December	1.05	0.0004	0.15	3.71	0.0071	1.44
Partab Bridge						
Annual	-	-	171	1.77	0.1299	56.62
January	3.81	0.0007	0.07	2.11	0.0018	0.94
February	-	-	0.08	-	-	0.77
March	-	-	0.12	-	-	0.83
April	1.01	0.0009	0.25	2.81	0.0045	1.08
May	3.41	0.0476	3.09	4.64	0.0506	3.37
June	1.39	0.2308	25.25	1.55	0.0380	9.32
July	-	-	64.14	1.00	0.0299	15.08
August	−1.26	−0.3333	65.59	−1.02	−0.0274	14.15
September	1.86	0.1304	12.20	0.95	0.0181	6.26
October	2.90	0.0041	0.33	2.85	0.0100	2.33
November	3.33	0.0008	0.09	3.50	0.0060	1.38
December	2.59	0.0003	0.06	2.65	0.0034	1.10

Interestingly, the magnitude of the increasing trend in SSLs over May at Partab Bridge

---

[3]Significant trend at 95% significance level (critical value = 1.96)

was higher than Besham Qila's SSLs, which makes their mean loads approximately the same after 1997 (Fig. 5.7). After 1997, there was no detectable increase in either parameter at either gauge station. Furthermore, September showed a significant increase of 60% no earlier than 1982, which is the highest magnitude or in the change in SSLs of the analyzed record. Compared to a noticeable increase in SSLs at Partab Bridge, surprisingly, the increasing loads are not being received at the downstream gauge (Fig. 5.7).
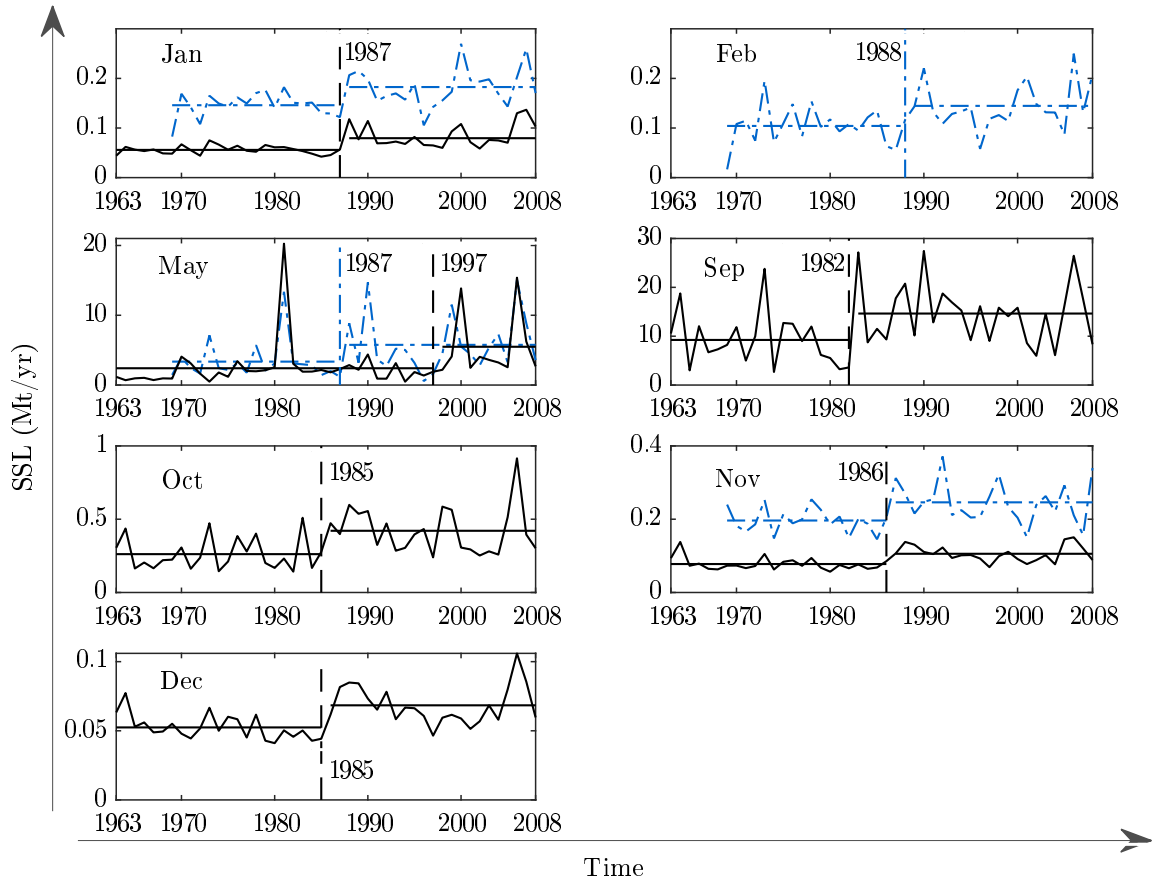
Figure 5.7: Significant change points in monthly SSLs determined using Pettitt test; black denotes Partab Bridge, and blue denotes Besham Qila.

Table 5.5: Significant change points in river flows determined using the Pettitt test.

Period	Annual	January	February	March	April	May	October	November	December
Besham Qila	-	1987	1987	1986	-	1997	1985	1986	1985
Partab Bridge	1987	1986	1987	1987	1987	1987	1985	1986	1985

5.4.5 Decadal analyses and linear regressions

The decadal analyses only show decreasing trends in SSLs during peak summer (June and July) at Besham Qila and only over August at Partab Bridge (Fig. S2, S3, 5.8a and 5.8b

(Supplementary material)). The directions of changes in monthly SSLs are similar to their corresponding discharges except for July at Partab Bridge and August at Besham Qila. It might be possible that the high SSLs recorded in July at Partab Bridge have been causing the SSLs in the following month of August at the downstream gauge to increase, as shown in Fig. 5.8. Similar deviations can be seen in effective discharges, where the SSL transport capacity of the river has been decreasing in summer (June, August and September) at Besham Qila and only over August at Partab Bridge (Fig. 5.9).

(a) Besham Qila   (b) Partab Bridge
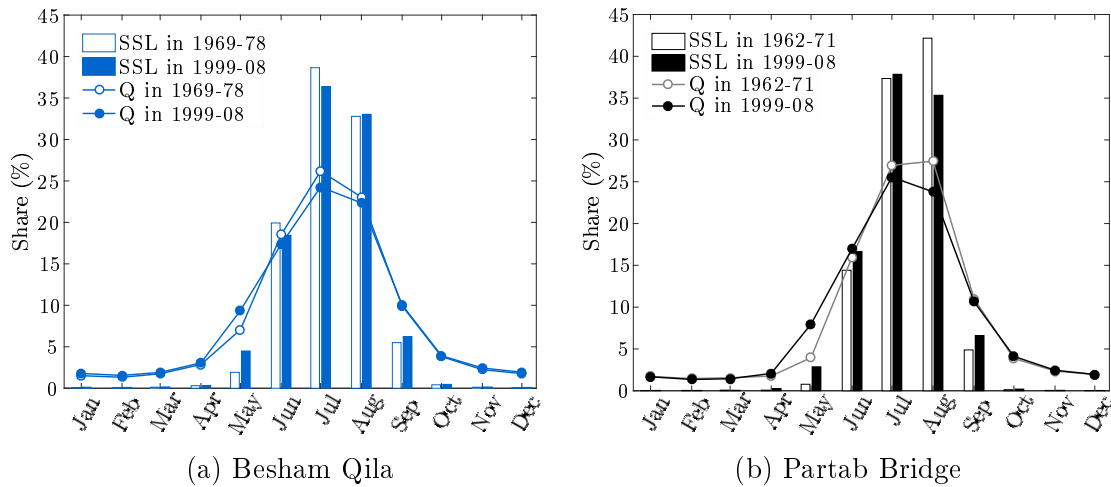
Figure 5.8: Monthly share of SSL and flow volume in the first and last decade of the analyzed record.

(a) Besham Qila   (b) Partab Bridge
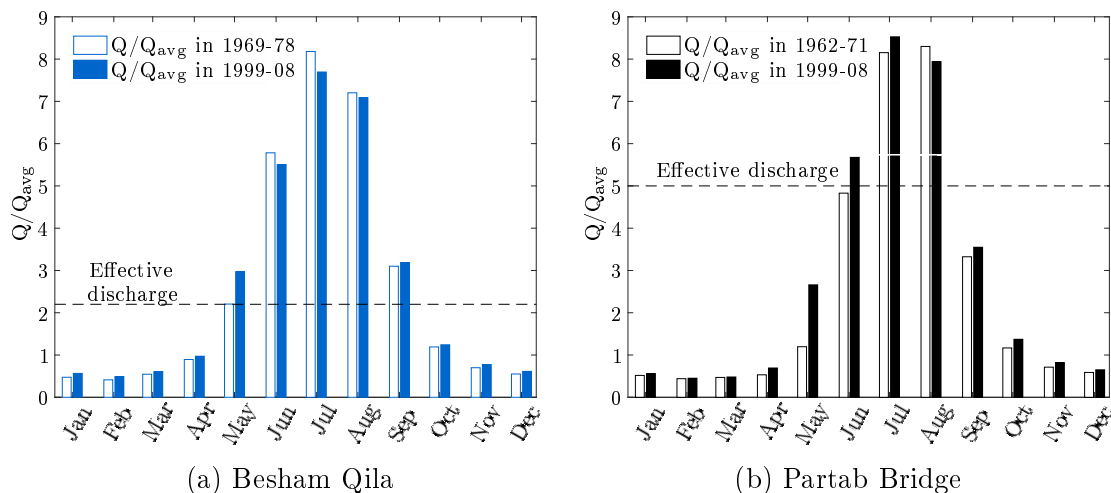
Figure 5.9: Monthly Q/Q_{avg} in first and last decade of the analyzed record following the monthly decadal trend of SSLs.

The linear regressions also showed identical directions in the changes of the monthly SSLs and their corresponding discharges, except for April at Besham Qila (Tab. 5.6),

where SSLs are decreasing against the increase in discharges. Nevertheless, there is a certain sensitive linear correlation between mean monthly SSLs and their corresponding discharges for the months in the effective discharges zone, depicted in Fig. 5.10, where the axes represent the change in mean monthly discharges and SSLs (since 1969 and 1962) determined by linear regression equations (Fig. S2 and S3 in the Supplementary material). As can be seen from Fig. 5.10, the change in SSLs is sensitive to the change in discharges, where a 1% change in discharges, on average, can cause a change of 3% in SSLs in the study area. However, compared to Besham Qila, the transport capacity of the river is more sensitive to the discharge change at Partab Bridge, where, for example, an 11% change in mean monthly discharges caused a 65% change in corresponding SSLs over September (Tab. 5.6). This may be due to the location of the major source of eroded sediments in the Karakoram parts of the basin that contributes SSLs disproportionate to its drainage area at Partab Bridge [101]. On the other hand, the river slope is mild from Partab Bridge to Besham Qila, which causes substantial sediment storage of the incoming SSLs, particularly in summer.

Table 5.6: Mean monthly linear variations in SSLs and discharges (flows) at both gauges (each month's regression plots are presented in Fig. S2 and S3 in the Supplementary material).

Period	Besham Qila [4]		Partab Bridge [5]	
	SSL (%)	Flow (%)	SSL (%)	Flow (%)
Annual	−7.40	3.90	13.50	16.00
January	44.64	29.49	93.56	12.85
February	77.58	29.8	10.27	6.28
March	59.43	20.8	3.36	5.01
April	-8.11	7.29	398.18	36.32
May	141.22	38.75	365.07	138.87
June	−13.41	−3.7	48.72	20.54
July	−9.04	−1.45	17.86	7.37
August	−12.79	−3.12	−8.16	−4.07
September	8.02	6.63	65.73	11.68
October	16.77	11.52	107.15	24.27
November	29.48	16.47	50.99	20.88
December	19.43	15.17	40.68	15.8

To gain an overall qualitative overview of the trends, we compared the results in

---

[4]from 1969–2008
[5]from 1962–2008

Tab. 5.7. The comparison reveals that SSLs have been increasing in May and decreasing in August in the study area. Apart from that, they have been monotonically increasing during winter months from November–February and also March and May. Although the annual SSLs at both gauge sites showed minor trends, they are statistically insignificant (Tab. 5.7).
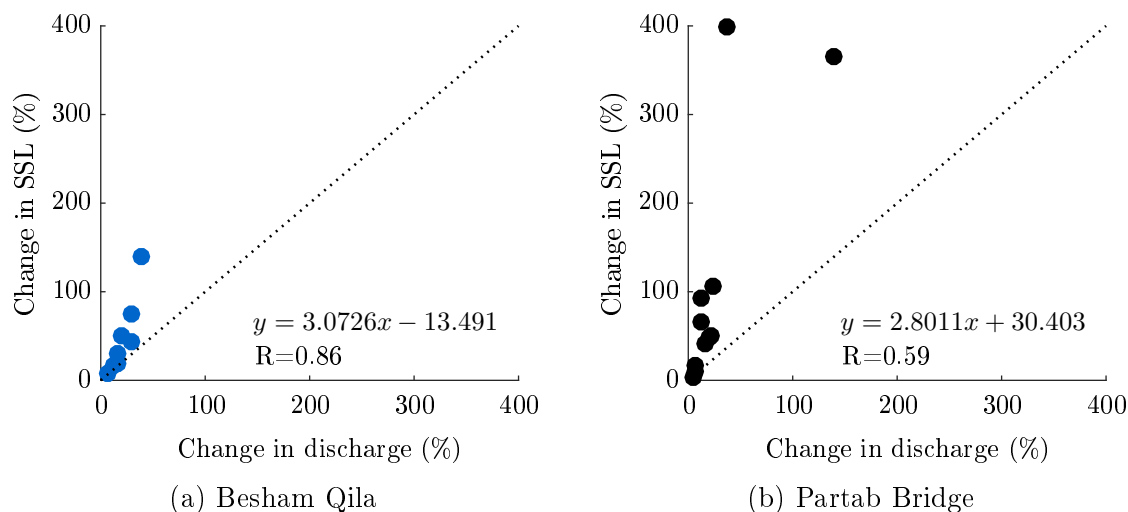

(a) Besham Qila (b) Partab Bridge

Figure 5.10: Linear regression of mean monthly changes in SSLs versus changes in discharges.

Table 5.7: Qualitative comparison of the trends in SSLs using different methods (blue triangles imply an upward trend, whereas red triangles imply a downward trend; a "-" represents statistically insignificant/no trend). ITA, innovative trend analysis.

Period	Besham Qila					Partab Bridge				
	ITA	MK	C.P[6]	D.C[7]	Regression	ITA	MK	C.P	D.C	Regression
Annual	▼	▼	-	▼	▼	▲	-	-	▲	▲
January	▲	▲	▲	▲	▲	▲	▲	▲	▲	▲
February	▲	▲	▲	▲	▲	▲	-	-	▲	▲
March	▲	▲	-	▲	▲	▲	-	-	▲	▲
April	▼	▼	-	▲	▼	▲	▲	-	▲	▲
May	▲	▲	▲	▲	▲	▲	▲	▲	▲	▲
June	▼	-	-	▼	▼	▲	▲	-	▲	▲
July	▼	-	-	▼	▼	▲	-	-	▲	▲
August	▼	▼	-	▲	▼	▼	▼	-	▼	▼
September	▲	-	-	▲	▲	▲	▲	▲	▲	▲
October	▲	-	-	▲	▲	▲	▲	▲	▲	▲
November	▲	▲	▲	▲	▲	▲	▲	▲	▲	▲
December	▲	▲	-	▲	▲	▲	▲	▲	▲	▲

[6]change point detection test
[7]decadal comparison

5.5 Discussion

The WA-ANN models with a decomposition level of 7 (256 days) and a lag time of two and one day for Besham Qila and Partab Bridge, respectively, can precisely find the missing suspended sediment load for a given circumstance of hydrological data of the study area. Our findings show that the variation in flow patterns have been causing a significantly increasing trend in suspended sediment loads (SSLs) in May and a significantly decreasing trend in August at both Besham Qila and Partab Bridge gauges in the upper Indus River (Tab. 5.7). Contrary to the increase in high frequencies in low annual SSLs and river flows at Besham Qila (which is additionally influenced by monsoon rainfall), the frequencies in high SSLs and river flows are increasing at the Partab Bridge gauge, which is located just downstream of high elevation glacierized areas of the Karakoram and Himalayas (Fig. 5.1 and 5.6). Even in the absence of hydraulic structures between both gauges, the high SSLs recorded at Partab Bridge during summer are not being transported to the downstream gauge. Furthermore, the mean monthly linear variations show that an average 1% change in monthly flows can cause a 3% change in SSLs (Fig. 5.10). However, the sediment transport capacity of the river is more sensitive to discharge change from May–August at Besham Qila and in September at Partab Bridge.

The sediment transport processes at the upper Indus River are influenced by hysteresis phenomenon and alternative cycles of dray and wet seasons. Applying simple relationship between water discharge and sediment concentration in the modeling process cannot adjust and model these impact factors. Therefore, a temporal resolution of approximately one year with a lag time of one day in the glacier-influenced zone and two days in the rainfall-influenced zone can reduce the variations in sediment load reconstruction. The reconstruction variations, in particular, increase when for example in conventional methods (sediment rating curves and ANN), temporary sediment storage in the main river channel and different transit times of discharges and sediment from their sources to the gauges are not included. Therefore, the quality of hydraulic design and sediment load trends based on poor sediment load estimation ultimately can affect the accuracy of subsequent studies and the efficiency of the overall hydraulic structure and associated benefits.

Partab Bridge gauge is located just downstream of the snow-fed and glacial melt zone of the upper Indus River. Therefore, the results indicate two types of patterns at Partab Bridge: (1) snowmelt- and (2) glacial melt-dependent SSLs. The former (snowmelt dependent) SSLs have been shifting to the spring months (April, May and June) due to an increase in early snowmelts at low altitudes [142, 37, 21]. Particularly in May, the

significant increasing effect of early snowmelt has increased the SSL from 3.3 Mt y^{-1}–5.6 Mt y^{-1}, over the last 50 years (Fig. 5.7). The effect of early snowmelt has also been noticed by [127], where they determined a 50 million m^3 increasing rate in May's flow at Partab Bridge. Interestingly, in comparison to Besham Qila (47 million m^3), the rate of increase in flow (50 million m^3) is higher at Partab Bridge and vice versa in SSLs (Tab. 5.4 and 5.6). However, this increasing trend in flows extraordinarily increased SSLs at Partab Bridge, where after 1993, SSLs are identical to those of Besham Qila. The identical loads at both gauges point out either no increase in SSLs at Besham Qila's catchment or deposition downstream of Partab Bridge.

On the other hand, retrieval of glacial size depreciates the SSLs in August due to less water availability [67, 36, 143, 40]; the SSLs have decreased to 34% (from 43%) over the past 50 years. It seems that glacial melt has shifted to July and September (Tab. 5.4). Although the increasing trend in both months is similar (Tab. 5.6), September's flow has remarkably increased the SSL from 9 Mt–15 Mt (similar to regressions where increase is 65%) at Partab Bridge (Fig. 5.7). This significant increasing trend may be caused by the small increase in most effective discharge. It also shows the degree of sensitivity where only an 11% change in discharge caused a 66% change in SSL (Tab. 5.6). Furthermore, the remarkable increase in SSLs in September may reduce the reservoirs' life by increasing trap efficiency, where according to existing operation rules, the dams are normally filled to the maximum conservation level as late as 31 of August, such as at Tarbela dam.

Contrary to monotonically-increasing trends in SSL at Partab Bridge (except August), the Besham Qila gauge, located in the snow and rain-fed zone, has diversified mean monthly trends from winter to spring (Tab. 5.7). The rise in spring' SSLs at Besham Qila might be due to early snowmelt as at Partab Bridge [127]. However, the most surprising trend outcome is the decrease in SSLs during April in contrast to the increase in discharges revealed by regressions (Tab. 5.6). In the MK test, April's SSLs also showed a decreasing trend, despite an increasing trends in proceeding and immediately succeeding months (Tab. 5.4). In April, half of the flow volume recorded at Besham Qila comes from Partab Bridge [144]; however, corresponding to a 36% linear mean monthly increase at Partab Bridge (Tab. 5.6), the increase in flow at Besham Qila is only 7%. Therefore, the corresponding increase in SSLs recorded at Partab Bridge during April may be deposited (due to less SSL transport capacity of the river) between Besham Qila and Partab Bridge, causing high SSLs during the succeeding month (May) at Besham Qila, when the river flows show a significant increasing trend at both gauges. Over August, on the contrary, the declining trend in SSLs at Besham Qila is statistically insignificant and seems to be

associated with the decrease in the contribution of SSLs (Tab. 5.4) and flow volume (from which 84% of flow comes) from Partab Bridge.

As can be seen in Fig. 5.2, over the past 40 years, at Besham Qila, the average annual volume of water was about 76 billion m^3 (BCMs), while the same average was 56 BCMs at Partab Bridge. That means the catchment at Partab Bridge (denoted by Zone 1) contributes 74.2% of the annual flow volume at Besham Qila. The remaining 25.8% in annual flow volume is contributed from the catchment between Partab Bridge and Besham Qila (denoted by Zone 2). The flow volume in Zone 2 is mostly generated from rainfall and snowmelt [21]. The linear trend from 1969–2008 in Fig. 5.5 shows an increase in flow volume at Besham Qila of around 3.90% (denoted by ΔQ), while the same increase at Partab Bridge is around 13.50% (denoted by ΔQ_1). The variation of water availability in the area between Partab Bridge and Besham Qila (denoted by ΔQ_2) can be approximated using the following mass balance equation:

$$100 \times \Delta Q = 74.2 \times \Delta Q_1 + 25.8 \times \Delta Q_2 \qquad\qquad 5.21$$

From this equation, we obtain the variation in flow in Zone 2 $\Delta Q_2 = -38\%$. As Zone 2 is influenced by rainfall and snowmelt, it seems that the negative variation is attributable to trends of these parameter. These parameters (snowmelt and rainfall) have further been causing a decrease in water availability (between both gauges) required to transport the increased SSLs coming from Partab Bridge. Thus, the annual SSL trends at Besham Qila have shown a decreasing tendency since 1969 (Fig. 5.5). Similar results have also been noted by [46], where the decrease in rainfall in the study area has been buffered by the increase in glacier melts. Additionally, the rise in glacier melt or precipitation over the western region of the upper Indus Basin noted by [38] might have been the cause of the 60% increase in SSLs during September at Partab Bridge. However, this increase has not been received at the downstream gauge, possibly due to a statistically insignificant increase in discharge downstream of the same gauge till Besham Qila (Tab. 5.4).

In the future at the upper Indus River, the overall increase in flow volume is expected to reach 7–12% [37]. This increase will mostly increase the flow share for the pre and post summer months, which will not be enough (it will be less than the most effective discharges) to transport an additional sediment load. Consequently, the annual SSLs will remain the same or will decrease slightly at Besham Qila. Therefore, in keeping with the current trends, the published sediment load estimates indicate an ongoing decline at Besham Qila (Tab. 5.1), since 1970 to the present. Regardless of the increase or decrease

in the flow volume, the researchers agree on the shift in flow patterns at the upper Indus River [19, 36, 145]. Since there are neither hydraulic structures at the upper Indus River/basin, nor land use changes that might have affected the situation, in contrast to [146, 147] studies for the East or Thames River, the temporal changes in SSLs can only be due to climate change factors. In addition, the statistically-significant monthly SSL trends contradict the previous reservoir sedimentation studies, which simply used the past SSCs without modification to the future predictions, particularly for the hydraulic structures planned upstream of Besham Qila [58, 15, 6, 33]. Thus, using modified boundary conditions for reservoir sedimentation studies in the presence of trends can improve the overall quality of hydraulic designs and reservoirs' lives in the study area.

Nevertheless, the variations in SSLs, overall, may have serious implications for water storage, as well as the management of peak supply, peak demand and dam safety, which will require certain changes in the existing reservoirs' operational rules. These changes may include the use of additional (increased) water for power generation during low flows (winter months) and for irrigation or flushing operations in May when more water is available. Flushing in May when crops are at a mature stage and do not require irrigation will also provide the opportunity to re-fill the reservoirs in the succeeding high flow months (June–July). Although the overall flow volume at Besham Qila has been increasing slightly, the flow contribution of the catchment between Partab Bridge and Besham Qila (Zone 2) has been decreasing and causing substantial sediment deposition and an overall decrease in the SSLs received at Besham Qila. Despite the fact that we did not include the impact of landslides on sediment deposition, the current findings are of crucial importance for 143 existing or planned dams and other construction projects in the upper Indus River, especially upstream of the Partab Bridge, which has a glacier-fed catchment and is sensitive to change in river discharges.

5.6 Conclusions

Reconstructed suspended sediment load (SSL) time series using wavelet neural networks (WA-ANNs) along with the innovative trend test, the Mann–Kendall test, Sen's slope estimator, the change point detection test and linear regressions have shown a shifting trend from the summer (June, July and August) to the spring and winter months due to a change in water availability at the upper Indus River over the past 50 years. The spatio-temporal trends between discharges and SSLs are disproportionate. This disproportional behavior and the significant trends strongly disconfirm the hypothesis that future inflows

and SSLs are similar to the previous ones for reservoir sedimentation studies for the upper Indus River. In addition, the SSLs recorded at Partab Bridge are depositing in the river channel between both gauges. This deposition process has led to a long-term decrease in SSLs, in contrast to a long-term increase in flow volume at the Tarbela dam. For future water and food security along the Indus River command area, it is necessary to estimate the impact of long-term SSL variations on the existing and planned water storage capacities of the reservoirs. Moreover, the impact of planned construction activities along the upper Indus River, which contains enormous sediment deposits, should be evaluated.

Chapter 6

An Innovative Approach for Modelling Sedimentation in Reservoirs

Abstract: A number of significant investigations have advanced our understanding of the parameters influencing reservoir sedimentation. However, a reliable modelling of sediment deposits and delta formation in reservoirs is still a challenging problem due to many uncertainties in the modelling process. Modelling performance can be improved by adjusting the uncertainty caused by sediment load boundary conditions. In our study, we diminished the uncertainty factor by setting more precise sediment load boundary conditions reconstructed using wavelet artificial neural networks for a morphodynamic model. The model was calibrated for hydrodynamics using a backward error propagation method. The proposed approach was applied to the Tarbela Reservoir located on the Indus River, in northern Pakistan. The results showed that the hydrodynamic calibration with coefficient of determination (R^2) =0.969 and Nash-Sutcliffe Efficiency (NSE) =0.966 also facilitated good calibration in morphodynamic calculations with R^2=0.97 and NSE=0.96. The model was validated for the sediment deposits in the reservoir with R^2=0.96 and NSE=0.95. Due to desynchronization between the glacier melts and monsoon rain caused by warmer climate and subsequent decrease of 17% in sediment supply to the Tarbela dam, our modelling results showed a slight decrease in the sediment delta for the near future (until 2030). Based on the results, we conclude that our overall state-of-the-art modelling

offers a significant improvement in computational time and accuracy, and could be used to estimate hydrodynamic and morphodynamic parameters more precisely for different events and poorly gauged rivers elsewhere in the world. The modelling concept could also be used for predicting sedimentation in the reservoirs under sediment load variability scenarios.

6.1   Introduction

Reservoir sedimentation is a serious issue in many parts of the world. On average, the annual rate of decrease in the world's reservoirs' storage capacity is approximately 1%. Together with the increase in world population, non-sustainable development and use of water resources, and the imminent threat associated with climate change, it may cause a crisis in water supply [53, 54]. In Asia alone, 80% of the useful storage capacity for hydropower production will be lost by 2035, while 70% of the storage volume used for irrigation will be lost to sedimentation by 2025 [52]. Pakistan, where no new large water storage has been constructed since the Tarbela dam in 1974, is facing a similar situation. The Tarbela dam has also lost 40.58% of its storage capacity due to high sediment trap efficiency [148]. Consequently, the country's reservoirs' water holding capacity is sufficient only to supply 30 days' requirements, and has been decreasing [45]. The decrease in water supply from reservoirs (such as the Tarbela) will affect millions of people who depend on the water supply and could lead to internal migration and severe geopolitical crises [20, 46]. Hence, it is necessary not only to operate the existing water storage capacities efficiently but also to construct reservoirs so as to trap less sediment. Especially in a scenario where reservoirs are the key infrastructure in mitigating the effects of climate change by their capacity to store and regulate water supply, the expected increase in hydrologic variability will demand more water regulatory capacity [52]. In addition, optimizing reservoir sedimentation will require new techniques for sediment load (SL) estimation, as conventional methods are no longer adequate or reliable.

The conventional method used to estimate SL, i.e. sediment rating curve (SRC), has limited accuracy due to complex sediment transport processes such as the hysteresis phenomenon [26, 3, 149]. For example, the mean deviation between the predicted SL using SRC and the measurements conducted for the Tarbela dam over a period of 26 years was approximately 40% [3]. A poor SL estimation affects the boundary conditions of the modelling process and may cause a circular error in reservoir sedimentation modelling, which subsequently results in the poor quality operation rules that ultimately contribute

to the structure's life cycle. Additionally, applying past data without modification for future modelling can also increase the circular error. [4] found a significant trend for the flow and SL in the Indus River, where summer flows have been decreasing, while pre-summer, post summer and winter flows have been increasing. Therefore, assuming that future flows and SLs are similar to past ones is not appropriate for reservoir sedimentation studies for the existing and planned dams on the Indus River [37, 43, 21, 44, 4]. Even the trap efficiency calculated using [66] curves may result in plausible over-or-underestimates of the trapped sediment volume. The same can also happen by calibrating a numerical model of a planned hydraulic structure with an (upstream or downstream) existing nearby dam.

The Tarbela dam is used as a standard for the design of planned (30,000 MW) hydraulic structures in the Upper Indus Basin (UIB). For studying reservoir sedimentation and designing of sediment routing facilities (invert level of low level outlets, bypass tunnels or location of power tunnels intakes), some numerical models have been developed [6]. In previous studies only 1D numerical models (HEC-RAS, HEC6-KC, RESSASS) have been used for Tarbela and other planned structures in UIB, due to their simplicity and lower computational time [57, 58, 15, 6, 1, 59]. The sediment boundary conditions in these models were based on SRC estimates. A 1D model can be used in simple topography to assess the cross-section averaged sediment deposition/erosion and the life of reservoirs. However, the SL boundary conditions based on SRC estimates may lead to false predictions. On the other hand, designers (in the detailed design stage) also need a more precise estimate of sediment concentrations with regard to different outlets, tunnels, etc., (and at different locations), to enable them to optimize sedimentation related facilities [60]. Since a 2D depth averaged model with more precise boundary conditions can provide more detailed information (in both simple and complex topographies) anywhere in the domain for shallow waters (when the 3D nature of the processes exists near the main dam body is of minor importance [150, 151]), its application is suitable for the Tarbela and other similar existing/planned hydraulic structures, where due to high width-depth ratio, vertical velocities are smaller than horizontal ones and pressure distribution is nearly hydrostatic.

For SL estimation, wavelet artificial neural networks (WA-ANNs) have performed well due to their ability to adjust for the hysteresis phenomena by decomposing the data time series in the time-frequency domain and revealing the information from a given data scenario [26]. However, there is a research gap in the literature with respect to reducing the uncertainty factor (contributing to accumulation of sediments in reservoirs) using WA-ANN estimated sediment loads (SLs) as a model of boundary conditions. In

addition, the computation time of 2D and 3D models for long term simulation of large systems such as the Tarbela dam is also very high. To address these research gaps, we employed a TELEMAC 2D open source model developed by Laboratoire National d'Hydraulique et Environnement (LNHE) France, which has also been modified by the Chair of Hydraulic and Water Resources Engineering, at the Technical University of Munich for graded sediment transport [63]. Since the modified code can run on computers with vector and parallel processing, the CPU time can be very significantly reduced.

Calibration is the process of setting the parameters of the model to ensure that the calculated values agree with observations. The validation process demonstrates whether the predictions of the calibrated model agree with the observed data set that is different from the data used in the calibration process. In this study, we calibrated our model using hydrological, and morphological data from the Besham Qila and Tarbela dam from 1983 (first comprehensive survey after its construction in 1974) to 1985, while the data from 1990 was used for the validation process. The calibration period of two years covers both, dry and wet, hydrological variations for the river. For example, 1984, with a flow volume of 83.8 billion m^3 (BCM) and SL of 209.6 million tons (Mt) was among the highest peak flow/SL years from 1969-2008, whereas 1985 had a lower flow/SL than corresponding averages. Similarly, the validation period of five years (1986-1990) also covers both dry and wet periods [4]. The computational time for hydrodynamic calibration was reduced using an automatic calibration method, which updated roughness for each mesh node using backward error propagation. The boundary condition of the morphodynamic model (in cascade modelling) was modified based on [3] studies where (due to the strong hysteresis phenomena) daily SL series was more precisely reconstructed from non-continuous suspended sediment (SSC) samples using WA-ANN. The overall performance of the modelling results was assessed using statistical performance parameters. To confine the length of this paper, detail of daily SL series reconstruction is not repeated here.

6.2 Methods

6.2.1 Study area

The Tarbela dam was constructed in 1974 on the Indus River to help in regulating the seasonal flows both for irrigation and power generation (Fig. 6.1). The dam supplies 50% of the total irrigation and 40% of the total energy production in Pakistan. The Tarbela Reservoir is embanked by three dams; the main embankment is 2,750 m long and 143

m high. The reservoir had an initial water storage capacity of 11.6 billion m^3 (BCM) with reservoir length extending approximately 80 km. The outlet works consist of four tunnels cut through the right abutment of the main dam plus a fifth tunnel between the main dam and the spillways on the left bank. The total installed capacity of the dam is currently 4,888 MW, 83% more than was originally envisaged in the initial design, with several turbines installed on tunnels 1-4 (Fig. 6.2). This also includes a recently installed scheme on tunnels 4 under Tarbela IV extension project, which has a power generation capacity of 1,410 MW [152].
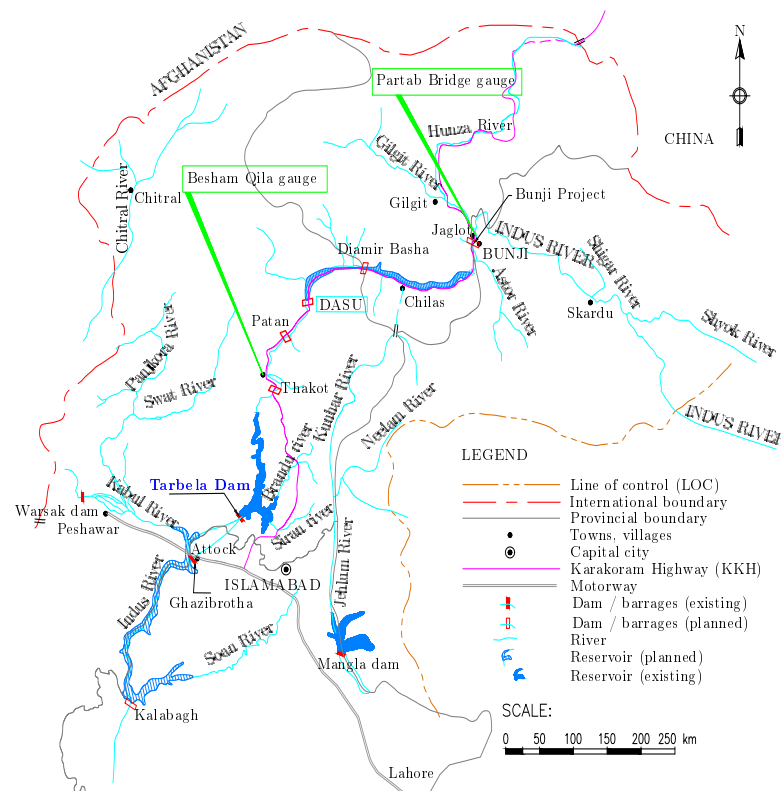

Figure 6.1: Location map of the study area, modified from [6]

Since commissioning, sedimentation in the Tarbela Reservoir has been a concern due to very high inflow of the sediments from the Upper Indus River, i.e. approximately 160-200 Mt/yr. This is largely due to the erosion effect of the glaciers that supply much of the flow. The Indus Basin upstream of the Tarbela dam has an area of about 169,650 km^2 (Fig. 6.1), of which over 90% lies between the great Karakoram and the Himalaya ranges. The snowmelt waters from this region contribute a major part of the annual flows regulated by the reservoir. The remainder of the Basin lying immediately upstream of the dam (Fig. 6.1) is subject to the monsoon rainfall primarily during the months of July to September. The peak flow due to snowmelt can be as high as 5,660 m^3/s to 11,300 m^3/s
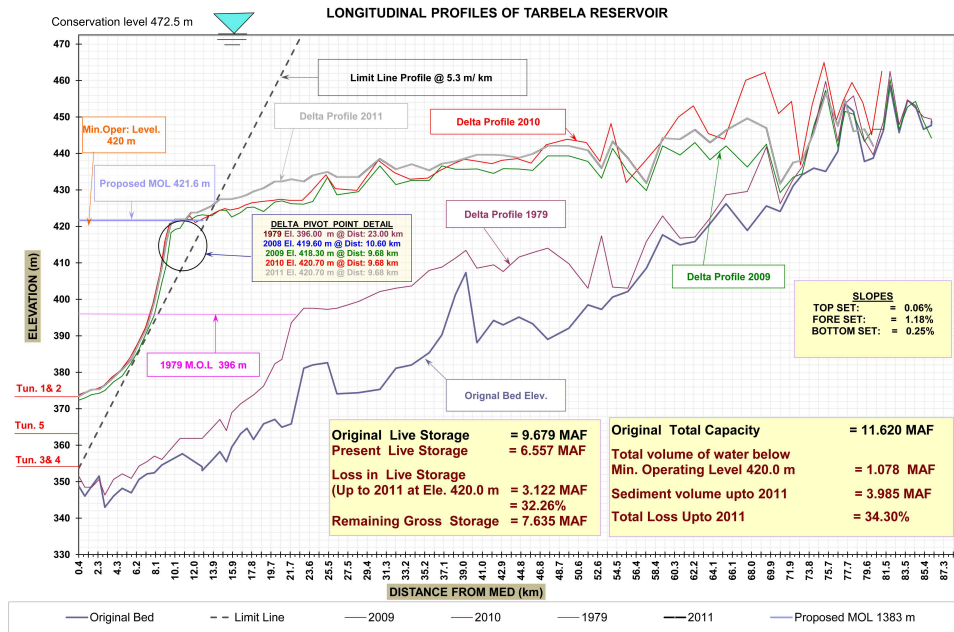
Figure 6.2: Sediment delta development in the Tarbela dam

with an additional rainfall contribution typically reaching a maximum of 5,660 m^3/s. The average annual inflow to the Tarbela Reservoir is 81 BCM [65].

Study of [3] noted that from 1969-2008 the annual sediment inflows into the reservoir varied between 92-270 Mt, which reduced the water storage capacity by 35% (Fig. 6.2) by 2011. The decrease in the storage capacity is a concern as it could result in reduction of irrigation supplies/allocations as per the Historic Apportionment Accord singed between the provinces in 1991 [153] and power supply. In addition, the impact of a delta created by the sediment deposits approaching the main dam is likely to block the power intakes. A recent alarming event at the Tarbela occurred in summer season of 2018 when reservoir levels dropped considerably, resulting in temporary blockage of power intakes. As the storage capacity of the reservoir reduces, more sediment will pass through the power intakes and likely to damage the turbine blades/runners. The problems may also be aggravated by the instability of the downstream sloping face of the delta [14] coupled with an occurrence of a earthquake [65].

6.2.2   Data description

The available sediment transport data for the dam consists of a long term hydrological database of published annual suspended sediment records and hydrographic surveys

conducted each year since 1983 (first comprehensive survey after the dam's construction in 1974). The hydrographic surveys are conducted using a systematic sounding method along the 73 cross sectional range lines, which covers the whole dam area, i.e. 161 km². Approximately 3,500-4,000 measurements of the bed level changes, water depths, and water surface elevations along these range lines are available, which were mostly collected during each survey conducted from September to November. The distance between the cross sections (range lines) and the (measured) data points along these cross sections is not uniform. An average distance between each cross section along the river thalweg is approximately 1.16 km. However, compared to the upstream (upper periphery of the reservoir), the distances between the cross sections are smaller near the dam. The distance between the measured data points along the cross sections (lateral distance in y direction) also varies with a mean of 39 m. The mean cross sectional width near the dam axis is approximately 4-5 km, which reduces to only 300-500 m at the upper periphery. Therefore, the major ponding area is near the dam axis and contains huge sediment deposits (Fig. 6.2).

Long-term continuous discharge and discontinuous suspended sediment concentration (SSC) sampling data is available at Besham Qila, which functions as an inflow gauge station for the Tarbela dam. On average, the SSC sampling frequency at the Besham Qila gauge station is 22% of annual daily sampling, therefore a daily time scale can be established using a sediment rating curve or an ANN and WA-ANN techniques [3]. In the present study, we used a WA-ANN technique from [4] study, which reconstructed the SSLs with Nash-Sutcliffe Efficiency (NSE)=0.837 for the calibration and NSE=0.871 for the validation period (Tab. 6.1). The Indus River transports more silt (47%) compared to sand and clay (Tab. 6.2), and 90% of it is trapped in the dam [19]. The density of sand, silt and clay is 1,535, 1,330, and 1,170 kg/m³. Although, observations show that there is no clear boundary of sizes between cohesive and non-cohesive sediments, the definition of cohesive sediment is usually site specific. Normally, cohesion plays a significant role for sediment sizes smaller than 2 μ m in reservoirs (including the Tarbela). We, therefore, used cohesionless modelling [154, 19, 155]). Most of the transport processes occur in the summer months; 84% of the total annual discharge and 99% of the SSL transport occur from May to September (Tab. 6.3 and Fig. 6.3).

Water depth in the reservoir varies from a maximum 150 m near the main dam to mostly 20 m upstream. To secure the stability of the dam and the slopes on the both banks along the reservoir, the maximum lowering and rising rate for the reservoir during operation, is 4 m/day and 3 m/day respectively between reservoir levels 396-460 m and

only 1 m/day up to the maximum conservation level (472.5 masl). The average slope upstream of the river bed in 1979 was $\frac{1m}{892m}$, which became flatter in 2010, with an average slope of $\frac{1m}{1,670m}$. More detail on data availability, data quality, re-construction and distribution can be found in [67, 3, 4].

Table 6.1: Statistical performance of WA-ANN for reconstructing SSL in study period (only high flows from May to September). Sediment load was calculated in [4]

Process	Duration	R²	RSR	NSE
Calibration	1984-1985	0.842	0.019	0.837
Validation	1986-1990	0.888	0.019	0.871

Table 6.2: Mean representative size classes of SSC

	Sand					
Grain size (mm)	1.0	0.5	0.25	0.125	0.0625	Pan
Fraction (%)	100	99.87	96.98	85.85	71.98	71.97
	Silt					
Grain size (mm)	0.0442	0.0312	0.0221	0.0156	0.011	0.0078
Fraction (%)	64.51	57.12	49.59	41.07	32.70	25.29
	Clay					
Grain size (mm)	0.0055	0.0039				
Fraction (%)	17.43	10.32				

Table 6.3: Suspended sediment load and flow volume distribution in million tons (MT) and billion cubic meters (BCM) from 1984-1990. Outflow also includes the minor contribution (0.04% and 0.16%) of the Siran and Brandu tributaries

Months	Average SSL (Mt)	Average inflow (BCM)	Average outflow (BCM)
Jan-Apr	0.98	5.67	11.85
May-Sep	157.9	65.54	55.18
Oct-Dec	1.11	5.50	11.25

6.2.3 Model system

TELEMAC is an open source finite element flow model on an unstructured, triangular mesh [61]. Whereas SISYPHE is a sediment transport model, which is capable of
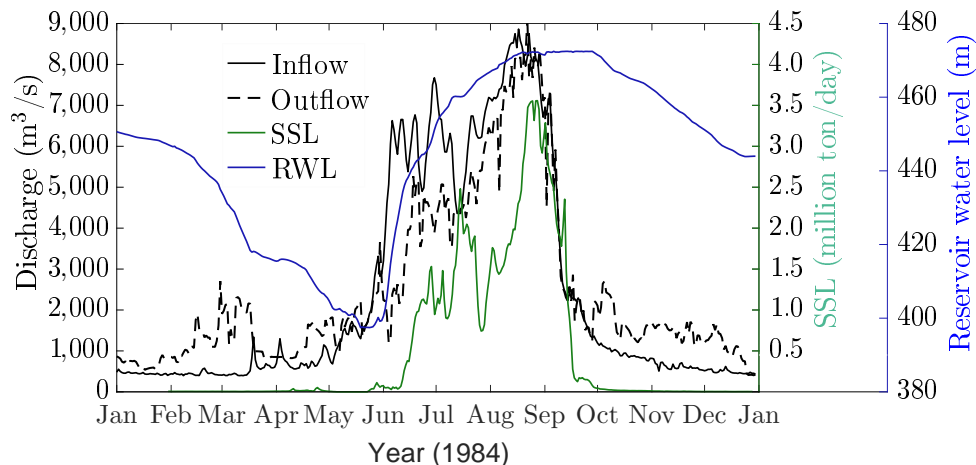
Figure 6.3: Sediment inflow, reservoir water level and discharges in 1984 (dash line represents outflow from the dam).

modelling sedimentary systems containing very fine to medium sand in suspension or as bedload [62]. Both models provide the opportunity to the users to adapt and modify the codes to facilitate a better simulation performance. In addition, the software package programmed for the parallel processing option, which significantly reduces the simulation time of study domains, have enormous mesh nodes. The opportunity to modify the source code also allows to implement an automatic calibration concept using Matlab or other programming languages. Different numerical schemes are available which can be selected according to study requirements, available computational power, time availability and desired accuracy. However, an edge based N-scheme based on a positive depth algorithm is a good compromise between accuracy and computational time [62]. The scheme is stable for the Courant number during each time step where it remains less than 1. Calculating a fixed time step over which the Courant number always stay below 1 is, nevertheless, challenging. Therefore, a variable time step option can be used where the model automatically executes intermediate time steps and the Courant number stays below a given value. The variable time step option is useful for simulations over several years or decadal, during which a river catchment undergoes several dry and wet hydrological cycles of run-off and subsequent sediment load.

The main factors controlling the sand transport are: advection by currents, settlement under gravity, turbulent diffusion in all directions, and exchange of sand between the flow and the bed. Two methods, chaining or internal coupling, are used to link the hydrodynamic and morphodynamic models[62]. In chaining, both hydrodynamic and morphodynamic models perform independently. For morphodynamic calculations the flow field is obtained from a previous hydrodynamic simulation where the bed is assumed to be non-moveable. Due to the difference in time scales of hydrodynamics and bed

evolution, this coupling method is normally used to model simple flows and small bed changes. The chaining coupling method does not conserve the mass due to change in the flow field while the bed evolves, which can lead to numerical instability. In internal coupling, the models communicate through a quasi-steady morphodynamic time stepping approach and both models (TELEMAC and SISYPHE) can be run fully coupled in such a way that after TELEMAC has computed the flow, the flow field can be used at each time step by the SISYPHE to calculate the sediment transport and resulting changes in the bed. The new bathymetry is passed back to the TELEMAC to calculate the new flow field on the next time step. If the flow is stationary and the bed changes in a time step are small compared to the water depth, a morphological speed up is used to reduce the computational time [156, 157, 158, 62, 159].

6.2.3.1   TELEMAC-2D for hydrodynamics

The TELEMAC 2D solves the following 2D shallow water equation for hydrodynamics. The equations were derived from the Navier-Strokes equations by taking the vertical average:

$$\frac{\partial h}{\partial t} + \frac{\partial (hu)}{\partial x} + \frac{\partial (hv)}{\partial y} = 0 \tag{6.1}$$

$$\frac{\partial (hu)}{\partial t} + \frac{\partial (hu^2)}{\partial x} + \frac{\partial (huv)}{\partial y} = -hg\frac{\partial Z_s}{\partial x} + \frac{\tau_{xx}}{\rho} \tag{6.2}$$

$$\frac{\partial (hv)}{\partial t} + \frac{\partial (hv^2)}{\partial y} + \frac{\partial (huv)}{\partial x} = -hg\frac{\partial Z_s}{\partial y} + \frac{\tau_{yy}}{\rho} \tag{6.3}$$

Where h = depth of water (m); u, v = depth-averaged flow velocity components in x and y direction, respectively (m/s); g = gravitational acceleration (m/s^2); Z_s = free surface elevation (m); t = time (s); x, y = horizontal Cartesian coordinates (m); ρ = density of water (kg/m^3); τ_{xx} and τ_{yy} = depth-averaged turbulent stresses. The bed shear stress is represented as a quadratic function of velocity:

$$\tau_{b(x,y)} = \frac{\rho C_f(u,v)|u|}{2} \tag{6.4}$$

Where C_f is roughness coefficient which can be calculated using Manning (n: $\frac{m^{1/3}}{s}$), Chezy (C: $\frac{\sqrt{m}}{s}$), or Nikuradse (N: mm) equations.

6.2.3.2   SISYPHE for morphodynamics

The sediment transport model, SISYPHE, simulates river bed morphodynamics by calculating temporal changes in bed elevation Z_b using the Exner equation:

$$(1 - p\prime)\frac{\partial Z_b}{\partial t} + \frac{\partial(\delta_b c_b)}{\partial t} + \frac{\partial(q_{t,x})}{\partial x} + \frac{\partial(q_{t,y})}{\partial y} + \eta\prime_e - \eta\prime_d = 0 \qquad\qquad 6.5$$

Where Z_b = bed elevation (m); δ_b = bed load layer thickness (m); $p\prime$ = bed porosity (-); c_b = sediment concentration in bed load layer (m^3/m^3); $q_{t,x}$ = total sediment transport in x-direction (m^2/s); $q_{t,y}$ = total sediment transport in y-direction (m^2/s); $\eta\prime_e$, $\eta\prime_d$ are erosion and deposition rates, respectively (m/s).

The SISYPHE model assumes the Rouse concentration profile, from which the equilibrium depth-averaged concentration is calculated.

6.2.4   Model setup

6.2.4.1   Grid mesh

The geometry of the Tarbela dam reservoir area was drawn from the Tarbela Reservoir Sedimentation Survey conducted in 1983. The survey along the Indus River was conducted from dam axis (0 km) to 88.10 km upstream. The reservoir bathymetric survey conducted by the Water and Power Development Authority Pakistan (WAPDA) proceeded from the left river bank to the right river bank, while looking downstream. The y distance (m) along each cross section starts from left river bank (with an absolute value of zero) to a maximum at the right river bank. The x distance (m) along the river starts from the main dam axis (central line) to a maximum at upstream (upper periphery of the reservoir (88.10 km)). The z is the river reservoir bed elevation in meters above sea level (masl) at each x and y distance. At each cross section, there was information of the distance along the left river bank, the distance along the main river channel (centre line), and the distance along the right river bank, i.e. at each cross section three values of x-distance. All measurements of z at each cross section were between the left and right river bank. On average 47 measurements were taken on each of the 73 cross sections, which resembles a total of 3,455, excluding the cross section (R/line) 62, where no data is available for 1983 (see Fig. 6.4). We excluded the Siran and Brandu tributaries (due to their minor contribution in the Tarbela dam) from the reservoir geometric model. To

create the geometry, SMS 12.2.9 developed by the Aquaveo and the open source software
BlueKenue was used. In order to convert the local coordinates of the data points on
each cross section to global coordinates (Cartesian coordinate system), the y distance was
transformed with AutoCAD Civil 3D 2018 (Fig. S4). The final geometry applied in the
numerical model is shown in Fig. 6.4.

An unstructured mesh of various sizes, particularly a finer one for the areas where the
river meanders, was generated. The final mesh contains 138,000 mesh elements repre-
senting 171 km^2. In selecting cell resolution, we tried to achieve a reasonable compromise
between accuracy and computational time.

To confirm the geometry approximation, we compared elevation-storage volume curve
with the observation (which does not include the volumes of the Siran and the Brandu
tributaries) as shown in Fig. 6.5. We obtained the statistical performance parameters
NSE=0.99, R^2=0.99, and a relative difference between the measured and the computed
volume=1%. Furthermore, the longitudinal profile of the mean measured and calculated
river bed is also shown in Fig. 6.6. The results confirmed a correct representation of the
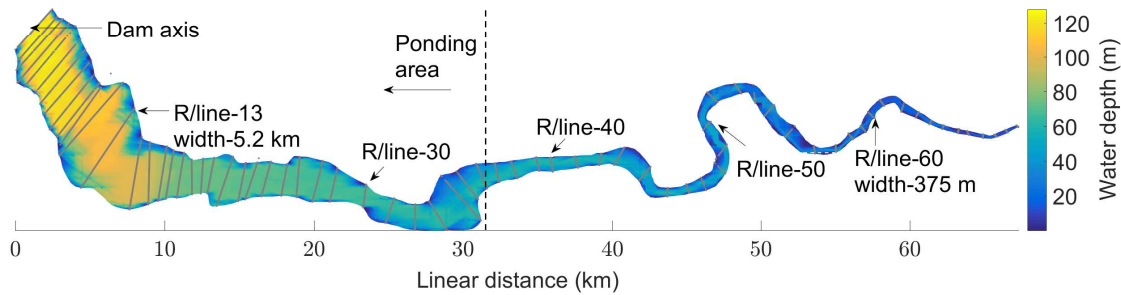grid mesh used in the numerical model.

Figure 6.4: Measured data points (grey) along cross sections/range lines and TELEMAC
simulated water depth at 30 September 1983

6.2.4.2   Initial and boundary conditions

As an initial condition, we filled the reservoir up to the maximum conservation level, i.e.
472.5 m, so that the model can attain a stable condition at the beginning. In addition,
we also set the SSC in equilibrium. In the numerical model, the vertical variations in the
SSCs and river flow were considered small compared to their horizontal counter parts.

The daily measured discharges and the WA-ANN reconstructed suspended sediment
loads (SSLs) were applied as upstream boundary conditions while the reservoir water
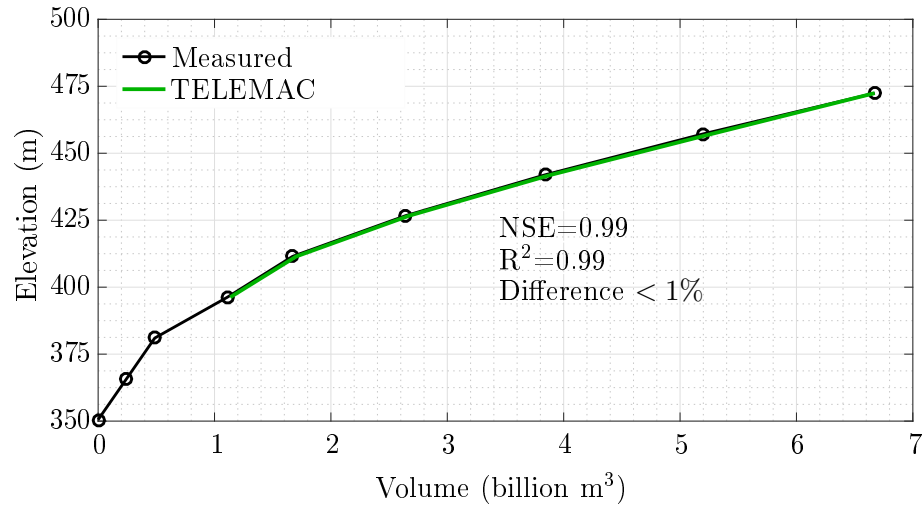
Figure 6.5: Comparison between the computed elevation-storage volume and observation for 1983

levels (RWL) were kept as the downstream boundary condition. We used the data from 1983 for hydrodynamic calibration while the data from 1984 to 1985 was used for the morphodynamic calibration and from 1985 to 1990 for the validation. We also omitted the low flow periods (from November to March (Tab. 6.3)) from the modelling due to their small contribution in the annual SSLs [4]. We also excluded small tributaries, i.e. the Siran and the Brandu, due to their minor (0.04% and 0.16%) contribution to the total sediment load entering the Tarbela Reservoir [19].
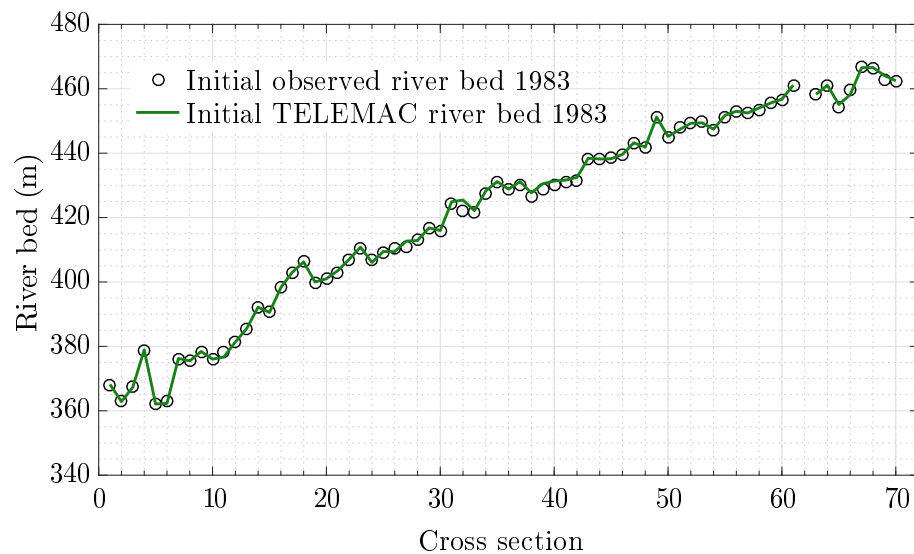
Figure 6.6: Mean observed and approximated river bed

6.2.5 Model performance

To evaluate the performance of the TELEMAC/SISYPHE model in terms of accuracy and consistency in predicting reservoir water depths and bed levels, the three following statistical measures were employed: (a) Coefficient of determination (R^2), which is an index of the degree of relationship between the observed and simulated data, ranging from 0 to 1, as follows:

$$R^2 = \left(\frac{\sum\limits_{i=1}^{P}(X_i^{obs} - \bar{X}^{obs})(X_i^{sim} - \bar{X}^{sim})}{\sqrt{\sum\limits_{i=1}^{P}(X_i^{obs} - \bar{X}^{obs})^2 \sum\limits_{i=1}^{P}(X_i^{sim} - \bar{X}^{sim})^2}} \right)^2 \qquad 6.6$$

Where X_i^{obs}, X_i^{sim} represent i^{th} value of observed and simulated parameters, respectively, where $\bar{X}$ denotes their mean values.

(b) Observations standard deviation ratio (RSR), which is the ratio of root mean square error (RMSE) and standard deviation (STDEV) of the observed data, as follows:

$$RSR = \frac{RMSE}{STDEV_{obs}} = \frac{\sqrt{\frac{1}{P}\sum_{i=1}^{P}(X_i^{obs} - X_i^{sim})^2}}{\sqrt{\sum\limits_{i=1}^{P}(X_i^{obs} - \bar{X}^{obs})^2}} \qquad 6.7$$

RSR varies from 0 to any positive value. A lower RSR value indicates a better performance of the model simulation.

(c) Nash-Sutcliffe Efficiency (NSE), which is a statistical measure to determine the relative magnitude of the residual variance compared to the measured data variance [160], as follows:

$$NSE = 1 - \frac{\sum\limits_{i=1}^{P}(X_i^{obs} - X_i^{sim})^2}{\sum\limits_{i=1}^{P}(X_i^{obs} - \bar{X}^{obs})^2} \qquad 6.8$$

Although negative values are possible, the NSE generally ranges from 0 to 1. NSE = 0 indicates that the model is no better than simply forecasting the mean value. The

closer the value of NSE to 1, the better the model performance. The simulated results
are normally referred as good when the NSE is higher than 0.75 and satisfactory when it
lies between 0.36 to 0.75 [115]. To define a stopping criteria (Eq. 6.17) for hydrodynamic
calibration, we assigned equal weight to all three statistical parameters in the form of a
statistical mix (S) as follows:

$$S = \frac{R^2 + (1 - RSR) + NSE}{3}$$

6.9

S can vary from 1 to a negative value, where 1 indicates a best performance of the
model.

6.2.6   Model parameters and automatic calibration

The information about the Tarbela dam other than daily inflows, reservoir water levels,
and WA-ANN reconstructed SSLs are: (a) volume of sediments deposited each year after
the flood season (between October-November), (b) 72 longitudinal profiles along the reser-
voir over the period 1983 to the present, (c) composition of the sediment deposits in some
areas, (d) flow velocities measured with an ADCP at several cross sections, (e) outflow
discharge and sediment concentration. This information were used for hydrodynamic and
morphodynaic calibrations. The automatic calibration algorithm was developed to save
computational time. We edited and controlled the TELEMAC and SISYPHE models
with a single Matlab code (Fig. 6.7). The TELEMAC and SISYPHE models required
specifying several parameters such as method for parametrising fraction coefficients, ini-
tial particle size distribution, sediment transport (suspended and bed load) formulae,
critical Shield parameter, and settling velocity. For the suspended sediment calculations
we tested different transport formulae. The critical Shield parameter was set to 0.047 for
the simulations. We provided settling velocities (m/s) to the model using the following
equation [161, 162]:

$$W_s = \begin{cases} \frac{(s-1)gd_{50}^2}{18\nu}, & \text{if } d_{50} \leq 10^{-4} \\ \frac{10\nu}{d_{50}}\left(\sqrt{1 + 0.01\frac{(s-1)gd_{50}^3}{18\nu}} - 1\right), & \text{if } 10^{-4} \leq d_{50} \leq 10^{-3} \\ 1.1\sqrt{(s-1)gd_{50}}, & \text{otherwise} \end{cases}$$

6.10

To deal with limitation of the numerical scheme, which can arise due to a numerical
error and can create negative water depths, we specified a minimum water depth of 1
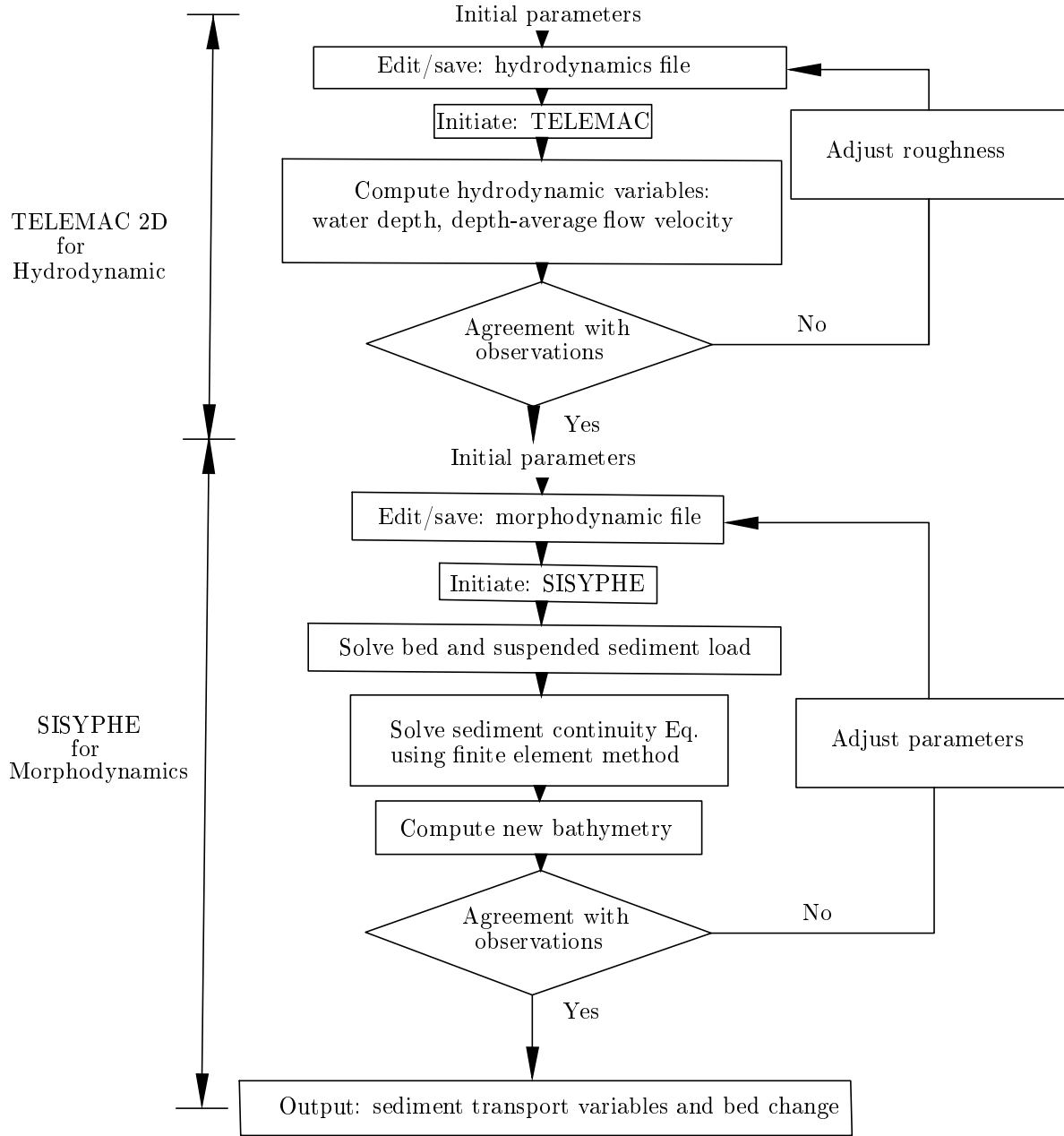
Figure 6.7: Algorithm for model calibration. The algorithm for TELEMAC and SISYPHE works in an uncoupled way where morphodynamic calibration only start after hydrodynamic calibration finished.

cm in the whole study domain. As the Indus River has an alluvial bed, we specified an erodible layer thickness of 100 m. The Manning roughness (n) was calculated using a back propagation error method (discussed below).

Based on preliminary results for the morphodynamic calibrations, we eventually used the [161] suspended sediment transport formula (Eq. 6.11) with different reference eleva-

tions (Z_{ref}) by changing total bed roughness (k_s). We also tested different friction angles and bedform correction factors for the sediment transport in the calibration process.

$$C_{eq} = 0.015 d_{50} \times \frac{(\frac{\tau'}{\tau_{cr}} - 1)^{0.66}}{Z_{ref} \times D_*^{0.3}} \qquad 6.11$$

Where τ_{cr} is critical shear stress (N/m^2), D_* is dimensionless grain diameter, Z_{ref} is reference elevation which can be calculated after [161] using $max(\frac{k_s}{2}; 0.01m)$, while k_s is total bed roughness (m) and is obtained from hydrodynamic calculations (Eq. 6.16: friction coefficients from hydrodynamic results) and type of bed-forms (flat, smooth or ripples bed). The τ' is total shear stress (N/m^2) includes skin friction which can be calculated using Eq. 6.12:

$$\tau' = \mu \times \tau_b \qquad 6.12$$

Where τ_b is total bed shear stress and μ is bed form coefficient calculated as follows:

$$\mu = \frac{C'_f}{C_f} \qquad 6.13$$

Where C_f is the combined friction of both drag forms and skin friction, and can be obtained from hydrodynamic results. C'_f is a friction coefficient due to skin friction and can be calculated as follows:

$$C'_f = 2 \times \left(\frac{k}{log(\frac{12 \times h}{k'_s})} \right)^2 \qquad 6.14$$

Where k is von Karman coefficient(=0.40), and k'_s is roughness height and can be computed as:

$$k'_s = \alpha_{ks} \times d_{50} \qquad 6.15$$

Where α_{ks} is a calibration coefficient and d_{50} mean particle diameter (m). Although the shallowness assumption is compromised due to non hydrostatic pressure distribution near the main dam, to model the bed level changes in the dam ponding area on a large scale we assumed that pressure distribution is virtually hydrostatic [150]. More details on morphodynamic calculations of the SISYPHE model can be found [62].

The Manning roughness (n) is used as one of the key parameters for flow calibration. The hydrodynamics was calibrated using the observed water levels at different locations along the 72 cross sections from 1983. The morphodynamics were calibrated using the river bed level changes along these cross sections from 1985. To compare the measurements (3,455) in the calibration process we created a 2D surface, to obtain interpolated values at the measured locations, by interpolating the simulated results using a 2D interpolation method. Based on the comparisons between the simulated and measured values, the relevant hydrodynamic and morphodynamic parameters were updated (Fig. 6.7). For interpolation we used: (a) linear, (b) nearest point, (c) natural, and (d) cubic interpolation methods.

Initially, for hydrodynamic calibration a constant hydraulic roughness n=0.04 from the literature [59, 76, 57] was used for the whole domain. In successive simulations, the model calculated n for each node using a backward propagation error method stated in Eq. 6.16:

$$
\begin{aligned}
n_{i,node} &= n_{i-1,node} - n_{i-1,node} \times P_{i-1,node} \times K \\
P_{i-1,node} &= \frac{2}{1 + e^{(-2 \times \eta_{i-1,node})}} - 1 \quad \text{where } -1 \leq P \leq +1 \\
\eta_{i-1,node} &= \frac{d^o_{i-1,node} - d^s_{i-1,node}}{d^o_{i-1,node}} \qquad \text{where } i = 2, 3, .., m
\end{aligned}
\tag{6.16}
$$

Where m represents numbers of simulations, d^o represents observed and d^s simulated water depths (m), and η is a dimensionless gradient used to arrive an optimal n. P is used to avoid over or undershoots of n. K is used to curtail significant changes in n due to continuous large gradients η at certain nodes. In subsequent iterations, the roughness to unmeasured nodes/points was assigned using a 2D linear interpolation method. The model stops when the difference between successive statistical mix (S) is a minimum, given here:

$$
S_i - S_{i-1} \leq 0.0001
\tag{6.17}
$$

Where S is given in equation Eq. 6.9. The convergence depends on the selection of an initial value of n.

6.3 Results

For the computational grid mesh we used 1983's comprehensive dam bathymetric survey. To calibrate the TELEMAC 2D model (with an automatic calibration algorithm) we use the hydrological data from 1985. To calibrate the SISYPHE model, we used the bathymetric survey from 1985. To validate the morphodynamic calculations, we use the bathymetric survey from 1990. The simulation results were evaluated using the coefficient of determinations (R^2), observed standard deviation ratio (RSR), and Nash-Sutcliffe Efficiency (NSE). The results are discussed in detail below.

6.3.1 Model calibration

Since a better representation of the study domain in the form of a numerical mesh plays a significant role in subsequent calculations, we tested different types of mesh sizes to obtain realistic results. Based on difference between measured and simulated water depths, we calibrated the hydrodynamic model by updating Manning roughness (n) for the whole domain using an automatic calibration approach mentioned above (Fig. 6.7). The calibrated flow model was used further for calibrating and validating morphodynamics as well as applying to predict (upto 2030) the bed level changes in the reservoir using more precise sediment load boundary conditions reconstructed with a WA-ANN (for WA-ANN model development please see [4]). The overall performance of the modelling concept was assessed using three statistical performance parameters, i.e. R^2, RSR, and NSE. The hydro-morphodynamic results of the study are described below.

To obtain the simulated water depths at the measured points, we applied a 2D scatter data interpolation method. The method interpolates the surface and returns the interpolated values at the desired points (x,y). The surface always passes through the mesh data points. In our study, we tested four different interpolation methods, namely, (a) linear, (b) nearest point, (c) natural, and (d) cubic. Due to the smooth river bed along the cross sections in the Tarbela Reservoir, a linear interpolation performed better than the other mentioned methods. Therefore, by using linear interpolation, we compared the interpolated and measured depths and updated n in the whole study domain using a back propagation method (Eq. 6.16). The final roughness (n) ranged from 0.035 to 0.045 with a mean of value of 0.0395. The roughness was lower downstream near the dam and in the middle of the channel, and vice versa (Fig. 6.8).
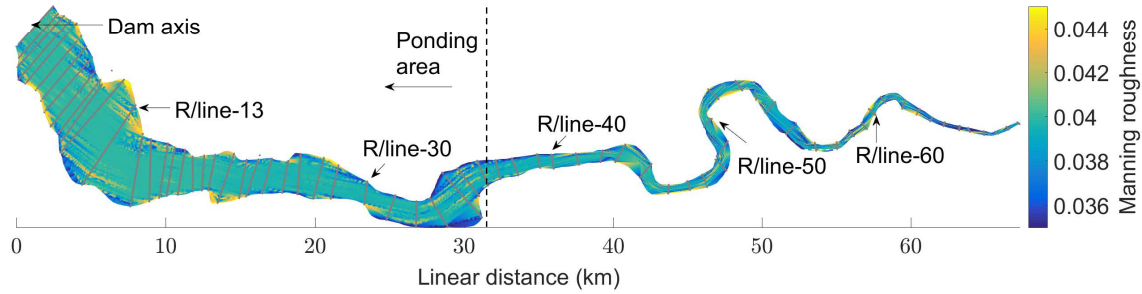
Figure 6.8: Interpolated Manning roughness (n). Grey lines represent the measurements along the cross sections/range lines (R/line).

Initially, using a uniform value of n=0.04, we obtained an absolute average difference of 1.6 m between the simulated and measured water depths. However, the difference decreased to only ±1 m after 5 iterations. The mean relative difference between the simulated and measured data points was only 0.072%. At some cross sections we only have measurements near the river banks, that is why their mean appears lower than neighbouring cross sections (Fig. 6.9). Comparison of water depths at some selected cross sections is shown in Fig. 6.10.

Water depth convergence depends upon an initial estimate of n. Using a single roughness (n=0.04) from the literature [59, 76, 57] for the whole domain of 171 km^2, initially we obtained a statistical mix (S)=0.933, R^2=0.90, and NSE=0.898 (Fig. 6.11). The performance of the model increased to a statistical mix=0.978, R^2=0.969, and NSE=0.966 by iterating n for each node point as per Eq. 6.16 and the process stated in Fig. 6.7. The approximated computational time in each simulation was 12-15 hours using a server with 20 physical cores (dual Intel XEON E5-2687W v3 @ 3.1 GHz) and 128 GB of RAM. Due to the large standard deviation (33.9 m) and small RMSE (0.0988) in the water depths, the observation standard deviation ratio (Eq. 6.7) remained in the range of 10^{-3} in all five simulations.

Further, we used the calibrated flow model for morphodynamic calibration and validation. As 90% of the sediment load (SL) entering the dam consists of suspended load [67, 4], we omitted bed load from the modelling process. For SL concentration, we used [161] formula (Eq. 6.11). The bed roughness was updated using a skin correction factor in the formula. The calibrated coefficient α_{ks}=3 (Eq. 6.15) provided the best results.

By varying different parameters (such as reference elevation, total roughness, etc.), we conducted a number of different simulations until a good agreement between the
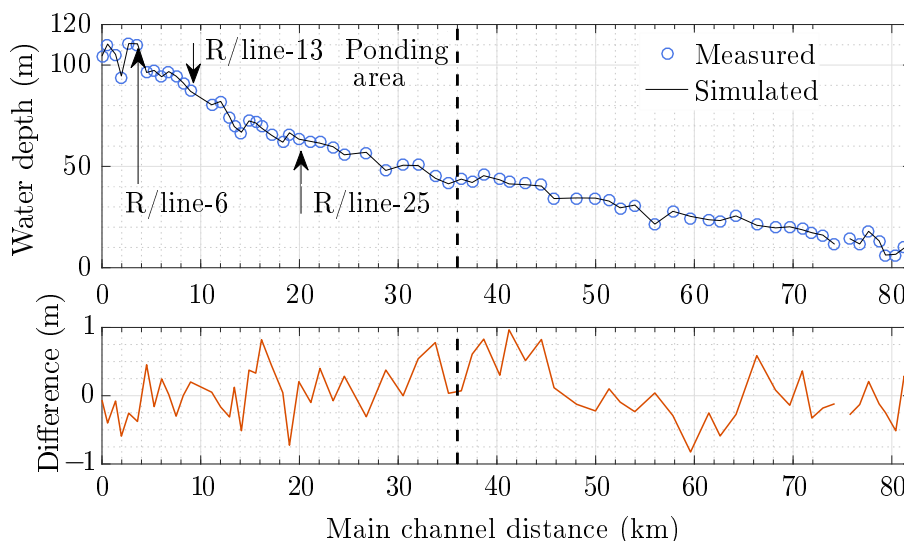
Figure 6.9: Comparison of mean measured and computed water depths at each cross section
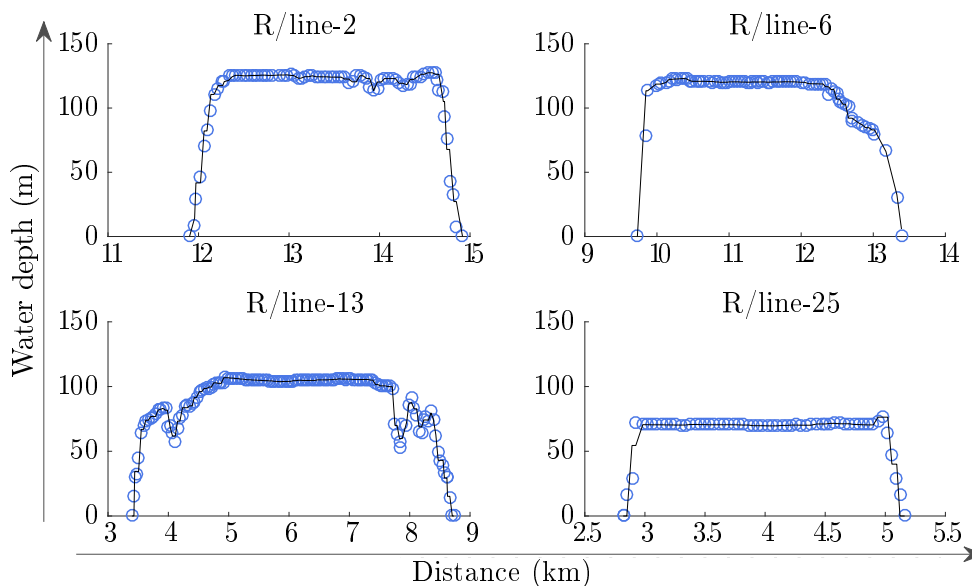

Figure 6.10: Comparison between measured (circles) and simulated water depths at selected cross sections (R/line) for 1983' event. Measurements starts from orographically left side of the reservoir.

measured and simulated result was found as presented in Tab. 6.4. We also updated the TELEMAC/SISYPHE 2D code for all fractions of suspended SL boundary conditions. In addition, the negative depth which arose due to numerical error was solved by specifying a minimum water depth of 1 cm in the whole study domain. However, this overall minimum water depth caused an excessive clay deposition due to its very low settling velocity= 2×10^{-5} m/s at some nodes on high river banks. We solved this issue by specifying no SL
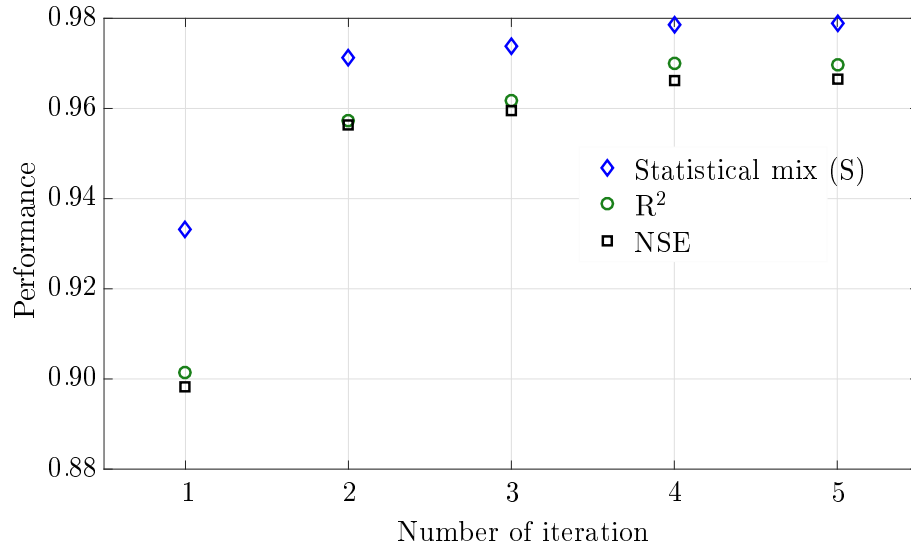
Figure 6.11: Statistical convergence of water depths for 1983' event

transport at equal or less than 1 cm water depth. Our final simulated results from May 1984 to October 1985 showed R^2=0.97, RSR=0.36%, and NSE=0.96 (Fig. 6.12). There was only 0.76% difference between the simulated and measured deposits in the reservoir. However, the mean differences between the simulated and observed river bed was in the range of -5 to 7 m.

Fig. 6.12 compared the mean computed and observed river bed along the river reach. The disagreement between measured and simulated results at some cross sections located in the upstream part of the river may be caused by large distance between the measured cross sections in this part of the river, distorting the in-between initial geometric information (see Fig. 6.4).

There was also a good agreement between each measurement along the cross sections in the ponding area (Fig. 6.13), where the Tarbela Reservoir has a sediment delta (Fig. 6.2). The approximated computational time in each simulation from 1983-1985 for only high flows (March to September - Tab. 6.3) was one week. After calibrating the model, we used the 1985 simulated river bed for the validation process.

6.3.2   Model validation

We validated the model using the sedimentation survey conducted in 1990, which (including cross section (R/line) 62) has 3,600 measured points of the river bed elevation along 73 cross sections. For validation, we ran the model for the five years (1986-1990) and

Table 6.4: Formulae and value of different hydro-morphodynamic parameters (stated in Eq. 6.10 to 6.16) used in the calibration process.

Parameter	Value/methods
Hydrodynamics	
Numerical scheme	Centred semi implicit scheme plus SUPG
Solver for hydrodynamic propagation step	Generalized minimum residual method
Equations	Saint-Venant finite element
Hydrodynamic calibration factor (K)	1.0
Manning roughness (n)	0.035-0.045
Mean Manning roughness (n)	0.0395
TELEMAC and SISYPHE model coupling	Internal
Morphodynamics	
Bed porosity ($p\prime$)	0.375
Fluids viscosity (ν)	1×10^{-6}
Suspended sediment transport formula	[161]
Calibration coefficient (α_{ks})	3
von Karman coefficient (k)	0.40
Shields parameter	0.047
Friction angle of sediment (ϕ_s)	32
Minimum depth required for sediment transport	1 cm
Formula for deviation	[163]
Parameter for deviation ($\beta2$) [163]	0.85
Stream wise slope effect (β)	1.3
Solver for suspension	Conjugate gradient
Critical evolution ratio	0.5
Numerical treatment of the advection term	Edge-based N-scheme

compared the measured and simulated river bed elevations. The statistical comparison showed R^2=0.96, RSR=0.37%, and NSE=0.95, whereas the difference between the measured and simulated deposits was only 0.54%. Similar to the morphodynamic calibration, the mean differences between the simulated and observed river bed were in the range of -5 to 7 m (Fig. 6.14).

As with the longitudinal profile in the calibration process, we obtained good results for the ponding area (Fig. 6.14). However, there were also disagreements between the measured and simulated results at some cross sections located upstream of the ponding area. In conformity with the calibration results, the model provided the results closed to river bed elevations measured along the cross sections in the ponding area (Fig. 6.15). The approximated computational time in each simulation from 1983-1990 for only high flows (March to September - Tab. 6.3) was three weeks.
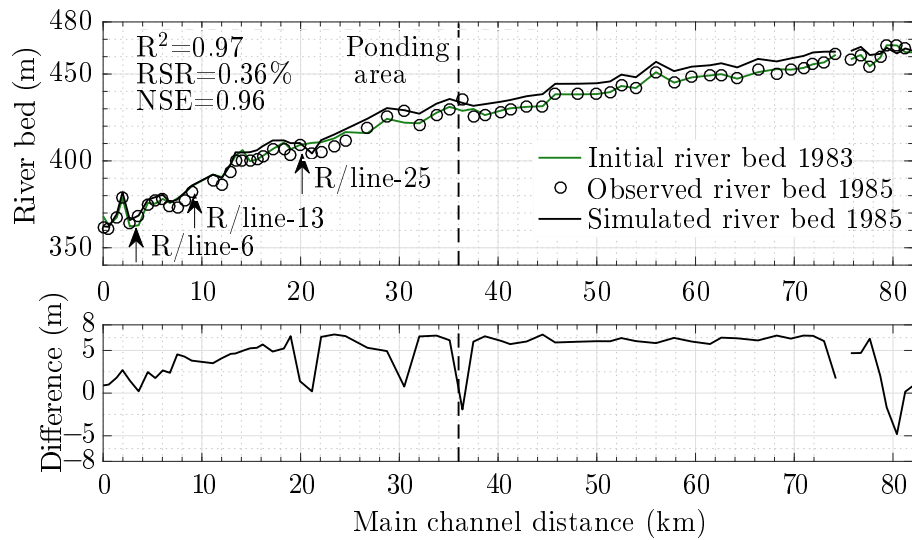
Figure 6.12: Longitudinal profile of mean measured and computed river bed at the end of calibration process
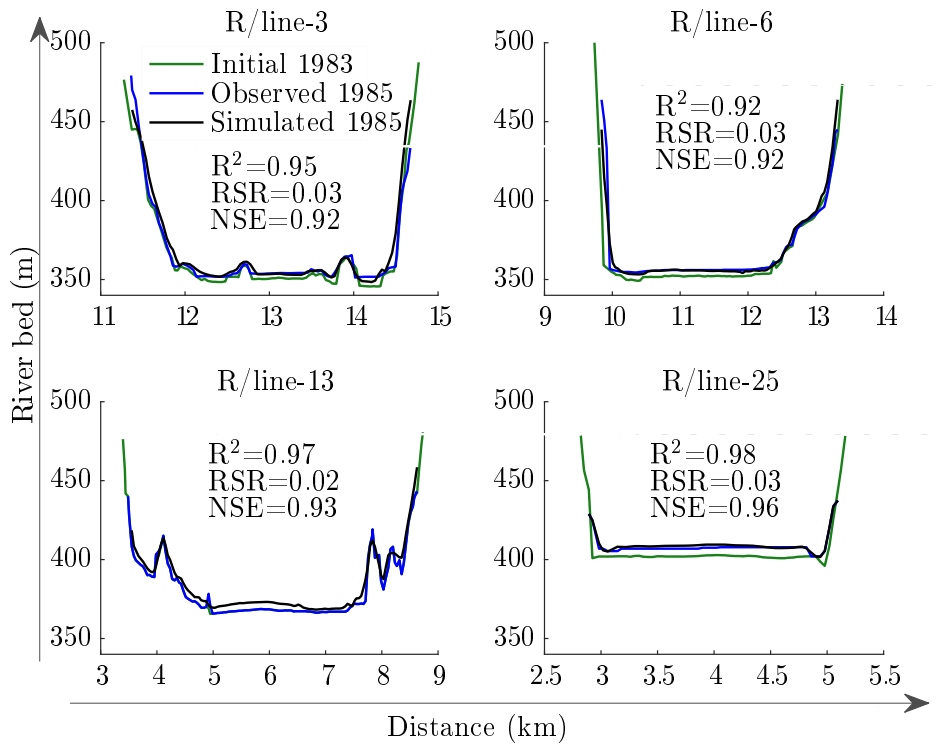

Figure 6.13: Comparison between measured and simulated river bed at four selected cross sections/range lines (R/line) at the end of calibration process. Measurements start orographically from left side of the reservoir.
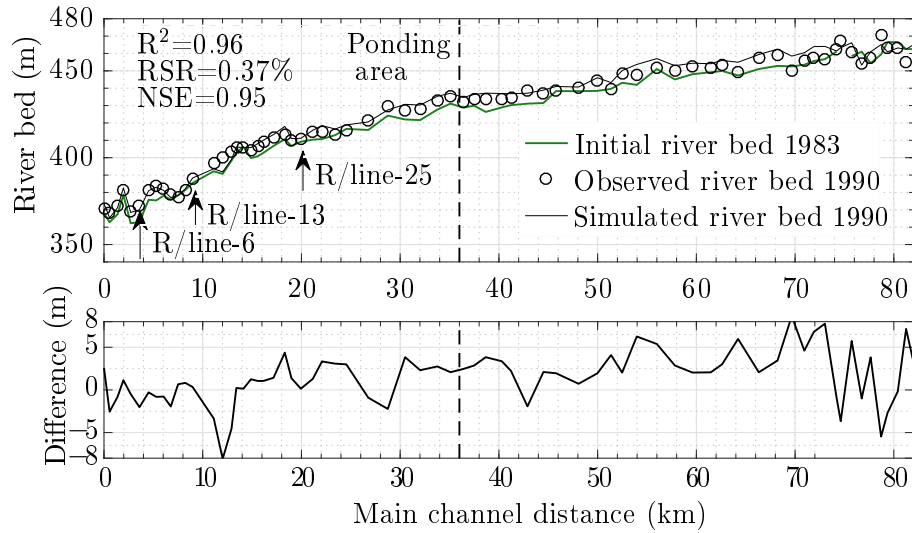
Figure 6.14: Longitudinal profile of mean measured and computed river bed at the end of validation process
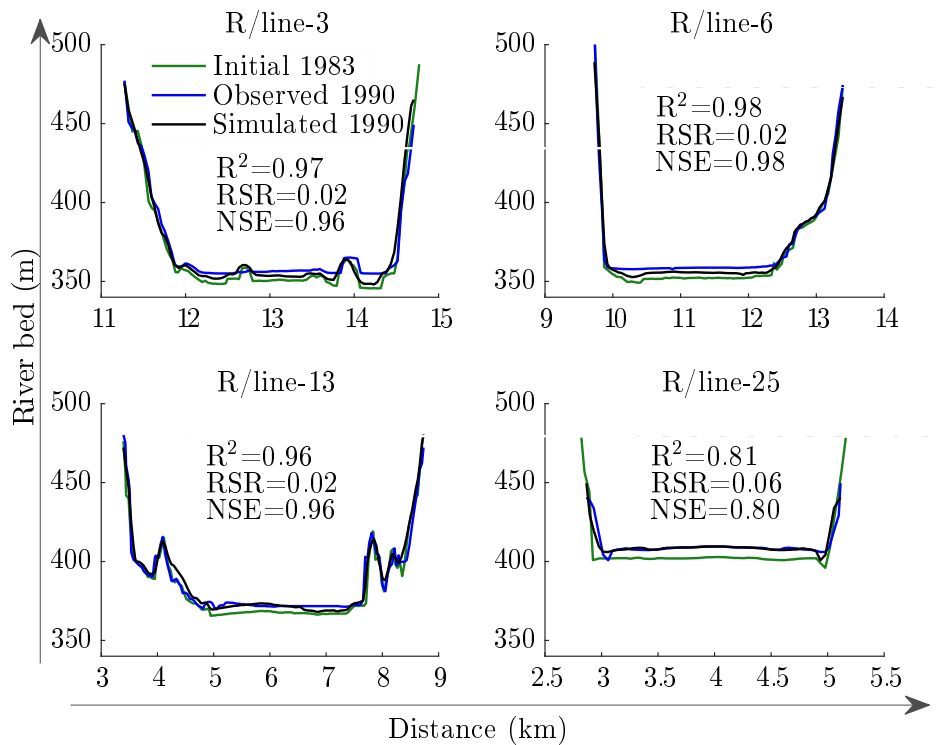

Figure 6.15: Comparison between measured and simulated river bed at four selected cross sections (R/line) at the end of validation process. Measurements start orographically from left side of the reservoir.

6.3.3 Model application

Since the people, economy and agriculture of the Pakistan rely heavily on the water supply from the Tarbela Reservoir, the current and future state of river discharges and corre-

sponding water storages are a matter of high political sensitivity due to climate change
[164]. The political tensions over water availability are further exacerbated by existing
dwindling and planned storages. Hence, to evaluate the effect of sediment transport vari-
ability on the reservoir sedimentation and water storage, we applied a future discharge
series for (2016-2030) calculated by [24] and corresponding SSLs estimated using WA-
ANN [3, 4] (Fig. 6.16). The reservoir water levels from 2016-2030 were kept same as
2000-2015. The near future scenarios of WA-ANN estimated sediment load suggest a
substantial decrease (20 million tons (Mt)) caused by drop in the glacier melt and one
month delay in peak of flows and overall reduction in water availability. The mean an-
nual sediment load (SL) from 1969-2008 was 160 Mt with a mean annual discharge of 76
billion m^3 [4]. However, the mean SL from 2000-2008 was decrease to 146 Mt/yr with a
mean discharge of 75 billion m^3/yr. Near future projections from 2010-2030 also suggests
a further decrease to 120 Mt/yr with a mean discharge of 75 billion m^3/yr. These dis-
proportional spatio-temporal trends between SL and discharges are primarily caused by
intra-annual shifts in flow discharges from summer to the winter under the influence of
warmer climates [24, 4]. Our modelling results also showed a stability in sediment delta
development due to an average 17% decrease in sediment supply in near future (Fig. 6.17).
Although, the overall water availability is expected to slightly decrease in the future, the
significant decrease in sediment load can help to store more water for multi-purpose use
(irrigation, hydropower, etc.) and was likely to increase the life span of the reservoirs.
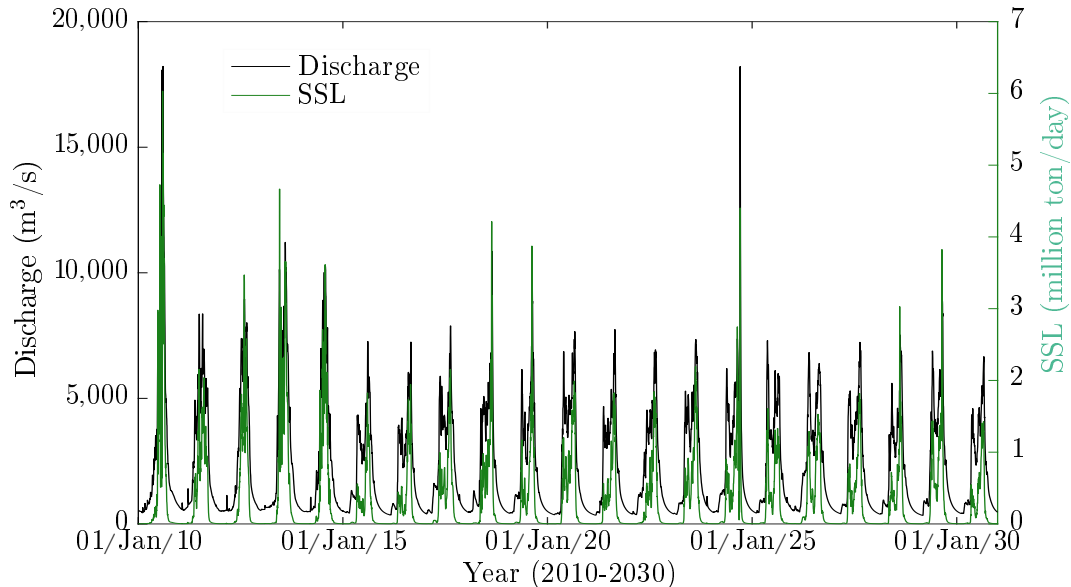

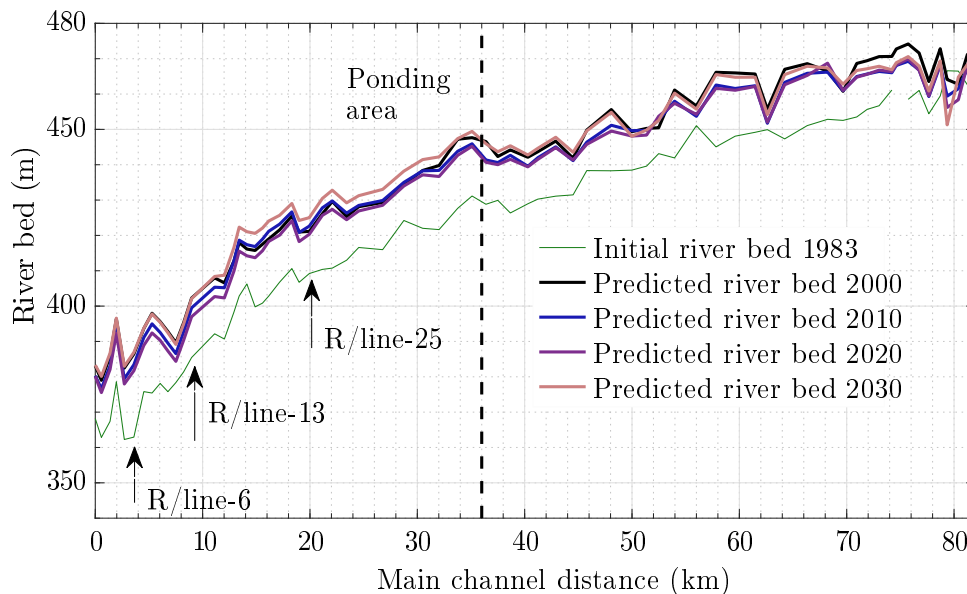Figure 6.16: Predicted flow discharge and sediment load at the Tarbela dam

Figure 6.17: Longitudinal profile of predicted river bed using WA-ANN predicted sediment boundary conditions

6.4 Discussion

The automatic hydrodynamic calibration algorithm for the Tarbela dam improved the model performance from R^2=0.90 and NSE=0.898 to R^2=0.969, and NSE=0.966 (Fig. 6.11). In addition, more precise sediment load (SL) boundary conditions obtained using the wavelet artificial neural network (WA-ANN) calibrated the model with R^2=0.97 and NSE=0.96 (Fig. 6.12). The model validated the results by predicting the reservoir bed for five years (1986-1990) with R^2=0.96 and NSE=0.95 (Fig. 6.14). Although the overall statistical performance of the model was good, it also over-predicted the river bed (0.76%) in the calibration process, particularly upstream of the ponding area (Fig. 6.12). However, the over-predictions were reduced to an average 0.54% in the validation process (Fig. 6.14). The calculations for bed level changes in the ponding area, particularly for the sediment delta, were close to the measurements in both the calibration and validation processes (Fig. 6.13 and 6.15). In addition, our modelling also shows a stability in the sediment delta development due to significant decrease (17%) in near future sediment load entering the reservoir (Fig. 6.16 and 6.17).

The back propagation method has been successfully used in the training of artificial neural networks for hydro-sedimentological studies [165, 105]. Using the same method along with a 2D linear interpolation during calibration process, we were able to update and interpolate the Manning roughness (n) for each node of the mesh. To achieve this,

the TELEMAC model passed the hydrodynamic information (water depths) to Matlab, which was compared with the observations in the form of matrices (Fig. 6.7). The difference was used to update n for the whole mesh using the linear interpolation method. The overall set-up not only reduced the computational effort but also saved computational time by using calculations in a more systematic way. Therefore, we were able to reduce the difference between predictions and measurements in only five iterations (Fig. 6.11) by employing the stopping criteria defined in Eq. 6.17, i.e. the difference between successive statistical mix (S) should be equal or less than 0.0001. The fast convergence with the minimum possible number of iterations not only saved computational effort but also provided us with an opportunity to curtail circular error in subsequent morphodynamic calculations. Fast convergence within minimum possible iterations is always required where large water bodies such as the Tarbela Reservoir (having hundreds of thousands of mesh nodes) are being simulated, which requires huge computational effort. Although the bed roughness has comparatively less influence in high water depths such as in the Tarbela (water depth approx. 100 m), the automatic calibration algorithm can also be used effectively in low water depth channels/rivers, where the influence of roughness on hydrodynamic parameters is high.

The more precise SL boundary conditions also improved the subsequent performance of SISYPHE calculations for bed level changes. In particular, the bed level changes in the ponding area, which contained the sediment delta. As the sediment delta progresses downstream towards the main dam, a precise representation of the delta in the modelling process can provide a better understanding of the impact of different management options necessary to preserve the functionality of the dam. In addition, the calibration period (1984-1985), which represents both dry and wet hydro-sedimentological events, favoured good calibration. Consequently, during the testing/validation period (1986-1990), which also contains the second highest flow and SL year (from 1969-2008), the model performed well. Therefore, the representativeness of the data sets used for calibration and validation should be considered, because when the model is calibrated with a data set that represents the characteristics of the hydro-sedimentological patterns will achieve good matching.

Although in terms of calculating total roughness using the [161] formula (Eq. 6.11) the automatic hydrodynamic calibration has improved the morphodynamic calculations by specifying the roughness for each mesh node, the main factors that influence reservoir sedimentation are: (a) inflow of both discharges and SLs, (b) particle size distribution of sediments, (c) specific weight of sediment deposits, (d) geometry of the reservoir, and (e) reservoir operation rules [64]. The influence of these factors may vary prior to

river and locational characteristics. Despite the fact that all these factors are to some extent uncertain, and also cause uncertainty in the model outcome, the inflow discharges and SLs are the most important factors contributing to the variation of accumulating sediments in the reservoirs [166]. Measurements taken twice daily successfully reduced the uncertainties in inflow discharge at Besham Qila. However, occasional/non-daily SSC sampling still contributed to variation in accumulating sediments in the Tarbela Reservoir, particularly when the occasional measurements were transferred on a daily time scale using conventional sediment rating curves. In a recent study, [59] modelled the Tarbela's delta using a 1D HEC-6 model. There was an average variation of 20 m (just in one year) between the observed and simulated river bed at some cross sections (during validation) in the dam ponding area. This variation could relate to uncertainty in sediment load (SL) boundary conditions, which were estimated using a sediment rating curve (SRC). The SRC has limited accuracy since it does not adjust complex sediment transport processes related to hysteresis phenomena and temporary sediment storage in the Upper Indus River [4]. For example, the mean deviation between the predicted SL using SRC and the measurements conducted for the Tarbela over a period of 26 years was as high as approximately 40%. However, using SL boundary conditions, estimated using the WA-ANN model, the variation was reduced to a range of -5 to 7 m (using TELEMAC/SISYPHE 2D model for 7 years) in the same domain (Fig. 6.12 and 6.14). In another study [151] used a TELEMAC 2D model to assess the impact of sediment distribution on the life of the Hirakud reservoir in India. The model slightly overestimated the deposits at the inlet due to sudden expansion of inlets, which reduced the water velocities, turbulences and shear stresses, and caused a delta there. However, with NSE=0.51-0.77, the model reasonably represented the overall changes in the bathymetry of the reservoir using daily measured sediment concentrations as SL boundary conditions. Therefore, the more precise modelling of reservoir sedimentation significantly depends on the quality of the input parameters and representation of geometry in the form of a numerical mesh. The use of a 2D model not only helps to design correct reservoir operation rules for the flushing of sediments but also contributes to diminishing circular error, particularly in the presence of complex topography, where 2D models can provide more accurate predictions in detail.

Interestingly a slight decrease in near future discharges caused by delaying glacier melt [24] are stabilizing the sediment delta by decreasing sediment supply to the Indus River at Tarbela dam (Fig. 6.16 and 6.17). Compared to an initial estimates by [11] of 480 million tons/year (Mt/yr) or by [12] of 400 Mt/yr at the time of Tarbela's construction, the sediment load in 2020 to 2030 will remain only at 120 Mt/yr. This is mainly caused

by a desynchronization between the glacier melt (major source of the flow discharges) and monsoon rain, which will result in a subsequent decrease in peaks flows and cause to reduced sediment transport due to decrease in effective discharges - the most effective discharge is defined as a midpoint of the range of flows, which over a certain period can transport a considerable proportion of the SSL [140]. Although, current findings contradict the previous claims of high reservoir sedimentation due to climate change [52, 167], the desynchronization has a positive effect on the life span and higher storage capacities of planned hydraulic structures on the Indus River. Additionally, the drop in short future sediment loads also negates the previous reservoir sedimentation studies, which simply used the past hydro-meteorological data without modification to the future predictions, particularly for the hydropower projects planned in the Indus River/Basin [6, 58, 15, 1, 59].

Despite the fact that the SISYPHE predictions for bed level changes in the Tarbela Reservoir are close to our measurements, omission of low flow/SL months from October to April (Tab. 6.3), when reservoir water levels are reduced to minimum level (Fig. 6.3), might have affected trap efficiency calculations and caused a 0.5-0.8% over-prediction. However, to compute seven years (1983-1990, only high flows and SLs) of reservoir sedimentation required a three week simulation time using a server with 20 physical cores (dual Intel XEON E5-2687W v3 @ 3.1 GHz) and 128 GB of RAM. To save computational time and assess the effects of only significant SL contributing periods, we decided to omit the low flow months from the modelling process.

The overall modelling approach can be used for better design of planned hydraulic structures and existing ones in the Indus Basin, particularly in the Upper Indus Basin, where the Tarbela dam is used as a standard/reference point for reservoir sedimentation studies of 30,000 MW planned hydraulic structures. In the absence of any hydraulic structure or land use changes in the Upper Indus River/Basin, there are statistically significant trends in discharges and SLs. Our cascade modelling approach using future SL can also be used to improve sediment management strategies and update reservoir operation rules for hydraulic structures. The SL boundary conditions for predictions can be estimated using WA-ANN models and future discharges. A coupling of the TELEMAC/SISYPHE model with a 1D model can reduce computation time, which could be useful for longer-range predictions.

6.5 Conclusions

In this paper the uncertainty factor related to sediment load (SL) boundary conditions were diminished using WA-ANN and TELEMAC-SISYPHE models, respectively. The flow model was calibrated using an automatic calibration algorithm along with more precise suspended SL boundary conditions. To predict the sediment delta movement in the ponding area, a hydrological and WA-ANN models were used to obtain the future discharge and corresponding sediment load boundary conditions. Based on the study results, we can draw the following main conclusions:

- More accurate WA-ANN estimated sediment load boundary conditions which better represent the hysteresis phenomenon and hydrological variations for the Indus River enabled the successive morphodynamic model to accurately predict the bed level changes in the Tarbela dam.

- Automatically calibrating hydrodynamics improved the overall statistical performance and reduced the calculation time for long-term simulations. In addition, specifying the bed roughness for each mesh node using the back propagation error method subsequently enhanced the performance of morphodynamic calculations by providing better hydrodynamic variables and total bed roughness for the calculation of sediment erosion, transport and deposit in the flow area.

- The desynchronization between glacier melt and monsoon rainfall due to warmer climate will also cause a significant decrease in future sediment loads and subsequent delta development. Therefore, past hydro-meteorological data (showing higher sediment loads) cannot be used without modification when making future predictions, particularly for the hydropower projects planned at the Indus River/Basin.

On the basis of these conclusions we would make the following recommendations:

- The presented modelling concept can be used to improve/design sediment management strategies for the existing and planned hydraulic structures in other un-gauged or poorly-gauged rivers.

- Although the effect of the bed roughness on the water depths in large dams is not always dominant, the concept of an automatic hydrodynamic calibration can also be used for other water bodies where roughness has a significant influence on water depths.

- In order to reduce computational time for long term morphodynamic predictions, coupling of the TELEMAC 2D model with a 1D model/ANN is recommended.

Notation

The following symbols are used in this paper:

ADCP	Acoustic Doppler Current Profiler
BCM	billion cubic meter
c_b	sediment concentration in bed load layer
C_eq	equilibrium near-bed concentration
C_f	roughness coefficient
C_f'	combined friction of both drag forms and skin friction
d_{50}	mean diameter
D_*	dimensionless grain diameter
d^o	observed water depth
d^s	simulated water depth
g	gravitational acceleration
h	water depth
HEC-RAS	Hydrologic Engineering Center-River Analysis System
k	von Karman coefficient
km	kilometre
k_s	bed roughness
k_s'	roughness height
masl	mean above sea level
Mt	million ton
MW	megawatt
n	Manning roughness

NSE	Nash-Sutcliffe Efficiency
$p\prime$	bed porosity
ppm	part per million
$q_{t,x}$ and $q_{t,y}$	total sediment transport in x and y direction
R^2	coefficient of determination
R/line	range lines or cross section
RESSASS	Reservoir Survey Analysis and Sedimentation Simulation
RSR	observations standard deviation ratio
RWL	reservoir water level
S	statistical mix
SL	sediment load
SRC	sediment rating curve
SSL	suspended sediment load
SSC	suspended sediment concentration
SUPG	Streamline-Upwinded Petrov-Galerkin
t	time
u, v	depth-averaged flow velocity components in x and y direction
µ	micro
ρ	density
τ_{xx} and τ_{yy}	depth-averaged turbulent stresses
δ_b	bedload layer thickness
$\eta\prime_e$	erosion rate
$\eta\prime_d$	deposition rate
X_i^{obs}	observed parameter
X_i^{sim}	simulated parameter
τ'	shear stress due to skin friction
τ_{cr}	critical shear stress

τ_b	total bed shear stress
μ	bed form coefficient
α_{ks}	calibration coefficient
UIB	Upper Indus Basin
W_s	settling velocity
WA-ANN	wavelet artificial neural network
WAPDA	Water and Power Development Authority
yr	year
Z_b	bed elevation
Z_{ref}	reference elevation
Z_s	free surface elevation

Chapter 7

Conclusion and Recommendations

7.1 Conclusions

The present study was designed in the context of numerical modelling of sediment management studies in Pakistani reservoirs. The study used more accurate sediment load boundary conditions with an automatic calibration algorithm which specify bed roughness for each mesh node and subsequently enhance the performance of morphodynamic calculations by providing better hydrodynamic variables and total bed roughness for the calculations of sediment erosion, transport and deposit in the flow area. Five different cases were documented with different types of sediment load estimation methods and boundary conditions. The conclusions drawn from this study are summarized in the following points.

- Estimation of sediment load deposits of Dasu Hydropower Project

To obtain a sediment deposition profile with pressure or free flow flushing in the reservoir, a 1D numerical model can be used in pre-feasibility studies.

- Reconstruction of missing sediment load

WA-ANN can accurately predict the sediment load time series with a temporal variation of more than one level for the Indus River. The new estimate of only 160 million tons per year for the Tarbela dam is close to the real time field measurements. In addition, the new estimate is lower than the published estimates, which can be attributed to the substantial sediment storage in the relatively flat Tibetan Plateau and the Indus River Valley between the Partab Bridge and Besham Qila gauge stations.

- Sediment load trends

The WA-ANN sediment load along with the innovative trend test, the Mann-Kendall test, Sen's slope estimator, the change point detection test and linear regressions have shown a shifting trend from the summer to the spring and winter months due to a change in water availability at the Upper Indus River over the past 50 years. The spatio-temporal trends between flow discharges and SSLs are disproportionate. This disproportional behaviour and the significant trends strongly disconfirm the hypothesis that future inflows and SSLs are similar to the previous ones for reservoir sedimentation studies for the Upper Indus River.

- TELEMAC 2D model

The well calibrated TELEMAC 2D model using more accurate sediment load boundary conditions (obtained using WA-ANN) enabled the successive morphodynamic model to accurately predict the bed level changes under a climate changing scenario in the Tarbela dam. The Climate change has been affecting existing reservoirs on the Indus River due to changes in boundary conditions, such as modified flow regimes, changed sediment loads, and natural hazards. Therefore, a projected desynchronization between glacier melt and monsoon rainfall can cause a significant decrease in future sediment loads due to change in most effective discharges.

7.2   Recommendation for further research

Modelling of sediment transport using TELEMAC 2D model is highly challenging and the following issues need further work:

- Reduction in computational time

Although the bed level predictions using TELEMAC model were close to the real time measurements, to compute seven year (1983-1990, only high flows and SLs) reservoir sedimentation required three weeks simulation time using a server with 20 physical cores (dual Intel XEON E5-2687W v3 @ 3.1 GHz) and 128 GB of RAM. Therefore, to reduce computational time for morphodynamic predictions, coupling of TELEMAC 2D model with a 1D model/ANN is recommended.

- Prediction of reservoir sedimentation and sediment delta

Since there are neither hydraulic structures at the Upper Indus River/Basin, nor land use changes that will change the situation, future sediment loads can be estimated with WA-ANN based on future long term discharge of hydrological models. Using these modified sediment load boundary conditions for reservoir sedimentation can improve the overall quality of hydraulic designs and the lifespan of reservoirs in the study area - in particular, the modelling of the movement of the sediment delta in the Tarbela dam.

- Data availability

2D modelling requires additional data of different parameters compared to 1D for calibration and validation processes. The data of these parameters is normally assumed or obtained using laboratory experiments. Therefore, the 2D modelling is still restricted to research institutions. Therefore, it is challenging to rely only on the outcome of WA-ANN reconstructed boundary conditions with 2D modelling. However, to implement the changeover to increase hydropower share in total energy mix and encounter climate changes, using state-of-the-art modelling (2D or 3D) will encourage data collection agencies to install new instruments for collecting more detailed data. This will not only provide an opportunity to the researcher to use actual field data in future but also bridge the gap between research and practice.

Bibliography

[1] Ateeq-Ur-Rehman, S.; Riaz, Z.; Bui, M.D.; Rutschmann, P., Application of a 1-D numerical model for sediment management in Dasu Hydropower Project. In *Proceedings of the 14th International Conference on Environmental Science and Technology*; Lekkas, D., Ed.; Global CEST: Rohdes, Greece, 2015; ISBN. 978-960-7475-52-7.

[2] Ateeq-Ur-Rehman, S.; Bui, M.D.; Riaz, Z.; Rutschmann, P., Estimation of sediment yield for Dasu Hydropower Project using artificial neural networks. In *18. Wasserbau-Symposium*; Rutschmann, P., Ed.; Freunde des Lehrstuhls für Wasserbau und Wasserwirtschaft, TU Munich: Wallgau, Germany, 2016; Vol. Nr. 134/2016, pp. 326–337, ISBN. 978-3-943683.

[3] Ateeq-Ur-Rehman, S.; Bui, M.D.; Rutschmann, P. Development of a wavelet-ANN model for estimating suspended sediment load in the upper Indus River. *Submitted to International Journal of River Basin Management* **2017**.

[4] Ateeq-Ur-Rehman, S.; Bui, M.D.; Rutschmann, P. Variability and trend detection in the sediment load of the Upper Indus River. *Water (Switzerland)* **2018**, *10*, 1–24, doi:10.3390/w10010016.

[5] Ateeq-Ur-Rehman, S.; Bui, M.D.; Hasson, S.u.; Rutschmann, P. An innovative approach to minimizing uncertainty in sediment load boundary conditions for modelling sedimentation in reservoirs. *Water (Switzerland)* **2018**, *10*, 1–27, doi:10.3390/w10101411.

[6] Dasu Hydropower Consultants. Detailed engineering design report, Part A; Engineering design, Volume 1; Project description. Report, Water and Power Development Authority, Lahore, Pakistan, 2013.

[7] Dasu Hydropower Consultants. Detailed engineering design report, Part A; Engineering design, Volume 7; Sediment management and reservoir operation. Report, Water and Power Development Authority, Lahore, Pakistan, 2013.

[8] McBean, E.A.; Al-Nassri, S. Uncertainty in suspended sediment transport curves. *Journal of Hydraulic Engineering* **1988**, *114*, 63–74, doi:10.1061/(ASCE)0733-9429(1988)114:1(63).

[9] Butt, M.J.; Waqas, A.; Mahmood, R.; Group, H.R. The combined effect of vegetation and soil erosion in the water resource management. *Water Resources Management* **2010**, *24*, 3701–3714.

[10] King, R.; Stevens, M. Sediment management at Warsak, Pakistan. *International Journal on Hydropower & Dams* **2001**, *8*, 61–68.

[11] Holeman, J.N. The sediment yield of major rivers of the world. *Water Resources Research* **1968**, *4*, 737–747, doi:10.1029/WR004i004p00737.

[12] Peshawar University. The sediment load and measurements for their control in rivers of West Pakistan. Report, Department of Water Resources, Peshawar University, Peshawar, Pakistan, 1970.

[13] Meybeck, M. Total mineral dissolved transport by world major rivers/Transport en sels dissous des plus grands fleuves mondiaux. *Hydrological Sciences Journal* **1976**, *21*, 265–284, doi:10.1080/02626667609491631.

[14] Lowe, J.; Fox, I., Sedimentation in Tarbela reservoir. In *Commission Internationale des Grandes Barrages. Quatorzieme Congres des Grands Barrages, Rio de Janeiro*; 1982.

[15] Roca, M., Tarbela Dam in Pakistan. Case study of reservoir sedimentation. In *Proceedings of River Flow*; Munoz, R.E.M., Ed.; CRC Press: London, UK, 2012; ISBN. 978-0-415-62129-8.

[16] Milliman, J.; Quraishee, G.; Beg, M., Sediment discharge from the Indus River to the ocean: past, present and future. In *Marine Geology and Oceanography of Arabian Sea and Coastal Pakistan*; Haq, B.U.; Milliman, J.D., Eds.; Van Nostrand Reinhold/Scientific and Academic Editions: New York, 1984; pp. viii, 382 p., ISBN. 978-0-44-223216-0.

[17] Summerfield, M.A.; Hulton, N.J. Natural controls of fluvial denudation rates in major world drainage basins. *Journal of Geophysical Research-Solid Earth* **1994**, *99*, 13871–13883, doi:10.1029/94jb00715.

[18] Collins, D. Hydrology of glacierised basins in the Karakoram: report on snow and Ice hydrology project in Pakistan with overseas development administration, UK [ODA] and water and power development authority, Pakistan [WAPDA]. Report, University of Manchester, Manchester, 1994.

[19] Ali, K.F. Construction of sediment budgets in large scale drainage basins: the case of the Upper Indus River. PhD thesis, Department of Geography and Planning, University of Saskatchewan, Saskatoon, 2009.

[20] Immerzeel, W.W.; Van Beek, L.P.; Bierkens, M.F. Climate change will affect the Asian water towers. *Science* **2010**, *328*, 1382–1385, doi:10.1126/science.1183188.

[21] Lutz, A.F.; Immerzeel, W.; Kraaijenbrink, P.; Shrestha, A.B.; Bierkens, M.F. Climate change impacts on the upper Indus hydrology: sources, shifts and extremes. *PLoS ONE* **2016**, *11*, 1–33, doi:10.1371/journal.pone.0165630.

[22] Bogen, J. The hysteresis effect of sediment transport systems. *Norsk Geografisk Tidsskrift-Norwegian Journal of Geography* **1980**, *34*, 45–54, doi:10.1080/00291958008545338.

[23] Hewitt, K. Gifts and perils of landslides: catastrophic rockslides and related landscape developments are an integral part of human settlement along upper Indus streams. *American Scientist* **2010**, *98*, 410–419.

[24] Hasson, S. Future water availability from Hindukush-Karakoram-Himalaya Upper Indus Basin under conflicting climate change scenarios. *Climate* **2016**, *4*, 40, doi:10.3390/cli4030040.

[25] Zhang, G.; Patuwo, B.E.; Hu, M.Y. Forecasting with artificial neural networks: The state of the art. *International journal of forecasting* **1998**, *14*, 35–62.

[26] Nourani, V.; Baghanam, A.H.; Adamowski, J.; Kisi, O. Applications of hybrid wavelet–artificial intelligence models in hydrology: A review. *Journal of Hydrology* **2014**, *514*, 358–377, doi:10.1016/j.jhydrol.2014.03.057.

[27] Tavakoli Targhi, A.; Abbaszadeh, S.; Arabasadi, Z. A hybrid method for forecasting river suspended sediments in Iran. *International Journal of River Basin Management* **2017**, *15*, 453–460.

[28] Shoaib, M.; Shamseldin, A.Y.; Melville, B.W.; Khan, M.M. A comparison between wavelet based static and dynamic neural network approaches for runoff prediction. *Journal of Hydrology* **2016**, *535*, 211–225, doi:10.1016/j.jhydrol.2016.01.076.

[29] Rajaee, T.; Nourani, V.; Zounemat-Kermani, M.; Kisi, O. River suspended sediment load prediction: application of ANN and wavelet conjunction model. *Journal of Hydrologic Engineering* **2010**, *16*, 613–627, doi:10.1061/(ASCE)HE.1943-5584.0000347.

[30] Ulke, A.; Tayfur, G.; Ozkul, S. Predicting suspended sediment loads and missing data for Gediz River, Turkey. *Journal of Hydrologic Engineering* **2009**, *14*, 954–965, doi:10.1061/(ASCE)HE.1943-5584.0000060.

[31] Olyaie, E.; Banejad, H.; Chau, K.W.; Melesse, A.M. A comparison of various artificial intelligence approaches performance for estimating suspended sediment load of river systems: A case study in United States. *Environmental Monitoring and Assessment* **2015**, *187*, 1–22, doi:10.1007/s10661-015-4381-1.

[32] Bui, M.D.; Rutschmann, P., Numerical investigation of hydro-morphological changes due to training works in the Salzach River. In *Proceedings of River Flow*; Munoz, R.E.M., Ed.; CRC Press: London, UK, 2012; Vol. 1, pp. 589–594, ISBN. 978-0-41-562129-8.

[33] Petkovsek, G.; Roca, M., Impact of reservoir operation on sediment deposition. In *Proceedings of ICE Water Management*; Hamilton, W.A.H., Ed.; ICE Publishing: UK, 2014; Vol. 167, pp. 577–584, ISBN. 1741-7589.

[34] Guerrero, M.; Rüther, N.; Haun, S.; Baranya, S. A combined use of acoustic and optical devices to investigate suspended sediment in rivers. *Advances in Water Resources* **2017**, *102*, 1–12, doi:10.1016/j.advwatres.2017.01.008.

[35] Chamoun, S.; De Cesare, G.; Schleiss, A.J. Venting of turbidity currents approaching a rectangular opening on a horizontal bed. *Journal of Hydraulic Research* **2017**, pp. 1–15, doi:10.1080/00221686.2017.1289266.

[36] Gardelle, J.; Berthier, E.; Arnaud, Y. Slight mass gain of Karakoram glaciers in the early twenty-first century. *Nature Geoscience* **2012**, *5*, 322–325, doi:10.1038/NGEO1450.

[37] Lutz, A.F.; Immerzeel, W.W.; Shrestha, A.B.; Bierkens, M.F.P. Consistent increase in High Asia's runoff due to increasing glacier melt and precipitation. *Nature Climate Change* **2014**, *4*, 587–592, doi:10.1038/nclimate2237.

[38] Böhner, J.; Lucarini, V. Prevailing climatic trends and runoff response from Hindukush-Karakoram-Himalaya, upper Indus Basin. *Earth System Dynamics* **2015**, doi:10.5194/esd-8-337-2017.

[39] Ul Hasson, S.; Pascale, S.; Lucarini, V.; Böhner, J. Seasonal cycle of precipitation over major river basins in South and Southeast Asia: a review of the CMIP5 climate models data for present climate and future climate projections. *Atmospheric Research* **2016**, *180*, 42–63, doi:10.1016/j.atmosres.2016.05.008.

[40] Forsythe, N.; Fowler, H.J.; Li, X.F.; Blenkinsop, S.; Pritchard, D. Karakoram temperature and glacial melt driven by regional atmospheric circulation variability. *Nature Climate Change* **2017**, *advance online publication*, doi:10.1038/nclimate3361.

[41] Azim, F.; Shakir, A.S.; Kanwal, A. Impact of climate change on sediment yield for Naran watershed, Pakistan. *International Journal of Sediment Research* **2016**, *31*, 212–219, doi:10.1016/j.ijsrc.2015.08.002.

[42] Yasarer, L.M.; Sturm, B.S. Potential impacts of climate change on reservoir services and management approaches. *Lake and Reservoir Management* **2016**, *32*, 13–26, doi:10.1080/10402381.2015.1107665.

[43] Khan, F.; Pilz, J.; Amjad, M.; Wiberg, D.A. Climate variability and its impacts on water resources in the Upper Indus Basin under IPCC climate change scenarios. *International Journal of Global Warming* **2015**, *8*, 46–69, doi:10.1504/IJGW.2015.071583.

[44] Khan, F.; Pilz, J.; Ali, S. Improved hydrological projections and reservoir management in the Upper Indus Basin under the changing climate. *Water and Environment Journal* **2017**, *31*, 235–244, doi:10.1111/wej.12237.

[45] Qiu, J. Stressed Indus River threatens Pakistan's water supplies. *Nature* **2016**, *534*, 600–601, doi:10.1038/534600a.

[46] Pritchard, H.D. Asia's glaciers are a regionally important buffer against drought. *Nature* **2017**, *545*, 169–174, doi:10.1038/nature22062.

[47] Şen, Z. Innovative trend analysis methodology. *Journal of Hydrologic Engineering* **2011**, *17*, 1042–1046, doi:10.1061/(ASCE)HE.1943-5584.0000556.

[48] Zhang, Q.; Xu, C.y.; Becker, S.; Jiang, T. Sediment and runoff changes in the Yangtze River basin during past 50 years. *Journal of Hydrology* **2006**, *331*, 511–523, doi:10.1016/j.jhydrol.2006.05.036.

[49] Shi, H.; Hu, C.; Wang, Y.; Liu, C.; Li, H. Analyses of trends and causes for variations in runoff and sediment load of the Yellow River. *International Journal of Sediment Research* **2016**, *32*, 171–179, doi:10.1016/j.ijsrc.2016.09.002.

[50] Pettitt, A.N. A non-parametric approach to the change-point problem. *Journal of the Royal Statistical Society Series C-Applied Statistics* **1979**, *28*, 126–135, doi:10.2307/2346729.

[51] Sun, L.; Yan, M.; Cai, Q.; Fang, H. Suspended sediment dynamics at different time scales in the Loushui River, south-central China. *CATENA* **2016**, *136*, 152–161, doi:10.1016/j.catena.2015.02.014.

[52] Schleiss, A.J.; Franca, M.J.; Juez, C.; De Cesare, G. Reservoir sedimentation. *Journal of Hydraulic Research* **2016**, *54*, 595–614, doi:10.1080/00221686.2016.1225320.

[53] Basson, G. Management of siltation in existing and new reservoirs. *General Report Q. 89. Proc. of the 23rd Congress of the Int. Commission on Large Dams (vol.2)* **2009**.

[54] Annandale, G., Sustainable water supply, climate change and reservoir sedimentation management: Technical and economic viability. In *Reservoir Sedimentation*; Schleiss, A.J.; Cesare, G.D.; Franca, M.J.; Pfister, M., Eds.; Taylor & Francis Group: London, 2014; ISBN. 978-1-138-02675-9.

[55] Babur, M.; Babel, M.; Shrestha, S.; Kawasaki, A.; Tripathi, N. Assessment of climate change impact on reservoir inflows using multi climate- models under RCPs−The case of Mangla Dam in Pakistan. *Water (Switzerland)* **2016**, *8*, 389, doi:10.3390/w8090389.

[56] Sönke Kreft, David Eckstein, I.M. *Global climate risk index 2017 who suffers most from extreme weather events? weather-related Loss events in 2015 and 1996 to 2015*; Germanwatch Nord-Sued Initiative e.V, 2016. Print.: Bonn, 2016; ISBN. 978-3-943704-49-5.

[57] Dasu Hydropower Project. Dasu Hydropower Project, feasibility report. Report, Water and Power Development Authority, Lahore, Pakistan, 2009.

[58] Bunji Consultants Joint Venture. Bunji Hydropower Project, design report, volume 2B sedimentation. Report, Water and Power Development Authority, Pakistan, 2010.

[59] Rehman, H.U.; Rehman, M.A.; Naeem, U.A.; Hashmi, H.N.; Shakir, A.S. Possible options to slow down the advancement rate of Tarbela delta. *Environmental Monitoring and Assessment* **2018**, *190*, doi:10.1007/s10661-017-6376-6.

[60] Malik, Y.I.; Munir, J. Hydraulic design of the low level outlets for Dasu dam, Pakistan. *International Journal on Hydropower & Dams* **2011**, *18*.

[61] EDF-R&D. *TELEMAC v7.0 User Manual*; Open TELEMAC-MASCARET: Chatou, France, 2014.

[62] EDF-R&D. *Sisyphe v7.2 User's mannual*; Open TELEMAC-MASCARET: Chatou, France, 2017.

[63] Reisenbüchler, M.; Bui, M.D.; Rutschmann, P., Implimentation of a new layer-subroutine for fractional sediment transport in SISYPHE. In *XXIIIrd TELEMAC-MASCARET user conference*; Bourban, S., Ed.; HR Wallingford Ltd.: Howbery Park, Wallingford, Oxfordshire, Oxfordshire OX10 8BA, 2016.

[64] USBR. *Design of small dams*; Water Resources Technical Publication, 860p, Water Resources Technical Publication, 1987.

[65] TAMS Consultants and HR Wallingford. Tarbela Dam sediment management study; Main report. Report, Water and Power Development Authority, Pakistan, 1998.

[66] Brune, G.M. Trap efficiency of reservoirs. *Eos, Transactions American Geophysical Union* **1953**, *34*, 407–418.

[67] Ali, K.F.; De Boer, D.H. Spatial patterns and variation of suspended sediment yield in the Upper Indus River Basin, northern Pakistan. *Journal of Hydrology* **2007**, *334*, 368–387, doi:10.1016/j.jhydrol.2006.10.013.

[68] McCully, P. Rivers no more: the environmental effects of dams. *Silenced rivers: the ecology and politics of large dams.* **1996**, pp. 29–64.

[69] World Commission on Dams. *Dams and Development: A New Framework for Decision-making: the Report of the World Commission on Dams*; Earthscan, 2000; ISBN. 1-85383-798-9.

[70] Sumi, T.; Kobayshi, K.; Yamaguchi, K.; Takata, Y. Study on the applicability of the asset management for reservoir sediment management. *International Congress on Large Dams, Brasilia, Q* **2009**.

[71] Haq, D.; Abbas, S.T., Sedimentation of Tarbela and Mangla reservoirs. In *70th Annual Session Proceedings of Pakistan Engineering Congress*; 2007; pp. 23–46.

[72] Sabir, M.A.; Shafiq-Ur-Rehman, S.; Umar, M.; Waseem, A.; Farooq, M.; Khan, A.R. The impact of suspended sediment load on reservoir siltation and energy production: A case study of the Indus River and its tributaries. *Polish Journal of Environmental Studies* **2013**, *22*, 219–225.

[73] Olsen, N.R. Two-dimensional numerical modelling of flushing processes in water reservoirs. *Journal of Hydraulic Research* **1999**, *37*, 3–16.

[74] Morris, G.L.; Fan, J. *Reservoir sedimentation handbook: design and management of dams, reservoirs, and watersheds for sustainable use*; McGraw Hill Professional, 1998; ISBN. 978-0-07-043302-1.

[75] Brunner, G.W. HEC-RAS river analysis system. Hydraulic Reference Manual. Version 4.1. Report, DTIC Document, 2010.

[76] HR Wallingford. Sedimentation study, Dasu Hydropower Project, Pakistan. Report EX 6801 R1, Dasu Hydropower Consultants, 2012.

[77] Martin, P.; Nishida, J.; Afzal, J.; Akbar, S.; Damania, R.; Hanrahan, D. Pakistan strategic country environmental assessment. *South Asia Region, World Bank* **2006**, *1*.

[78] Falkenmark, M. The massive water scarcity now threatening Africa: Why isn't it being addressed? *Ambio* **1989**, *18*, 112–118.

[79] Ministry of Water and Power Pakistan. Pakistan's vision of water resources management **2003**.

[80] Ministry of Water and Power Pakistan. Pakistan water vision 2025 **2004**.

[81] Food and Agriculture Orgnization of the United Nations. Pakistan, water report 37, 2012 **2011**.

[82] Chaudhary, M.M.; Hasan, Z.; Sufi, A.B. Addressing water and power needs of Pakistan through construction of major storage dams. *72nd annual session of Pakistan Engineering Congress* **2013**, pp. 235–258.

[83] ASCE. Artificial neural networks in hydrology. I: Preliminary concepts. *Journal of Hydrologic Engineering* **2000**, *5*, 115–123, doi:10.1061/(ASCE)1084-0699(2000)5:2(115).

[84] ASCE. Artificial neural networks in hydrology. II: Hydrologic applications. *Journal of Hydrologic Engineering* **2000**, *5*, 124–137, doi:10.1061/(ASCE)1084-0699(2000)5:2(124).

[85] Bui, M.; Penz, P.; Rutschmann, P. Application of an artificial neuronal network for estimation of contraction scour. *3rd IAHR Europe Congress, Porto, Portugal* **2014**, *Book of Proceedings*.

[86] Fayaed, S.S.; El-Shafie, A.; Alsulami, H.M.; Jaafar, O.; Mukhlisin, M.; El-Shafie, A. Augmentation of an artificial neural network and modified stochastic dynamic programing model for optimal release policy. *Hydrology Research* **2015**, *46*, 689–704, doi:10.2166/nh.2015.186.

[87] Boukhrissa, Z.A.; Khanchoul, K.; Le Bissonnais, Y.; Tourki, M. Prediction of sediment load by sediment rating curve and neural network (ANN) in El Kebir catchment, Algeria. *Journal of Earth System Science* **2013**, *122*, 1303–1312, doi:10.1007/s12040-013-0347-2.

[88] Jothiprakash, V.; Garg, V.; ASCE, S.M. Reservoir sedimentation estimation using artificial neural network. *Journal of Hydrologic Engineering* **2009**, *14*, 1035–1040, doi:10.1061/(ASCE)HE.1943-5584.0000075.

[89] Rahim, A.; Akif, A. Optimal artificial neural network modeling of sedimentation yield and runoff in high flow season of Indus River at Besham Qila for Terbela Dam. *Int. J. of Science and Research* **2015**, *4*, 479–483.

[90] Rezaeianzadeh, M.; Kalin, L.; Anderson, C. Wetland water-level prediction using ANN in conjunction with base-flow recession analysis. *Journal of Hydrologic Engineering* **2015**, *0*, D4015003, doi:10.1061/(ASCE)HE.1943-5584.0001276.

[91] Yang, C.T.; Marsooli, R.; Aalami, M.T. Evaluation of total load sediment transport formulas using ANN. *International Journal of Sediment Research* **2009**, *24*, 274–286, doi:10.1016/S1001-6279(10)60003-0.

[92] Agarwal, A.; Singh, R.; Mishra, S.; Bhunya, P. ANN-based sediment yield models for Vamsadhara river basin (India). *Water SA* **2005**, *31*, p. 95–100, doi:10.4314/wsa.v31i1.5125.

[93] Wang, Y.M.; Traore, S.; Kerh, T. Using artificial neural networks for modeling suspended sediment concentration. *Proceedings of the 10th WSEAS International Conference on Mathematical Methods and Computational Techniques in Electrical Engineering, Sofia, Bulgaria* **2008**.

[94] Singh, P.; Jain, S.K. Streamflow simulation of Satluj River in the Western Himalayas **1993**.

[95] Bui, M.D.; Rutschmann, P., Numerical modelling for reservoir sediment management. In *ASIA 2016. Sixth Intern. Conf. and Exhibition on Water Resources and Hydropower Development in Asia, Vientiane, Lao*; Aqua-Media International Ltd: Wallington, Surrey, UK, 2016; p. 9pp.

[96] Subramanian, V. Input by Indian rivers into the world oceans. *Proceedings of the Indian Academy of Sciences - Section A, Earth and Planetary Sciences* **1978**, *87*, 77–88, doi:10.1007/bf03182097.

[97] Collins, D.N., Sediment transport from glacierized basins in the Karakoram mountains. In *Erosion and Sediment Yield: Global and Regional Perspectives*; Walling, D.E.; Webb, B.W., Eds.; International Association of Hydrological Sciences Publication, 1996; pp. 85–96, ISBN. 0-947571-89-2.

[98] Shoaib, M.; Shamseldin, A.Y.; Khan, S.; Khan, M.M.; Khan, Z.M.; Melville, B.W. A wavelet based approach for combining the outputs of different rainfall runoff models. *Stochastic Environmental Research and Risk Assessment* **2018**, *32*, 155–168, doi:10.1007/s00477-016-1364-x.

[99] Rantz, S. *Measurement and computation of stream flow. Vol. 1. Measurement of stage and discharge; Vol. 2. Computation of discharge*; Water-supply paper (Washington, D.C.), 2175., United States Geological Survey, 1982.

[100] Edwards, T.K.; Glysson, G.D.; Guy, H.P.; (U.S.), G.S. *Field methods for measurement of fluvial sediment*, rev. ed.; Techniques of water-resources investigations of the United States Geological Survey, U.S. Geological Survey : Information Services: Reston, Va. Denver, Co., 1998; pp. viii, 89 p., ISBN. 978-0-607-89738-8.

[101] Ali, K.F.; De Boer, D.H. Spatially distributed erosion and sediment yield modeling in the upper Indus River basin. *Water Resources Research* **2010**, *46*, 1–16, doi:10.1029/2009WR008762.

[102] Khan, A.; Richards, K.S.; Parker, G.T.; McRobie, A.; Mukhopadhyay, B. How large is the Upper Indus Basin? The pitfalls of auto-delineation using DEMs. *Journal of Hydrology* **2014**, *509*, 442–453.

[103] Munir, S. Role of sediment transport in operation and maintenance of supply and demand based irrigation canals: Application to Machai Maira branch canals. PhD thesis, Institute for Water Education, UNESCO-IHE, Delf, Netherlands, 2011.

[104] Graf, W.H. *Hydraulics of sediment transport*; Water Resources Publication, 1984; ISBN. 978-0-91-833456-5.

[105] Jain, S.K. Development of integrated sediment rating curves using ANNs. *Journal of Hydraulic Engineering* **2001**, *127*, 30–37, doi:doi:10.1061/(ASCE)0733-9429(2001)127:1(30).

[106] Crowder, D.W.; Demissie, M.; Markus, M. The accuracy of sediment loads when log transformation produces nonlinear sediment load discharge relationships. *Journal of Hydrology* **2007**, *336*, 250–268, doi:http://dx.doi.org/10.1016/j.jhydrol.2006.12.024.

[107] Jansson, M.B. Estimating a sediment rating curve of the Reventazón River at Palomo using logged mean loads within discharge classes. *Journal of Hydrology* **1996**, *183*, 227–241, doi:10.1016/0022-1694(95)02988-5.

[108] Khan, N.M.; Tingsanchali, T. Optimization and simulation of reservoir operation with sediment evacuation: a case study of the Tarbela Dam, Pakistan. *Hydrological Processes* **2009**, *23*, 730–747, doi:10.1002/hyp.7173.

[109] Haykin, S. *Neural networks : a comprehensive foundation*, 2nd ed. ed.; Pearson Education: Delhi, 1999; p. 842 p. : ill. ; 24 cm., ISBN. 0-13-273350-1.

[110] Fletcher, D.; Goss, E. Forecasting with neural networks: an application using bankruptcy data. *Information & Management* **1993**, *24*, 159–167, doi:10.1016/0378-7206(93)90064-Z.

[111] Sundararajan, D. *Discrete wavelet transform: a signal processing approach*; John Wiley and Sons, 2016; ISBN. 978-1-119-11311-9.

[112] Mallat, S. *A wavelet tour of signal processing*; Academic press, 1999; ISBN. 978-0-08-052083-4.

[113] Labat, D.; Ababou, R.; Mangin, A. Rainfall runoff relations for karstic springs. Part II: Continuous wavelet and discrete orthogonal multiresolution analyses. *Journal of Hydrology* **2000**, *238*, 149–178.

[114] Shoaib, M.; Shamseldin, A.Y.; Melville, B.W. Comparative study of different wavelet based neural network models for rainfall runoff modeling. *Journal of Hydrology* **2014**, *515*, 47–58.

[115] Moriasi, D.N.; Arnold, J.G.; Van Liew, M.W.; Bingner, R.L.; Harmel, R.D.; Veith, T.L. Model evaluation guidelines for systematic quantification of accuracy in watershed simulations. *Transactions of the ASABE* **2007**, *50*, 885–900, doi:10.13031/2013.23153.

[116] Duraes, M.F.; de Mello, C.R.; Beskow, S. Sediment yield in Paraopeba River Basin – MG, Brazil. *International Journal of River Basin Management* **2016**, *14*, 367–377, doi:10.1080/15715124.2016.1159571.

[117] Rajaee, T.; Mirbagheri, S.A.; Zounemat-Kermani, M.; Nourani, V. Daily suspended sediment concentration simulation using ANN and neuro-fuzzy models. *Science of The Total Environment* **2009**, *407*, 4916–4927, doi:10.1016/j.scitotenv.2009.05.016.

[118] WAPDA. *Tarbela Dam Project, residency survey and hydrology organization*; Water and Power Development Authority: Lahore, Pakistan, 2011.

[119] Khan, S.M. Management of river and reservoir sedimentation in Pakistan. *Water international* **1985**, *10*, 18–21.

[120] Ackers, J.; Hieatt, M.; Molyneux, J.D. Mangla reservoir, Pakistan - Approaching 50 years of service. *Dams and Reservoirs* **2016**, *26*, 68–83, doi:10.1680/jdare.16.00036.

[121] Tfwala, S.S.; Wang, Y.M. Estimating sediment discharge using sediment rating curves and artificial neural networks in the Shiwen River, Taiwan. *Water (Switzerland)* **2016**, *8*, 1–15, doi:10.3390/w8020053.

[122] Ulke, A.; Tayfur, G.; Ozkul, S. Investigating a suitable empirical model and performing regional analysis for the suspended sediment load prediction in major rivers of the Aegean Region, Turkey. *Water Resources Management* **2017**, *31*, 749–764, doi:10.1007/s11269-016-1357-z.

[123] Partal, T.; Cigizoglu, H.K. Estimation and forecasting of daily suspended sediment data using wavelet–neural networks. *Journal of Hydrology* **2008**, *358*, 317–331, doi:10.1016/j.jhydrol.2008.06.013.

[124] Adamowski, K.; Prokoph, A.; Adamowski, J. Development of a new method of wavelet aided trend detection and estimation. *Hydrological Processes* **2009**, *23*, 2686–2696, doi:10.1002/hyp.7260.

[125] Partal, T.; Cigizoglu, H.K. Prediction of daily precipitation using wavelet—neural networks. *Hydrological Sciences Journal* **2009**, *54*, 234–246, doi:10.1623/hysj.54.2.234.

[126] Hasson, S.; Lucarini, V.; Khan, M.R.; Petitta, M.; Bolch, T.; Gioli, G. Early 21st century snow cover state over the western river basins of the Indus River system. *Hydrology and Earth System Sciences* **2014**, *18*, 4077–4100, doi:10.5194/hess-18-4077-2014.

[127] Hasson, S.; Böhner, J.; Lucarini, V. Prevailing climatic trends and runoff response from Hindukush–Karakoram–Himalaya, upper Indus Basin. *Earth System Dynamics* **2017**, *8*, 337–355, doi:10.5194/esd-8-337-2017.

[128] The International Journal on Hydropower & Dams. *World atlas & industry guide*; Aqua Media International Ltd: Wallington, UK, 2017; pp. 183–186.

[129] Railean, I.; Moga, S.; Borda, M.; Stolojescu, C.L., A wavelet based prediction method for time series. In *Stochastic Modeling Techniques and Data Analysis (SMTDA2010)*; Janssen, J., Ed.; ASMDA International: Chania, Greece, 2010.

[130] Şen, Z. Trend identification simulation and application. *Journal of Hydrologic Engineering* **2013**, *19*, 635–642, doi:10.1061/(ASCE)HE.1943-5584.0000811.

[131] Kisi, O. An innovative method for trend analysis of monthly pan evaporations. *Journal of Hydrology* **2015**, *527*, 1123–1129, doi:10.1016/j.jhydrol.2015.08.051.

[132] Mann, H. Nonparametric tests against trend. *Econmetrica* **1945**, *13*, 245–259, doi:10.2307/1907187.

[133] Kendall, M.G. *Rank correlation methods*, 4th ed.; Charles Griffin: London,, 1975; ISBN. 978-0-85-264199-6.

[134] Gilbert, R.O. *Statistical methods for environmental pollution monitoring*; John Wiley & Sons, 1987; ISBN. 978-0-47-128878-7.

[135] Yue, S.; Pilon, P.; Phinney, B.; Cavadias, G. The influence of autocorrelation on the ability to detect trend in hydrological series. *Hydrological Processes* **2002**, *16*, 1807–1829, doi:10.1002/hyp.1095.

[136] Von Storch, H., Misuses of statistical analysis in climate research. In *Analysis of Climate Variability*; Springer, 1999; pp. 11–26.

[137] Yue, S.; Wang, C.Y. Regional streamflow trend detection with consideration of both temporal and spatial correlation. *International Journal of Climatology* **2002**, *22*, 933–946, doi:10.1002/joc.781.

[138] Sen, P.K. Estimates of the regression coefficient based on Kendall's tau. *Journal of the American Statistical Association* **1968**, *63*, 1379–1389, doi:10.1080/01621459.1968.10480934.

[139] Gibbons, R.D.; Bhaumik, D.; Aryal, S. *Statistical methods for groundwater monitoring*, 2nd ed.; Statistics in practice, Wiley: Hoboken, N.J., 2009; pp. xxvi, 374 p., ISBN. 978-0-47-016496-9(cloth).

[140] Pickup, G. Adjustment of stream-channel shape to hydrologic regime. *Journal of Hydrology* **1976**, *30*, 365–373, doi:10.1016/0022-1694(76)90119-0.

[141] Hassan, M.; Shamim, M.A.; Sikandar, A.; Mehmood, I.; Ahmed, I.; Ashiq, S.Z.; Khitab, A. Development of sediment load estimation models by using artificial neural networking techniques. *Environmental Monitoring and Assessment* **2015**, *187*, 1–13, doi:10.1007/s10661-015-4866-y.

[142] Khattak, M.S.; Babel, M.; Sharif, M. Hydro-meteorological trends in the upper Indus River basin in Pakistan. *Climate Research* **2011**, *46*, 103–119, doi:10.3354/cr00957.

[143] Mukhopadhyay, B.; Khan, A. A reevaluation of the snowmelt and glacial melt in river flows within Upper Indus Basin and its significance in a changing climate. *Journal of Hydrology* **2015**, *527*, 119–132, doi:10.1016/j.jhydrol.2015.04.045.

[144] Mukhopadhyay, B.; Khan, A. A quantitative assessment of the genetic sources of the hydrologic flow regimes in Upper Indus Basin and its significance in a changing climate. *Journal of Hydrology* **2014**, *509*, 549–572, doi:10.1016/j.jhydrol.2013.11.059.

[145] Laghari, A.; Vanham, D.; Rauch, W. The Indus basin in the framework of current and future water resources management. *Hydrology and Earth System Sciences* **2012**, *16*, 1063–1083, doi:10.5194/hess-16-1063-2012.

[146] Zhang, W.; Wu, Y.; Wang, W.G.; Xing, W.Q. Characterizing the seasonal changing patterns of hydrological variables in the East River, Southern China. *Journal of Hydrologic Engineering* **2016**, *21*, 1–7, doi:10.1061/(asce)he.1943-5584.0001445.

[147] Bussi, G.; Dadson, S.J.; Bowes, M.J.; Whitehead, P.G. Seasonal and interannual changes in sediment transport identified through sediment rating curves. *Journal of Hydrologic Engineering* **2016**, *22*, 1–8, doi:10.1061/(ASCE)HE.1943-5584.0001466.

[148] WAPDA. *Tarbela Dam Project, residency survey and hydrology organization*; Water and Power Development Authority: Lahore, Pakistan, 2017.

[149] Juez, C.; Buhlmann, I.; Maechler, G.; Schleiss, A.J.; Franca, M.J. Transport of suspended sediments under the influence of bank macro-roughness. *Earth Surface Processes and Landforms* **2018**, *43*, 271–284, doi:10.1002/esp.4243.

[150] Rüther, N. Computational fluid dynamics in fluvial sedimentation engineering. Thesis, 2006.

[151] Dutta, S.; Sen, D. Sediment distribution and its impacts on Hirakud Reservoir (India) storage capacity. *Lakes & Reservoirs: Research & Management* **2016**, *21*, 245–263, doi:10.1111/lre.12144.

[152] The International Journal on Hydropower & Dams. First power from Tarbela IV in Pakistan. *The International Journal on Hydropower & Dams* **2018**, *25*, 15.

[153] Anwar, A.A.; Bhatti, M.T. Pakistan's water apportionment Accord of 1991:25 years and beyond. *Journal of Water Resources Planning and Management* **2018**, *144*, doi:10.1061/(ASCE)WR.1943-5452.0000831.

[154] Mehta, A.J.; Lee, S.C. Problems in linking the threshold condition for the transport of cohesionless and cohesive sediment grain. *Journal of Coastal Research* **1994**, *10*, 170–177.

[155] Klassen, I. Three-dimensional numerical modeling of cohesive sediment flocculation processes in turbulent flows. PhD thesis, Bauingenieur-, Geo- und Umweltwissenschaften, Karlsruher Instituts für Technologie (KIT), 2017.

[156] Roelvink, J.A. Coastal morphodynamic evolution techniques. *Coastal Engineering* **2006**, *53*, 277–287, doi:10.1016/j.coastaleng.2005.10.015.

[157] Duc, B.M.; Bernhart, H.H.; Kleemeier, H. Morphological numerical simulation of flood situations in the Danube River. *International Journal of River Basin Management* **2005**, *3*, 283–293, doi:10.1080/15715124.2005.9635268.

[158] Juez, C.; Murillo, J.; Garcia-Navarro, P. A 2D weakly-coupled and efficient numerical model for transient shallow flow and movable bed. *Advances in Water Resources* **2014**, *71*, 93–109, doi:10.1016/j.advwatres.2014.05.014.

[159] Reisenbüchler, M.; Bui, M.D.; Skublics, D.; Rutschmann, P. An integrated approach for investigating the correlation between floods and river morphology: A case study of the Saalach River, Germany. *Science of The Total Environment* **2019**, *647*, 814–826, doi:10.1016/j.scitotenv.2018.08.018.

[160] Nash, J.E.; Sutcliffe, J.V. River flow forecasting through conceptual models part I - A discussion of principles. *Journal of Hydrology* **1970**, *10*, 282–290, doi:10.1016/0022-1694(70)90255-6.

[161] Rijn, L.C.v. Sediment transport, part II: suspended load transport. *Journal of Hydraulic Engineering* **1984**, *110*, 1613–1641, doi:doi:10.1061/(ASCE)0733-9429(1984)110:11(1613).

[162] Van Rijn, L.C. *Principles of sediment transport in rivers, estuaries and coastal seas*; Aqua publications Amsterdam, 1993; ISBN. 9080035629.

[163] Talmon, A.M.; Struiksma, N., S.; van Mierlo, M.C.L.M. Laboratory measurements of the direction of sediment transport on transverse alluvial-bed slopes. *Journal of Hydraulic Research* **1995**, *33*, 495–517, doi:10.1080/00221689509498657.

[164] Bolch, T. Hydrology: Asian glaciers are a reliable water source. *Nature* **2017**, *545*, 161–162, doi:10.1038/545161a.

[165] Rumelhart, David E. ; McClelland, J.L. *Parallel distributed processing, v. 1, Foundations explorations in the microstructure of cognition foundations*; Cambridge, Mass. : MIT Press : 1986 : 1 Online-Ressource, 1986.

[166] Salas, J.D.; Shin, H.S. Uncertainty analysis of reservoir sedimentation. *Journal of Hydraulic Engineering* **1999**, *125*, 339–350, doi:doi:10.1061/(ASCE)0733-9429(1999)125:4(339).

[167] Kumar, R.; Kumar, R.; Singh, S.; Singh, A.; Bhardwaj, A.; Kumari, A.; Randhawa, S.S.; Saha, A. Dynamics of suspended sediment load with respect to summer discharge and temperatures in Shaune Garang glacierized catchment, Western Himalaya. *Acta Geophysica* **2018**, *66*, 1–12, doi:10.1007/s11600-018-0184-4.

Appendices

.1 Supplementary material

Table S1: Statistical parameters of annual linear and quadratic trends of reconstructed SSLs and observed discharges for the Besham Qila and the Partab Bridge sites. Note: Q_s is annual SSL in Mt, Q is annual flow volume in BCM for Besham Qila ($1969 \leq y \leq 2008$) and Partab Bridge ($1962 \leq y \leq 2008$).

Trend	Besham Qila		Partab Bridge	
	Equation	$\mathbf{R^2}$	Equation	$\mathbf{R^2}$
SSL linear	$Q_s = -0.315097y + 786$	0.0087	$Q_s = 0.555835y - 932$	0.0148
SSL quadratic	$Q_s = -0.029615y^2 + 117.465y - 116,312$	0.0169	$Q_s = 0.131748y^2 - 522.485y + 518,161$	0.1368
Flow linear	$Q = 0.075016y - 72$	0.0082	$Q = 0.155112y - 251$	0.0863
Flow quadratic	$Q = -0.006747y^2 + 26.908y - 26,750$	0.0153	$Q = 0.002850y^2 - 11.158y + 10,976$	0.0906

PSfrag replacements   PSfrag replacements
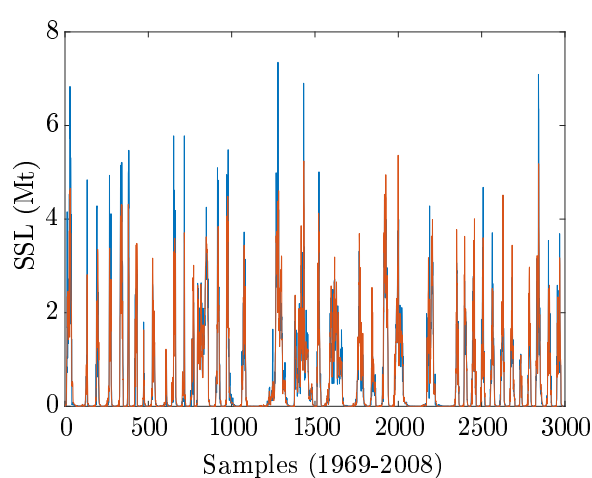
(a) Besham Qila
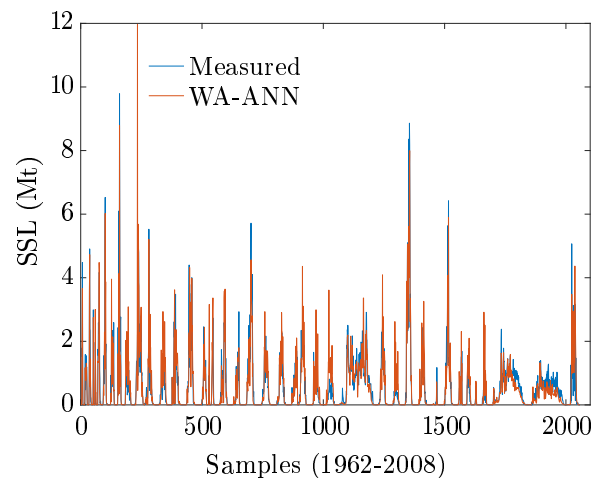
(b) Partab Bridge

Figure S1: Comparison between the mass of suspended sediment sampled daily and computed results using WA-ANN models., (legends for Fig. S1b also apply for Fig. S1a).
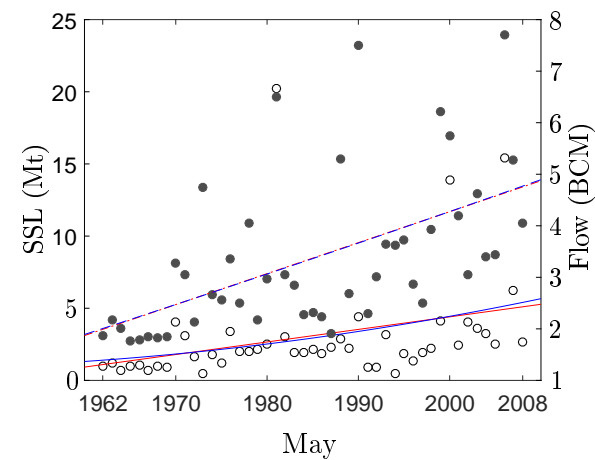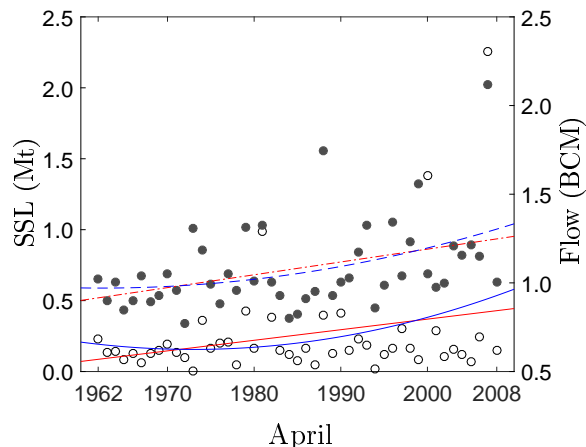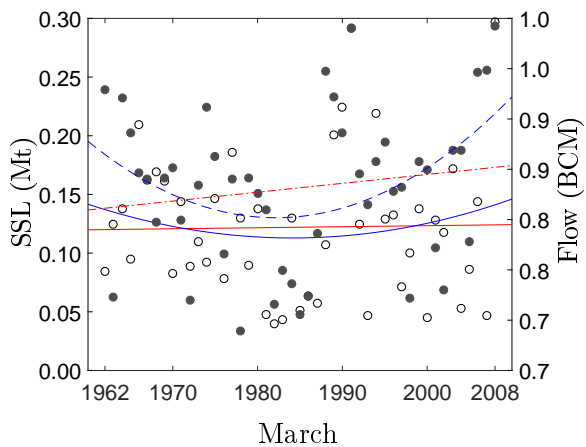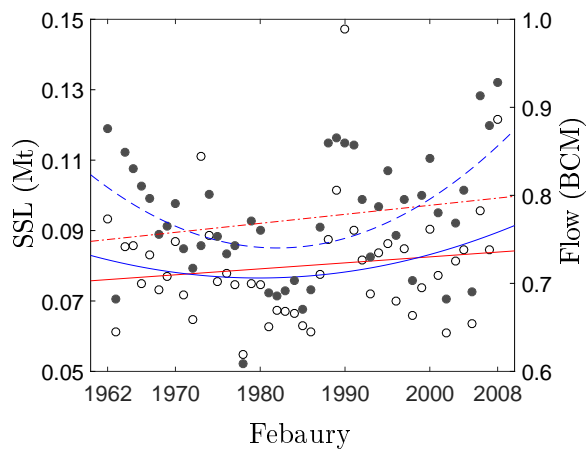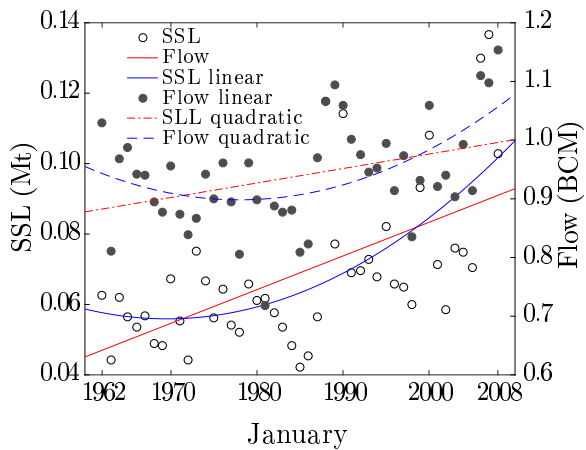
January

February

March

April

May

June
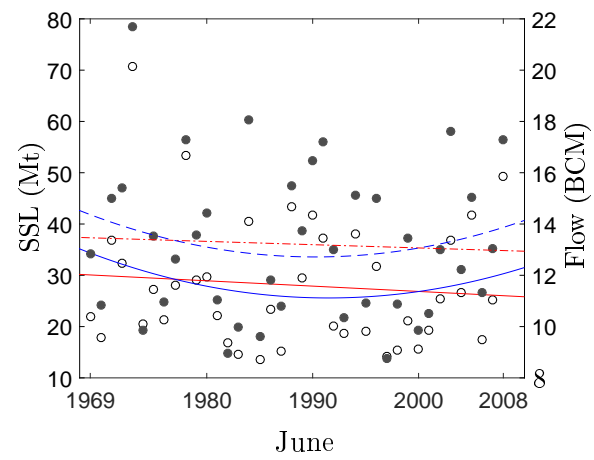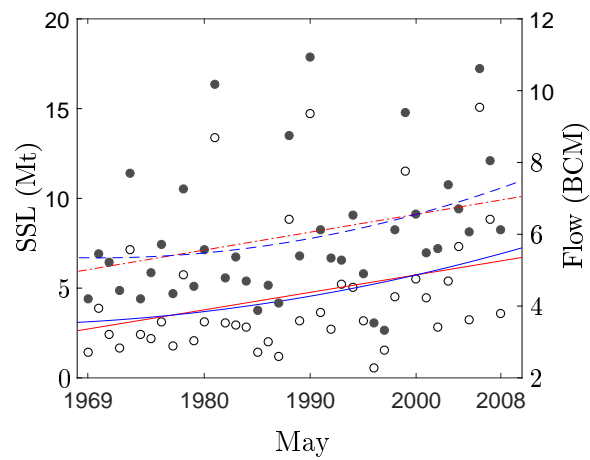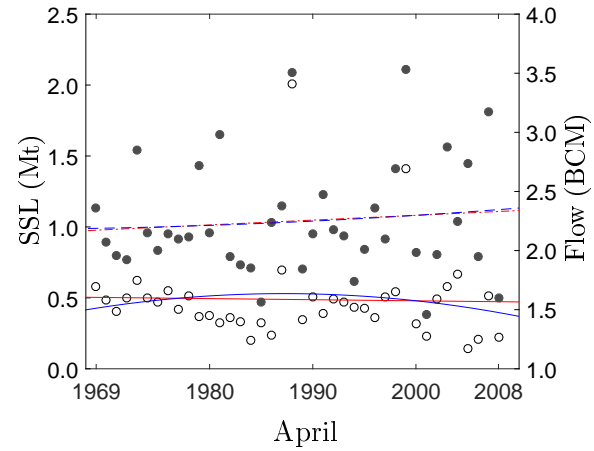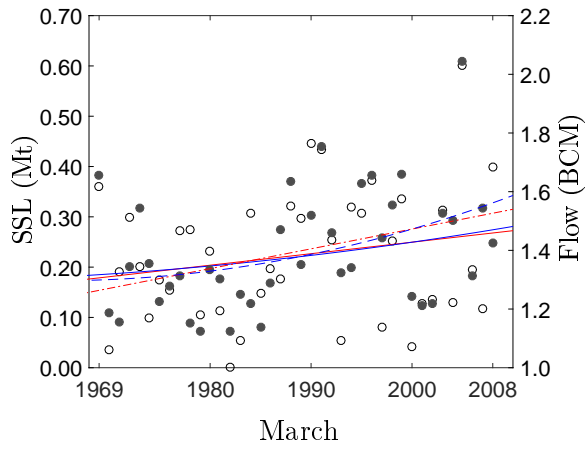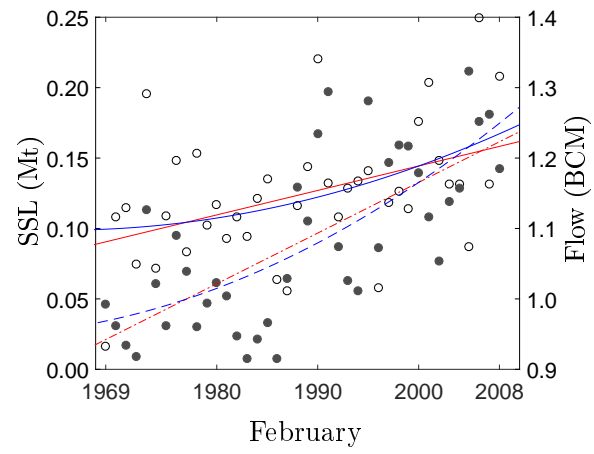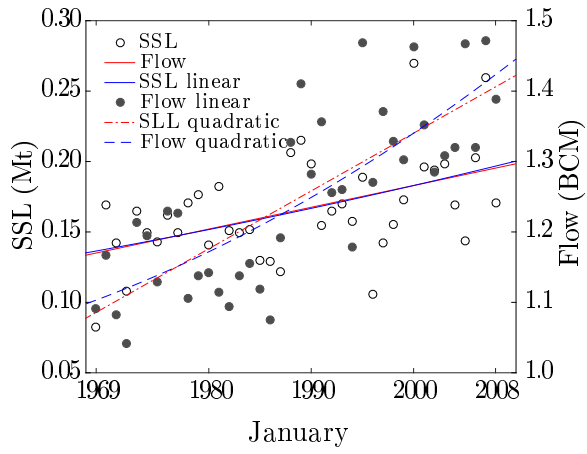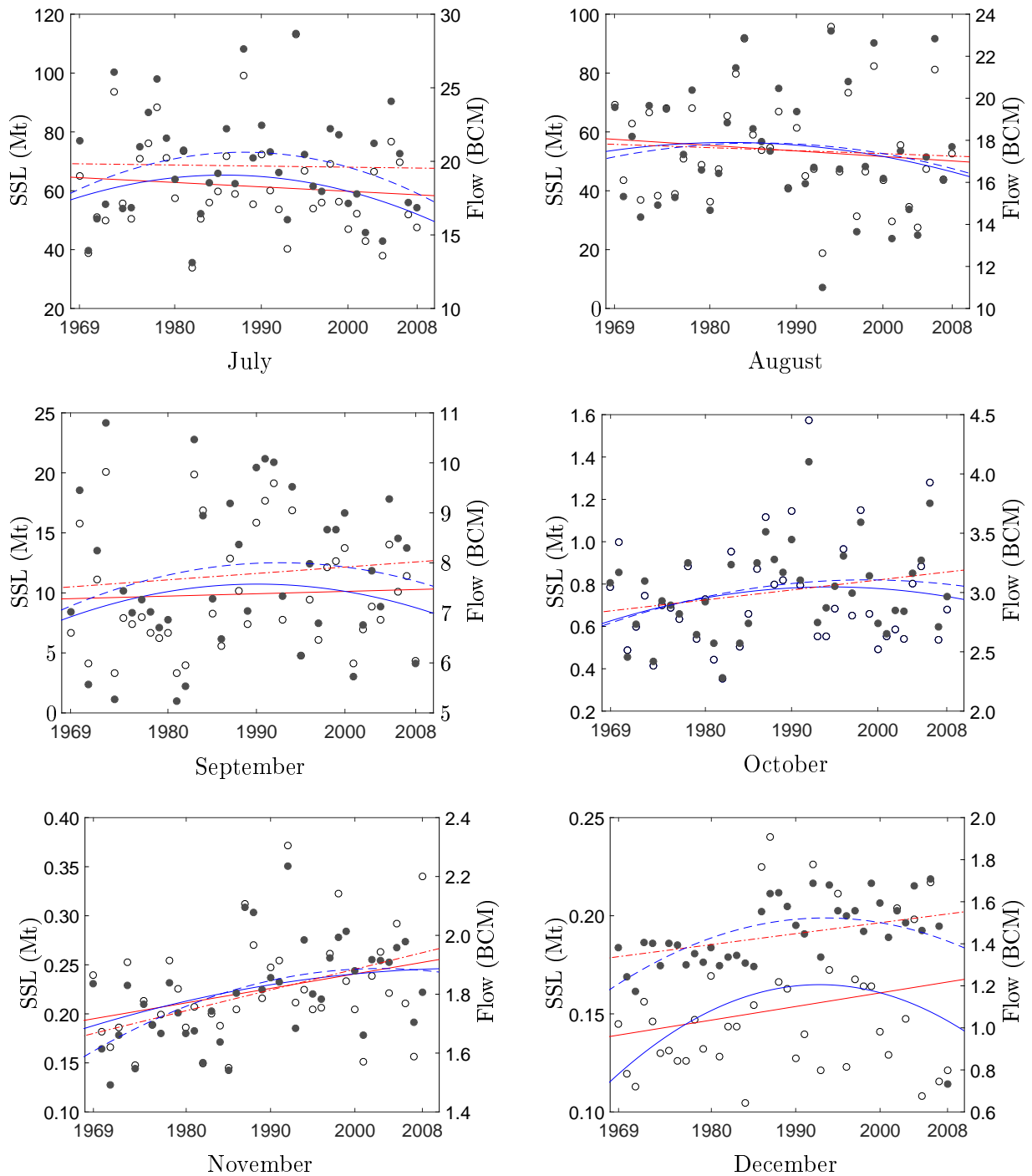
Figure S2: Mean monthly linear and quadratic trends in SSLs and discharges at Besham Qila site from 1969-2008.
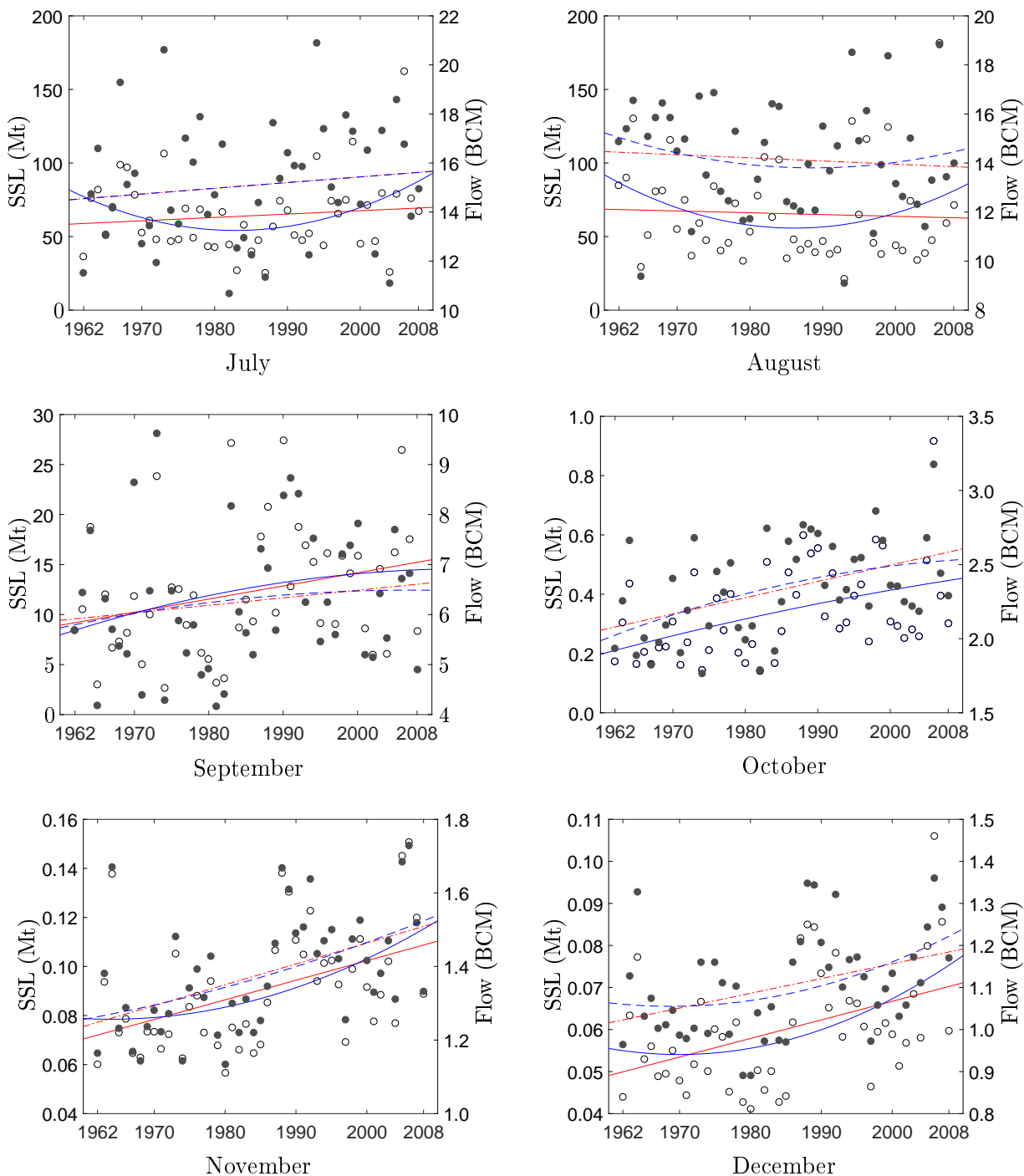
January

Febaury

March

April

May

June
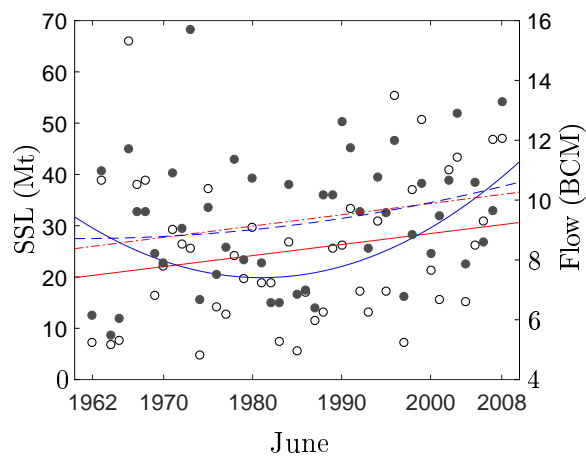
Figure S3: Mean monthly linear and quadratic trends in SSLs and discharges at Partab Bridge site from 1962-2008.
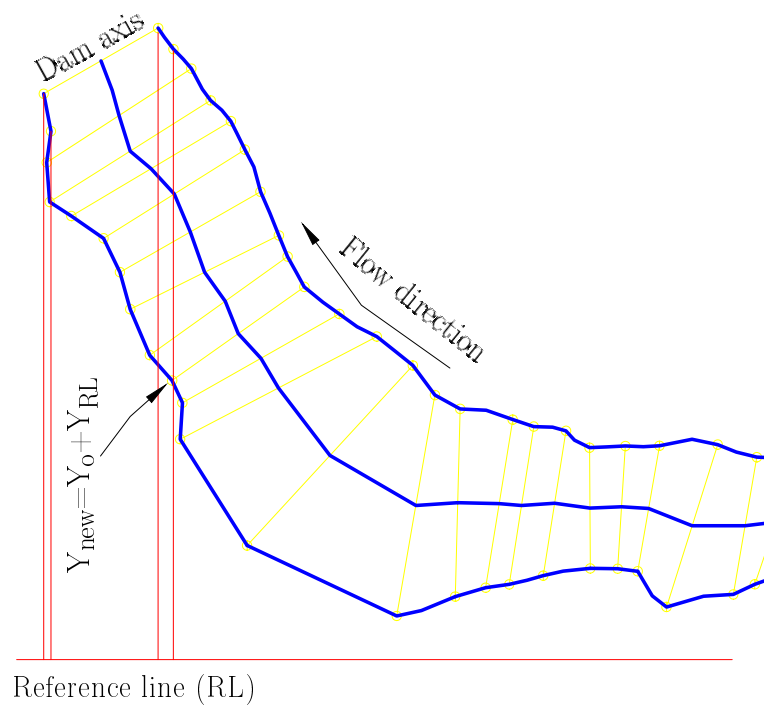
Figure S4: Transformation of Tarbela Reservoir Sedimentation Survey's local coordinates to global coordinates (Cartesian coordinates system) using AutoCAD Civil 3D 2018